UNIVERSITÄT ZU LÜBECK

From the Institute for Human Genetics

of the University of Lübeck

Director: Prof. Malte Spielmann

One miR to rule them all – epigenetic regulation of local thyroid hormone action in metabolic dysfunction-associated steatotic liver disease

Dissertation

for Fulfillment of

Requirements

for the Doctoral Degree

of the University of Lübeck

From the Department of Natural Sciences

Submitted by

Alison-Michelle Naujack

from Hamburg

Lübeck 2025

First referee: Prof. Dr. Henriette Kirchner

Second referee: Prof. Dr. Henrik Oster

Date of oral examination: 26.09.2025

Approved for printing: Lübeck, 02.10.2025

Eigenständigkeitserklärung

Ich versichere, dass ich die Dissertation ohne fremde Hilfe angefertigt und keine anderen als die angegebenen Hilfsmittel verwendet habe. Weder vorher noch gleichzeitig habe ich andernorts einen Zulassungsantrag gestellt oder diese Dissertation vorgelegt. Ich habe mich bisher noch keinem Promotionsverfahren unterzogen

Lübeck,

Contents

Figures

Tables

1. Abstract

Metabolic dysfunction-associated steatotic liver disease (MASLD) affects 30% of the global population. With rising numbers it presents a risk for global health and health care systems. The development of MASLD and the more severe stage, metabolic dysfunction-associated steatohepatitis (MASH), is driven not only by comorbidities like obesity and type 2 diabetes, but also by hypothyroidism. Independent of the systemic thyroid hormone levels, dysregulation of hepatic thyroid hormone signaling plays an important role in MASLD pathogenesis, with the only approved medication for MASH treatment, resmetirom, being a thyroid hormone receptor beta (*THRB*) agonist. While the effect of thyroid hormone signaling dysregulation on the hepatic metabolism has been investigated thoroughly there is little information on whether epigenetic regulations contribute to this dysregulation in MASLD. Therefore, the aim of this thesis was the investigation of epigenetic regulations on hepatic thyroid hormone signaling in MASLD.

Since the expression of *THRB* negatively correlates with the disease progression marker MASLD activity score (MAS) and since miRNAs have inhibiting effects on their target genes, miRNAs that potentially bind to *THRB* were identified. The expression of miRNAs and mRNAs potentially involved in the regulation of thyroid hormone action in the liver was measured in human and mouse liver tissue using qPCR. Verification of increased expression of potential *THRB* targeting miRNAs was performed in a cohort of obese individuals (BMI > 30 kg/m ^{2}) which was divided into a non-MASH group (n = 41, MAS ≤ 3) and MASH group (n = 27, MAS ≥ 4), as well as in multiple mouse models mimicking different stages of MASLD. Binding of miRNA to target mRNAs was verified using luciferase reporter assays, as well as RNA-interacting protein immunoprecipitation-sequencing. Furthermore, cell culture models were metabolically stimulated to induce a MASLD-like state in the cells and investigate the effect on the expression of thyroid hormone metabolism genes. Additionally, DNA methylation was measured at THRB and miRNA genes, to further investigate involvement of additional epigenetic regulators. Unfortunately, no suitable THRB antibody was available to verify the results of mRNA measurements on the protein level. To address this, plasmids were designed to identify tags, that when added to *THRB* do not interfere with thyroid hormone signaling.

miR-34a-5p was identified to be increased in MASLD and was predicted to bind not only *THRB* but also the thyroid hormone receptor alpha, the thyroid hormone activating enzyme *DIO1* as well as the thyroid hormone transporters *SLC10A1* and *SCL16A2*. The binding to THRB and *DIO1* was verified and induced overexpression of miR-34a-5p reduced the levels of *THRB* regulated genes after stimulation with thyroid hormones. Cell culture experiments further showed induction of miR-34a-5p by stimulation with fatty acids. Interestingly, the results of the overexpression of miR-34a-5p on potential target genes could also be induced by stimulation with fructose and insulin without miR-34a-5p involvement. Repression of thyroid hormone signaling through miR-34a-5p, reducing the expression of *THRB* as well as *DIO1* which reduces the amount of available active thyroid hormone further, is exacerbated by increased DNA methylation in the *THRB* gene, which negatively correlates with *THRB* expression. Finally, treatment of high-fat diet fed mice with metformin reduced the expression level of miR-34a-5p. This reduced dysregulation of the miRNA could potentially recover *THRB* expression and signaling and might also be of use to patients unresponsive to resmetirom due to low *THRB* levels.

2. Zusammenfassung

Metabolische Dysfunktions-assoziierte Steatotische Lebererkrankung (MASLD engl. *Metabolic dysfunction-associated steatotic liver disease*) betrifft 30% der globalen Population mit steigenden Zahlen und stellt eine Bedrohung für die globale Gesundheit und Gesundheitssysteme dar. Die Entstehung von MASLD und dem schwerwiegenderen Stadium Metabolische Dysfunktions-assoziierte Steatohepatitis (MASH, engl. *metabolic dysfunction-associated steatohepatitis*), wird nicht nur durch Komorbiditäten wie Adipositas und Typ 2 Diabetes vorangetrieben, sondern auch durch Hypothyreose. Unabhängig von den systemischen Schilddrüsenhormonleveln, spielt die Dysregulation des Schilddrüsensignalweges in der Leber eine wichtige Rolle in der MASLD Pathogenese. Tatsächlich ist das einzige zugelassene Medikament für die Behandlung vom MASH, Resmetirom, ein Schilddrüsenhormonrezeptor Beta (*THRB*) Agonist. Obwohl die Auswirkung der Störung des Schilddrüsenhormonsignalweges auf den Lebermetabolismus umfassend untersucht und bewiesen wurde, gibt es wenig Informationen über den Einfluss der epigenetischen Regulierung auf den gestörten Lebermetabolismus in MASLD.

Da die Expression von *THRB* negativ mit dem MASLD Krankheitsverlaufsmarker MASLD Aktivitätsscore (MAS engl. *MASLD activity score*) korreliert und miRNAs einen inhibierenden Effekt auf ihre Zielgene haben, wurden miRNAs identifiziert, die potentiell THRB binden. Die Expression von potentiell in die Regulation des Schilddrüsenhormonwirkung involvierten miRNAs und mRNAs wurde in Lebergewebe mittels qPCR ermittelt. Die erhöhte Expression der potentiell THRB-bindenden miRNAs wurde in einer Kohorte aus Individuen mit Adipositas (BMI > 30 kg/m ^{2}), welche in die Gruppen non-MASH (n = 41, MAS $\leq$ 3) und MASH (n = 27, MAS $\geq$ 4) eingeteilt wurden, sowie in mehreren Mausmodellen, die unterschiedliche MASLD-Stadien imitieren, untersucht. Die Bindung zwischen miRNA und Zielgen wurde mittels Luciferase-Reporter-Assays und RNA-Protein-Interaktion Immunpräzipitation Sequenzierung nachgewiesen. Darüber hinaus wurden verschiedene Zellkulturmodelle metabolisch stimuliert, um MASLD ähnliche Zustände zu imitieren und der Effekt auf die Expression der Gene des Schilddrüsenhormonsignalweges gemessen. Zusätzlich wurde die DNA Methylierung der *THRB* und miRNA Gene gemessen, um die Relevanz weiterer epigenetischer Mechanismen zu untersuchen. Da es keine *THRB*-Antikörper gibt, welche die Proteinexpression zuverlässig nachweisen, wurden Plasmide konzipiert, um Tags zu identifizieren, welche die *THRB* Funktion nicht stören, sodass mRNA und Proteinlevel verglichen werden können.

Die Überexpression der miRNA miR-34-5p in MASLD wurde bestätigt und die Bindung der miRNA zu *THRB*, dem Schilddrüsenhormonrezeptor Alpha, dem Schilddrüsenhormon-aktivierende Enzym *DIO1* und den Schilddrüsenhormontransportern *SLC10A1* und *SLC16A2* prognostiziert. Die Bindung an *THRB* und *DIO1* konnte nachgewiesen werden und die induzierte Überexpression von miR-34a-5p führte zu einer reduzierten Expression von *THRB*-regulierten Genen nach Stimulation mit Schilddrüsenhormonen. Weitere Zellkulturexperimente zeigten, dass die Expression der miR-34a-5p durch Stimulation mit Fettsäuren induziert werden kann. Interessanterweise konnte derselbe Effekt der Überexpression von miR-34a-5p auf Gene des Schilddrüsenhormonsignalweges ohne Zutun von miR-34a-5p durch Stimulierung der Zellen mit Fructose und Insulin erzielt werden. Die Unterdrückung des Schilddrüsenhormonsignalweges durch die Bindung von miR-34a-5p an *THRB* und *DIO1* wird durch die vermehrte DNA Methylierung am *THRB* Gen, welches negativ mit der *THRB* Expression korreliert, verstärkt. Abschließend führt die Behandlung von Mäusen, die mit einer Diät mit hohem Fettgehalt gefüttert wurden, mit Metformin zu einer Reduzierung der miR-34a-5p Expression. Diese reduzierte Expression der dysregulierenden miRNA könnte potentiell einen positiven Effekt auf die *THRB* Expression und den Schilddrüsenhormonsignalweg haben. Dies könnte die Wirkung von

Resmetirom verstärken und Patienten helfen, die durch eine geringe *THRB* Expression nicht auf die Behandlung mit Resmetirom ansprechen.

3. Introduction

3.1. The Liver – a metabolic organ

The liver is a central organ of metabolic homeostasis and reacts to episodes of feeding and fasting by regulation of biochemical pathways. Hepatocytes are not only the main epithelial cells in the liver, but also possess a nutrient-sensing system that contributes to the metabolism regulating role of the liver [1,2]. Cholangiocytes, the epithelial cells of the bile duct, are the second most abundant epithelial cell population of the liver. Stellate cells regulate collagen organization and production and therefore contribute to fibrosis development after liver injury. Additionally, the liver contains macrophages, called Kupffer cells, that perform anti- and pro-inflammatory roles [2]. Apart from the Kupffer cells, the cells of the liver are organized in hexagonal lobules with the central vein in the middle surrounded by hepatocytes and the portal triads that contain the portal vein, the hepatic artery and the bile duct at the vertices [2]. Hepatocytes are distinguished into three different zones, depending on their location in the lobule. Located at the portal vein, they are referred to as periportal, followed by the intermediate hepatocytes and the ones at the central vein as pericentral [3]. Considering the differences in nutrient and oxygen supply in the different zones, the cells show heterogeneity in their metabolic activity, with periportal hepatocytes being more involved in β-oxidation and gluconeogenesis and pericentral hepatocytes in glycolysis and lipogenesis [3,4]. This zonation can be disturbed in metabolic diseases like metabolic dysfunction-associated steatotic liver disease (MASLD) [3].

Glucose metabolism

The glucose uptake and release in the liver is conducted primarily through glucose transporter GLUT2 and depends on the energy state of the body [5,6]. In the fed state, the liver stores glucose as glycogen, while under fasting conditions glucose is mobilized from glycogen storage [7]. Therefore, the liver plays an essential role in the maintenance of the blood glucose levels which is tightly regulated by insulin and glucagon [5]. High insulin levels under fed conditions stimulate glycolysis and lipogenesis but suppress gluconeogenesis. Glucagon counteracts insulin actions and is increased under fasting conditions. After the uptake the glucose is phosphorylated by the enzyme glucokinase to glucose-6-phosphate and is either used for glycogen synthesis or glycolysis depending on the energy status of the organism. Glycolysis is limited by the glucokinase, liver pyruvate kinase and 6-phosphofructo-1 kinase. The nascent product, pyruvate, can be used for the generation of ATP through complete oxidation in the citric acid cycle or used for *de novo* lipogenesis [5]. On the transcriptional level, glycolysis is regulated by carbohydrate-response element-binding protein (ChREBP) and sterol regulatory element binding protein 1c (SREBP-1c) that are also responsible for the regulation of fatty acid biosynthesis [8]. Under fasting conditions, glucose is primarily generated though glycogenolysis, but can additionally be produced by gluconeogenesis from 3-carbon precursors. The rate limiting steps of gluconeogenesis are performed by phosphoenolpyruvate carboxy kinase (PEPCK) and glucose-6-phosphatase (G6PC) which are activated under fasting conditions [8,9].

Lipid metabolism

Similar to the glucose metabolism, the lipid metabolism is also regulated by metabolic hormones, for example by the regulation of lipogenesis via the transcription factors SREBP-1c and liver X receptor (LXR) [10]. Excess glucose is converted into lipids in the liver using *de novo* lipogenesis (DNL). The pyruvate generated during glycolysis is processed amongst others by acetyl-CoA carboxylase (ACACA) and fatty acid synthase (FASN) resulting in palmitic acid, a component of triglycerides (TG) [5]. TGs are either incorporated in to very low density lipoproteins (VLDL) and secreted into the blood or stored within the liver as lipid droplets [11]. Additionally, fatty acids are transported to the

hepatocytes via the bloodstream mainly through the fatty acid transport protein 2 (FATP2), FATP4, FATP5 and CD36 and are derived from food as well as from adipose tissue [12–14]. The liver stores fatty acids as TGs to prevent lipotoxicity [15]. To release stored TGs they are degraded by lipolysis, the hydrolysis of TG, resulting in the release of fatty acids and glycerol, which is conducted by lipases [11]. The degradation of short, medium and long chained fatty acids is conducted by β-oxidation and takes place in the mitochondria while very long chained fatty acids are oxidized in peroxisomes [10].

Alternatively, fatty acids are used for the production of cholesterol, which is an important component of membranes but also needed for the production of bile acid. While SREBP-1c regulates lipogenesis, Sterol regulatory element-binding protein 2 (SREBP-2) controls the uptake and biogenesis of cholesterol in the liver through transcriptional activation of genes like low density lipoprotein receptor (LDLR), 3-hydroxy-3-methylglutaryl-coenzyme A reductase (HMGCR), hydroxy-3-methylglutaryl-coenzyme A synthase 1 (HMGCS1), and farnesyl diphosphate synthase (FDPS) [8].

3.2. Metabolic dysfunction-associated steatotic liver disease

According to the WHO noncommunicable diseases (NCD) account for 41 million death s yearly worldwide, which translates to 74% of all deaths. The main types of chronic diseases are cardiovascular diseases, cancer, respiratory diseases and diabetes. While there are multiple risk factors and environmental contributors, metabolic risk factors play a big role in disease development. The metabolic risk factors are hypertension, overweight and obesity, hyperglycemia and hyperlipidemia [16]. These risk factors correspond to the metabolic syndrome which needs to meet at least three of the risk factors for diagnosis [17]. Metabolic dysfunction-associated steatotic liver disease (MASLD) is considered the liver manifestation of the metabolic syndrome [18]. Affecting more than 30% of the global population and with increasing prevalence in adults and children MASLD has developed into a serous worldwide health concern [19,20]. MASLD is defined as the accumulation of fatty acids in more than 5% of hepatocytes in the absence of infectious diseases, limited consumption of alcohol and no evidence of hepatic injury [21]. MASLD is the new term for the formerly known non-alcoholic fatty liver disease (NALFD). The change in nomenclature included an adjustment in diagnosis criteria. Patients now need to present with an additional symptom of metabolic syndrome to be diagnosed as MASLD, emphasizing the connection between MASLD and metabolic syndrome [22]. Despite the change in criteria, analysis of NAFLD cohorts show that over 97% of NAFLD patients also qualify for MASLD [23] and are therefore used synonymously throughout this thesis.

While MASLD manifests in the liver it is a systemic disease that involves many other organs. The hallmarks of MASLD development are the accumulation of fatty acids in hepatocytes, which is often accompanied by a dysfunction of the adipose tissue and is known as metabolic dysfunction-associated steatotic liver (MASL). In 10-25 % of MASL patients the disease progresses further into metabolic dysfunction-associated steatohepatitis (MASH) [24]. In this case the liver is inflamed, the injured hepatocytes increase in size (ballooning) and the liver tissue shows first signs of scaring (fibrosis) [25] with increased production of extracellular matrix, which can later develop into cirrhosis (Figure 1) and hepatocellular carcinoma (HCC) [20]. At this stage of disease patient often suffer from dysbiosis, a disruption of healthy gut microbiome which has a negative effect on the liver and vice versa [26]. To determine the severity of the disease the MASLD activity score (MAS) is used. Using histology of liver biopsies the degree of steatosis, ballooning hepatocytes, fibrosis and inflammation are determined [21]. While the MAS is the gold standard of diagnosis, biopsies are a risky and not widely accessible procedure. Instead the liver markers alanine aminotransferase (ALT) and aspartate

aminotransferase (AST) are often used to determine liver health and upon suspicion of MASLD fibro scans and ultrasounds are used to determine fibrosis and steatosis respectively [25].

MASLD development and progression is associated with obesity and type 2 diabetes (T2D), which are associated with a westernized diet high in processed foods, refined carbohydrates, meats, dairy products and soft drinks. Indeed, patients with MASLD consume more calories daily compared to healthy control [27,28] and three times as much fructose [29]. 90% of patients with obesity and 70% of overweight people have MASLD while the prevalence of MASLD in patients with T2D is at 60% [20]. Despite the tight association of obesity and MASLD it can occur in people with an BMI below 25 kg/m2. The prevalence of lean MASLD varies strongly between ethnicities and can be partially attributed to genetic variations. Polymorphisms in Patatin-like phospholipase domain containing protein 3 (PNPLA3), a TG lipase, as well as in transmembrane 6 superfamily member 2 (TM6SF2), resulting in less secretion of VLDL from the liver [30], are risk factor for MASLD development though studies are not conclusive regarding MASH and fibrosis risk [20]. An additional well established risk factor is systemic hypothyroidism [31], but also a dysregulation of thyroid hormone signaling in the liver has been associated with disease severity [32].

3.2.1. Molecular mechanisms of MASLD pathogenesis

Steatosis and lipotoxicity

The first stage of MASLD is steatosis, the accumulation of lipids in hepatocytes. Under normal conditions hepatocytes balance lipid synthesis with lipid degradation and export depending on hormone and energy levels, however this balance is disrupted in MASLD. This disruption can be caused by excess fructose consumption, which induces insulin resistance and DNL increasing enzyme levels [33–35] and reduces beta oxidation. Patients with MASLD show increase of DNL compared to healthy controls [36]. While accumulation of TGs is not toxic, the liver lipid profile changes in MASLD with an increase in diacylglycerol, ceramides, free cholesterol and phospholipids which are contributing to lipotoxicity [37,38]. The accumulation of cholesterol is further aggravated by a reduction in cholesterol excretion from hepatocytes in bile, as either cholesterol or bile acid [39]. Lipotoxicity is the accumulation of toxic lipids, which results in organelle dysfunction and cell injury or death. The lipid overload leads to a stress response in the endoplasmic reticulum (ER). This triggers a protein unfolding response, that is used to re-establish the homeostasis of the ER, but under prolonged activity induces apoptotic pathways [40]. Excess of toxic lipids also stimulates the release of extracellular vesicles, which enables the transport of inflammation, fibrosis and angiogenesis inducing compounds throughout the liver and organism [41]. The increase in fatty acids also affects the mitochondria, in early stages of MASH the mitochondria show an increase in β-oxidation, which in turn results in an increased production of reactive oxygen species (ROS) [42]. In later stages mitochondrial function is impaired and oxidative stress increases. The damage of ROS on lipids, proteins and DNA impair organelle and cell function, with evidence suggesting an impact on inflammation, insulin sensitivity and the gut microbiome [33,43–45]

Insulin resistance

The development of insulin resistance is a driving factor of MASLD progression. During insulin resistance the liver becomes resistant to the effects of insulin on the glucose metabolism, resulting in an increase in glucose production. Simultaneously, the effect of insulin on the lipid metabolism remains the same, though the increase in insulin expression consequently increases the production of lipids, leading to steatosis [46]. Additionally hyperinsulinemia promotes lipolysis and the release of fatty acids from adipose tissue [47]. The high amount of insulin also stimulates the release of pro-inflammatory cytokines from the adipose tissue like tumor necrosis factor α (TNFα) [48]. Insulin

resistance and T2D in turn induce a dysfunction of adipocytes, disrupting their ability to store lipids [49], which increases circulating free fatty acids (FFA) that are then taken up by the liver. Dysfunctional adipose tissue also reduces excretion of adiponectin, which is insulin -sensitizing and has hepatoprotective effects by reducing DNL, hepatic FFA intake, gluconeogenesis and induction of beta oxidation and is anti-inflammatory [50]. This reduction of anti-inflammatory signals is accompanied by an increased secretion of pro-inflammatory adipocytokines [19].

Dysbiosis

The gut-liver-axis also plays an important role in MALSD pathogenesis. Microbial compounds and metabolites circulate from the gut throughout the body, the majority is transported to the liver via the portal vein. This gut-liver axis can influence liver function [51]. Tissue damaging diets like a long term high-fat diet can damage the gut barrier, which leads to an accumulation of microbiota derived substances in the liver [26]. Chronic liver diseases are associated with small intestine bacterial overgrowth syndrome, which due to the increase of microbial-associated molecular patterns (MAMPs) and pathogen-associated molecular patterns (PAMPs) alters the liver immune microenvironment and can lead to chronic inflammation [52]. Overabundance of *E.coli* derived lipopolysaccharides (LPS) has been reported in patients with MASLD [53]. LPS are well studied MAMPs and PAMPs. They bind to toll-like receptor 4 (TLR-4) activating nuclear factor kappa B subunit 1 (NFκB) mediated inflammation, accelerating MASH and fibrosis progression [54]. The other way around, the liver influences the gut by producing and releasing bile acids and antimicrobial molecules into the biliary tract which reach the gut and contribute to eubiosis [26]. While circulating the liver bile acids act as signaling molecules binding to nuclear receptors like FXR (farnesoid X receptor) and therefore, regulating glucose and lipid metabolism as well as the synthesis of hepatic bile acids [26].

Inflammation

Due to the livers exposure to blood-borne pathogens it is one of the bodies first line of defense against external disease-causing agents and is therefore, well equipped to deal with inflammation. While hepatocytes are not innate immune cells, they do carry out immune functions under stressed conditions [55]. Hepatocytes detect pathogens and metabolic molecules via pattern recognition receptors like TLRs, inducing the production of innate immunity proteins [56]. The first cells of the innate immune system reacting to metabolic disturbances in MASLD are Kupffer cells. Generally macrophages can be categorized into two different types M1 and M2 cells, with M1 generally considered to be pro-inflammatory and M2 immunoregulating, with involvement in tissue remodeling [57]. This distinction does not hold true for macrophages in the liver, as Kupffer cells show simultaneous expression of M1 and M2 markers [58]. Induction of the more pro-inflammatory M1 expression is initiated by LPS, known PAMPs and MAMPs. This leads to the expression of inflammatory cytokines like TNF-α and IL-12. The resulting local inflammation in turn leads to hepatocyte injury, which is visible in histology as enlarged hepatocytes with granular cytoplasm (hepatocyte ballooning), and the release of damage-associated molecular patterns (DAMPs). DAMPs further activate the Kupffer cells, leading to a circle of inflammation [59]. Indeed, patients with MASH not only show higher levels of inflammation marker TNFα in the liver, but also in adipose tissue [60] as well as increased NFκB levels [61]. Additionally Kupffer cells can be activated by lipid overload, which is observed during MASLD and increases the inflammatory response to LPS [62]. The activation of Kupffer cells not only contributes to the inflammation, but also to insulin resistance and the development of fibrosis [63]. In addition to Kupffer cells, monocytes are recruited into the liver, where they differentiate into monocyte-derived macrophages with a more pro-inflammatory profile compared to Kupffer cells [64]. Another type of immune cells present in the liver are dendritic cells, which are located around the central veins. They

are antigen-presenting cells and infiltrate the liver under MASH conditions, though their role in MASH is not fully understood, with studies providing contradictory data [59]. Neutrophils also infiltrate the liver of MASH patients, with the severity of neutrophil infiltration being associated with disease progression [55]. They contribute to the activation of Kupffer cells and therefore, play an important role in the initiation of liver inflammation. Studies have shown that activated neutrophils release peroxidases, like myeloperoxidase, that induce liver damage, through mitochondrial injury which causes hepatocyte death but also the activation of hepatic stellate cells, resulting in fibrosis [55].

Fibrosis

A consequence of chronic inflammation is the development of fibrosis, the excess production of extracellular matrix without degradation. In the liver hepatic stellate cells are mainly responsible for the production and degradation of extracellular matrix. As described above, multiple aspects of MASLD play a role in the activation of hepatic stellate cells and the induction of fibrosis. Several studies have shown that fibrosis is the main indicator for the severity of disease progression and mortality [65]. During MASLD the amount of extracellular matrix not only increases, but the composition changes, compared to healthy liver tissue. This results in an extracellular matrix that is more resistant to degradation and therefore, contributes to the increase of fibrosis in MASH. While the role of the extracellular matrix in healthy liver is to provide structure to the organ and control proliferation and cell survival [65,66], increased deposition of type-I collagen contributes to portal hypertension and the reduction of functional liver tissue. While fibrosis can be reversed in MASH patients, there is no current evidence that cirrhosis caused by MASLD can be reversed. Fibrosis and chronic injury can lead to the development of cirrhosis, that is defined by the fibrosis caused portal hypertension, as well as abnormal blood flow and changes in the liver structure [67].

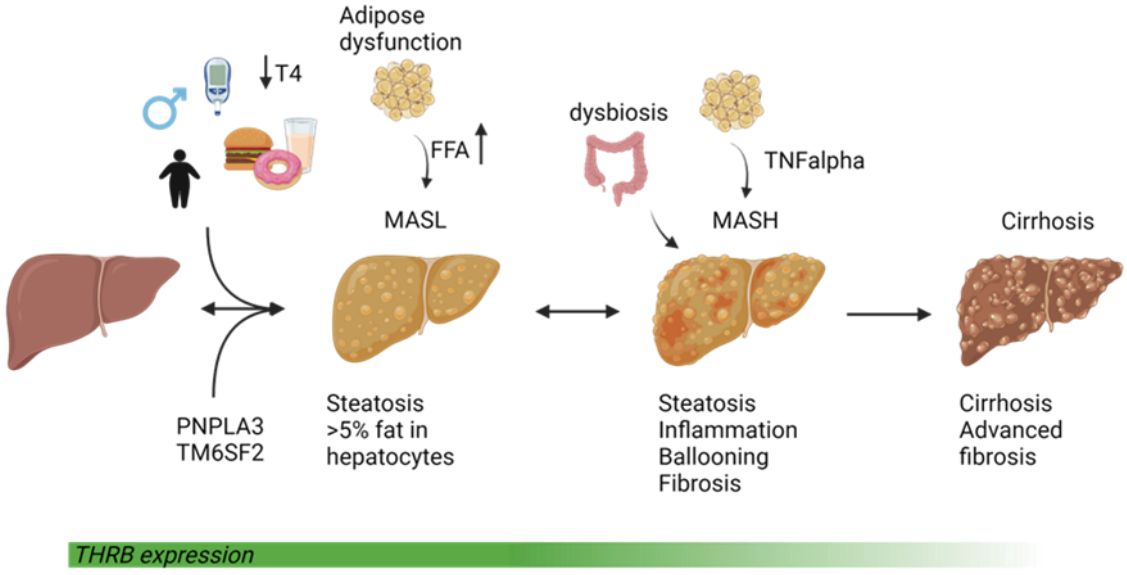

Figure 1. Metabolic dysfunction-associated steatotic liver disease (MASLD) development and progression. Environmental risk factors like a diet high in refined carbohydrates and fructose, obesity and type 2 diabetes, but also hypothyroidism and genetic factors like polymorphisms in Patatin-like phospholipase domain containing protein 3 (PNPLA3) and transmembrane 6 superfamily member 2 (TM6SF2) can induce development and progression of MASLD. The first stage metabolic dysfunction-associated steatotic liver (MASL) shows an increased influx of free fatty acids (FFA) from diet and dysregulated adipose tissue into the liver and is defined as at least an accumulation of fat in 5% of

hepatocytes. The disease can progress further into metabolic dysfunction-associated steatohepatitis (MASH) in which hepatocyte injury and inflammation are aggravated by dysbiosis and proinflammatory adipokines like tumor necrosis factor alpha (TNFα). Further dysregulation of the liver can lead to cirrhosis and hepatocellular carcinoma.

Considering the complexity of MASLD it is not surprising that the treatment is difficult. First line therapy is the reduction of weight in overweight or obese individuals and an increase of physical activity together with treatment of underlying metabolic diseases like hypertension or T2D [68]. In concert with the already mentioned disruption of thyroid hormone (TH) metabolism in MASLD, studies have shown an improvement of the disease after treatment with TH [69]. Indeed, the thyroid hormone receptor beta (TRβ) agonist resmetirom is the first drug designed to specifically treat MASLD and has been approved by the United Stated Food and Drug Administration (FDA) recently [70].

3.2.2. Mouse and cell models of MASLD

To investigate MASLD development, progression and the development of potential treatments, different *in vivo* and *in vitro* models are utilized. Due to little standardization between models there is a huge variety of different methods to induce MASLD in different model organisms. Since this thesis focuses on mouse and cell culture models other animal models are not included in this introduction.

3.2.2.1. Mouse models

MASLD mouse models can be roughly categorized into genetic modifications, dietary modifications and models treated with chemicals. Some models utilize more than one method. While no available model is able to completely mimic all aspects of human MASLD, different models imitate different aspects and are used accordingly, depending on the research question. In Table 1 different models are compared for their ability to mimic aspects of metabolic syndrome (obesity, insulin resistance, dyslipidemia), development of MASH (hepatocyte ballooning, steatosis, fibrosis, inflammation) and increase of liver markers AST and ALT. There is little standardization within the models considering diet composition and length of treatment, resulting varying phenotypes. Similarly, the susceptibility of the treatment varies between mouse strains [71]. The main advantage of animal models compared to cell culture is that the animal model has the potential to mimic the systemic disease throughout the different organs, while cell models are limited to only a few cell types in co-culture. Still not all animal models suitably mimic the whole phenotype of MASLD. While the differing models are suitable to mimic different aspects of MASLD in mice, meta-analysis have shown that there is little overlap between gene expression profiles of liver tissues from different mouse models and patients with MASLD [72]. Vacca *et al.* propose an MASLD human proximity score (MHPS) ranking different models concerning their metabolic relevance to induce MASH and identify models with profiles relevant to the human disease [73]. The proposed MHPS ranks diets according to body weight, triglycerides, cholesterol, liver to body weight ratio, ALT and AST, MAS, fibrosis and transcriptomics.

Dietary models

According to the MHPS the western diet (WD) containing cholesterol mimics the gene expression and histology comparable to human progression with obesity and dyslipidemias. Nevertheless, there is a high variance between experiments, due to differences in diet composition and duration of the experiment [73]. Meanwhile choline deficient models (CDD, CD-HFD, CDHFHCD) despite developing fibrosis did not perform well overall due to low metabolic ranking. And while the HFD

model shows the expected increase in body weight, insulin resistance and hyperlipidemia and therefore, mimics the human phenotype quite well [74]. The reduction of the choline content of a high-fat diet (CD-HFD) impairs hepatic lipid metabolism, reducing VLDL secretion which leads to fat accumulation, cell death, oxidative stress and inflammation with fibrosis. CD-HFD animals do not show the increase in body weight that is expected for a HFD and deviates from the human phenotype [74]. The additional lack of methionine in the MCDD model leads to inflammation and early development of fibrosis with increase in AST and ALT. MCDD mice show a fast onset of MASH phenotype in the liver but no other phenotypes like insulin resistance and dyslipidemia, similar to some CD-HFD mice they lose body weight [74]. MCDD treated mice are only suitable to investigate MASLD within the liver. With a loss of body weight and a lack of insulin resistance this model does not mimic the metabolic syndrome, a necessity diagnosis criteria for MASLD in humans. Meanwhile, high-fructose diet (HFrD) fed mice develop the metabolic syndrome phenotype but do not progress further into MASH without additional stimulation with a high fat (HFrHFD) or a diet with added high fat and cholesterol (HFrHFHCD) [71,74,75]. Similarly, the American lifestyle diet (AMLD) uses a HFD or a WD content with refined sugars in the drinking water to mimic the conditions of MASLD development in humans. Depending on diet composition and duration of treatment the AMLD mimics the majority of MASLD parameters with steatosis detection as early as 8 weeks, but inflammation only after 16 weeks [73].

Chemical models

To reduce the time of disease progression and to induce more severe phenotypes chemicals are utilized in some animal models. Streptozotocin (STZ) is used to induce type 1 and type 2 diabetes. Low doses of STZ combined with a HFD induce insulin resistance, while treatment with a high dose of STZ destroys pancreatic β-cells leading to the development of type 2 diabetes [76,77]. In the STAM diet, a high fat diet paired with STZ the MASLD progression is sped up greatly. The mice present steatosis after 7 weeks and show all histological signs of MASH, before development of cirrhosis after 12 weeks and HCC after 20 [71]. While the use of STZ leads to a similar histological pattern in mice compared to diabetic MASLD patients, the molecular mechanisms differ and the use of STZ induces insulin deficiency rather than insulin resistance [78]. Another chemical used in MASLD models is carbon tetrachloride (CCl_4), which induces liver injury, fibrosis and cirrhosis. Therefore, animals treated only with CCl_4 are commonly used as a fibrose control, but not as a separate MASLD model. The repeated administration of CCl_4 combined with a HFD triggers chronic oxidative stress and inflammation in the liver before causing fibrosis and also shows histologic similarities to human MASLD patients [79]. However, the STAM treated mice show a reduction of body and liver weight, indicating chronic damage [79]. Similarly, other studies observed less weight gain in HFD mice treated with STZ or CCl_4 than in mice only treated with HFD [73].

Genetic models

Mice with a deficiency in either leptin (ob/ob) or the leptin receptor (db/db) develop obesity under a normal chow diet. The lack of leptin signaling results in a hyperphagic state and the mice develop insulin resistance, dyslipidemia and steatosis [80]. While these mice develop severe hepatosteatosis within 12 weeks, they do not develop MASH without further stimulation by either a diet or chemicals [74]. Therefore, leptin signaling deficient mice present a model for the early stages of MASLD, though the metabolic changes caused by the lack of leptin signaling should be taken into consideration.

Table 1. Comparison of different MASLD mouse models according to their diet and use of chemicals, as well as the resulting phenotype

Model	Mouse strain[1]	Diet	Chemicals	Metabolic syndrome Obesity (1) Insulin resistance (2) Dyslipidemia (3)	MASH Histology Hepatocyte ballooning (1) Steatosis (2) Fibrosis (3) Inflammation (4)	ALT (1) AST (2)	Advantage/ Disadvantage	Reference
High fat (HFD)	C57BL/6J	45-75% fat	NA	(1) + (2) + (3) +	(1) -/+ (2) + (3) + (4) +	(1) + (2) +	Dysbiosis after one week of HFD	[71,73–75,81–84]
High fructose (HFrD)		Fructose supplemented drinking water	NA	(1) – (2) +	(2) + (3) – (4) +		Metabolic syndrome, but no progression to MASH phenotype	[71]
High fructose high fat (HFrHFD)	C57BL/6J	Fructose supplemented drinking water HFD	NA	(1) +	(2) + (3) + (4) +	(1) -		[74,75]

[1] No entry indicates no specification of strain

+ indicates presence or increase of phenotype or disease marker, - indicates lack of phenotype or decrease of marker, blank indicates no information, NA not applicable.

Model	Mouse strain[1]	Diet	Chemicals	Metabolic syndrome Obesity (1) Insulin resistance (2) Dyslipidemia (3)	MASH Histology Hepatocyte ballooning (1) Steatosis (2) Fibrosis (3) Inflammation (4)	ALT (1) AST (2)	Advantage/ Disadvantage	Reference
HFrHF + high cholesterol (HFrHFHCD)	C57BL/6J	40% fat 40 g/l fructose 0.2% cholesterol	NA	(2) +	(1) + (2) + (3) + (4) +			[75]
Western diet (WD) (atherogenic)		0.2-2% cholesterol 0.5% cholic acid	NA	(1) + (2) +/- (3) +	(1) +/- (2) + (3) +/- (4) +/-	(1) + (2) +	High variance in disease severity between experiments	[73,74]
American lifestyle (AMLD)		HFD or WD supplemented with refined sugar in drinking water	NA	(1) - (3) +	(1) +/- (2) + (3) +/- (4) +/-	(1) + (2) +		[73]

Model	Mouse strain[1]	Diet	Chemicals	Metabolic syndrome Obesity (1) Insulin resistance (2) Dyslipidemia (3)	MASH Histology Hepatocyte ballooning (1) Steatosis (2) Fibrosis (3) Inflammation (4)	ALT (1) AST (2)	Advantage/ Disadvantage	Reference
Methionine and choline deficient (MCDD)	C57BL/6J	40% sucrose 10% fat Deficient in methionine and choline	NA	(1) - (2) -	(1) + (2) + (3) + (4) +	(1) + (2) +	No metabolic syndrome, only suitable as intrahepatic model. Fast development of phenotype	[71,74,75]
Choline deficient (CDD)		Diet deficient in choline	NA	(1) - (2) - (3) -	(1) + (2) + (3) + (4) +	(1) + (2) +	Ballooning of hepatocytes only occurs after 8 weeks of treatment	[73,82]
Choline deficient-HFD (CD-HFD)		71% (45-75%) fat 11% carbohydrates 18% proteins With reduced choline	NA	(1) -/+ (2) +	(1) + (2) + (3) + (4) +	(1) + (2) +	Ballooning of hepatocytes only occurs after 8 weeks of treatment	[73,82]

Model	Mouse strain[1]	Diet	Chemicals	Metabolic syndrome Obesity (1) Insulin resistance (2) Dyslipidemia (3)	MASH Histology Hepatocyte ballooning (1) Steatosis (2) Fibrosis (3) Inflammation (4)	ALT (1) AST (2)	Advantage/ Disadvantage	Reference
CCl_4		NA	CCl_4	(1) - (2) -	(1) + (3) + (4) +	(1) + (2) +	Fibrosis control, not a MASLD model in itself	[73,74]
HFD CCl_4	C57BL/6J	HFD	CCl_4		(1) + (2) + (3) + (4) +	(1) + (2) +		[74,79]
HFD Streptozotocin (STAM)	C57BL/6J	HFD	Streptozotocin	(2) -	(1) + (2) + (3) + (4) +	(1) + (2) +	Development of cirrhosis and HCC, STZ induces insulin deficiency not insulin resistance	[71,74,78]

Model	Mouse strain[1]	Diet	Chemicals	Metabolic syndrome Obesity (1) Insulin resistance (2) Dyslipidemia (3)	MASH Histology Hepatocyte ballooning (1) Steatosis (2) Fibrosis (3) Inflammation (4)	ALT (1) AST (2)	Advantage/ Disadvantage	Reference
Lep^{ob}/Lep^{ob}	Lep^{ob}/Lep^{ob}	NA	NA	(1) + (2) + (3) +	(1) – (2) + (3) – (4) –/+		No spontaneous development of MASH, similar MASLD development to humans	[71,73,74,80]
$Lepr^{db}/Lepr^{db}$	$Lepr^{db}/Lepr^{db}$	NA	NA	(1) + (2) + (3) +	(2) + (3) – (4) +		No spontaneous development of MASH, similar MASLD development to humans	[71,73,74,80]

3.2.2.2. Human cell culture models

Besides mouse models, cell culture models are commonly used to ascertain liver toxicity of compounds and investigate cell signaling pathways. There are different complexity levels of cell culture, the easiest and most common one being 2D monoculture, culturing only one type of cell. To improve imitation of liver tissue 2D co-culture combines hepatocyte cell culture with other hepatic cells like stellate or Kupffer cells. 3D cultures of cells growing in spheroids both in mono and co-culture further increase the complexity and liver-likeness of the models. Lastly, body-on-a-chip models combine multiple cell culture organ models to mimic the exchange between different organs.

The gold standard for hepatocyte-like cells are primary human hepatocytes, which are derived from liver resections or tissue not usable for transplantation. While these cells express all hepatocyte typical enzymes and show a similar metabolic profile compared to *in vivo* hepatocytes they rapidly dedifferentiate within hours after plating, losing their hepatic function [85,86]. Co-cultures prevent dedifferentiation to an extent, though primary human hepatocytes are difficult to acquire and the high variance between cell donors proves to be problematic with poor reproducibility of results [87]. More readily available hepatocyte-like cell models are immortalized cancer cell lines HepG2 and Huh-7. HepG2 cells were derived from a hepatoblastoma of a 15 year old Caucasian male [88] while Huh-7 cells are from the hepatocellular carcinoma of a 57 year old Japanese male. While both cell lines originate from the liver their cancerous nature comes along with changes in their expression patterns compared to hepatocytes [89]. On the other hand, spheroids of HepG2 show a different expression pattern than monolayer HepG2 with hepatocyte-like morphology [90,91]. Meanwhile HepaRG cells are bipotent progenitor cells of hepatocytes and biliary cells, originating from a liver tumor with chronic hepatitis C [92]. After differentiation the cells show largely hepatocyte-like expression and can be used for studies of metabolism [89]. 3D co-culture of hepatic stellate cells and HepaRG are used as a fibrosis model [93]. Lastly human induced pluripotent stem cells are also used for differentiation into hepatocyte-like cells as they can be used in mono, co and 3D culture. The most complex type of cell culture is the body-on-a-chip model where multiple organ cell types are combined to simulate the interaction between organs in an organism [94]. This model tries to solve the main problem of cell culture models of being unable to simulate the situation in a complete organism with only one or two cell types. To induce a MASLD state in any of the aforementioned cell culture models, the cells can be challenged with metabolic stimulants. For example fatty acids with oleate and palmitate mixtures have been shown to indues steatosis as well as treatment with fructose [87,95]. Considering the advances made in *in vitro* techniques and when using the models conscious of their limitations cell culture models pose a valuable asset for MASLD research.

3.3. Thyroid hormone signaling

The thyroid hormones (TH) thyroxine (T_4) and to a lesser extent the active triiodothyronine (T_3), are produced in the thyroid gland, regulated by the hypothalamus-pituitary-thyroid (HPT) axis. The hypothalamus secretes the thyrotropin releasing hormone (TRH) which stimulates the pituitary into the secretion of thyroid stimulating hormone (TSH) which in turn regulates production of thyroid hormones in the thyroid gland. TH concentrations regulate the production of both TRH and TSH in a negative feedback loop [96] (Figure 2A). The THs are transported throughout the body using carrier proteins and delivered into various tissues by transporters with many of them regulating both influx and efflux dynamically [97,98]. In the liver monocarboxylate transporter 8 (MCT8), encoded by the *SLC16A2* gene) transports both T_3 and T_4 across the membranes of hepatocytes [98] similar to the Na^+/taurocholate cotransporting polypeptide (NTCP, encoded by the *SLC10A1* gene) [99]. The

concentration of thyroid hormones and their metabolites in tissues and circulation is regulated by the selenoproteins deiodinase type I-III (DIO) [100]. The different types of DIOs have varying capabilities in activating and deactivating TH products and show tissue specific expression, with DIO1 being the main DIO in the liver [96]. There are 4 different types of thyroid hormone action [101]. In type 1, also known as canonical action of TH, T_3 binds to thyroid hormone receptors (TR). The genome encodes two TR genes, thyroid hormone receptor alpha (*THRA*) and thyroid hormone receptor beta (*THRB*) with their splice variants [102]. While THs and their receptors fulfill a multitude of essential functions throughout the body in different tissues, in the liver the main expressed TR is the TRβ1 regulating liver metabolism [96]. TRs are part of the family of nuclear hormone receptors and bind to the thyroid hormone response element (TRE) either by building a homodimer or a heterodimer by binding to other nuclear receptors, mainly to retinoid X receptor (RXR) isoforms [102]. TRs bind to the DNA also in absence of TH, at both positive and negative enhancers, the binding of TH does not function as a switch but rather changes the ratio of corepressors and coactivators bound to the TR [103]. Alternatively, there is evidence of type 2 signaling of T_3-bound to TR binding to other DNA bound transcription factors, modulating their function, though more research is necessary [104]. Type 3 action describes protein-protein interactions between TR and for example phosphoinositide 3-kinase (PI3K) [105], meanwhile in type 4 action TH bind to other proteins than TRs like T_3 or T_4 binding to integrin αvβ3 [106] (Figure 2B). While thyroid hormones have a variety of functions throughout the body in different tissues, e.g. regulating heartbeat, brain development and skeletal function. Their main function in the liver is regulation of metabolism [96]. In hepatocytes TRs regulate lipid, glucose and cholesterol metabolism [107] with multiple of the presented modes of action.

Lipogenesis

In TRβs function as transcription factor, T_3 binding induces the expression of lipogenesis genes like fatty acid synthase (*FASN*), acetyl-CoA carboxylase (*ACACA*), malic enzyme (*ME*) and Thyroid hormone responsive (*THRSP*) and additionally regulates the expression of other transcription factors like sterol regulatory element-binding protein 1c (*SREBP1c*), liver X receptor (*LXR*) and carbohydrate-responsive element-binding protein (*ChREBP*) that also play a role in lipogenesis regulation. Meanwhile the synthesis of triglycerides is negatively regulated by TH, directly reducing the expression of apolipoprotein B100 (*APOB100*), stearoyl-CoA desaturase (*SCD1*), the main desaturase enzyme of triglyceride synthesis, though the regulation mechanism of SCD1 is not yet known [108]. In addition the binding of TRβ to PI3K results in the repression of the AKT/MAPK/AMPK cascade [105], indirectly regulating lipogenesis, gluconeogenesis and mitochondrial biogenesis [109].

Lipolysis and fatty acid oxidation

Thyroid hormones induce degradation of stored hepatic lipid droplets, containing triglycerides, using the autophagy-lysosomal pathway [110] by increasing the amount of autophagosomes [111]. Lipid degradation through β-oxidation mainly occurs in mitochondria, with TR acting on both nuclear and mitochondrial genome [112]. THs induce both the expression of the rate limiting enzyme of β-oxidation carnitine palmitoyltransferase 1 (*CPT1-Lα*) [113] and PPARγ co-activator 1α (*PGC-1α*) which induces mitochondrial biogenesis via the PGC-1α-NRF1-mTFA axis [112,114]. In addition, TRβ regulates mitochondrial gene expression indirectly by regulating the expression of estrogen-related receptor α (*ESRRA*) and *PGC-1α* [114]. Furthermore, T_3 acts directly in the mitochondria by binding to TRα and its isoforms [115], therefore, regulating mitophagy and O2 consumption [116]. The expression of other mitochondrial enzymes involved in β-oxidation, medium-chain acyl-CoA

dehydrogenase (*MCAD*) [117], pyruvate dehydrogenase kinase isoform 4 (*PDK4*) [118] and mitochondrial uncoupling protein 2 (*UCP2*) [119] are also all induced by TH action.

Cholesterol metabolism

TRβ indirectly regulates the rate limiting step of cholesterol synthesis by regulating Sterol regulatory element-binding protein 2 (*SREBP2*) expression which in turn regulates the expression of 3-hydroxy-3-methylglutaryl coenzyme A (*HMG-CoA*) [120], *SREBP2* also plays a role in endocytosis of cholesterol by regulating expression of LDLR [121]. Treatment of hypothyroid patients has shown a reduction of total cholesterol after treatment with TH [122] possibly by the reduction of proprotein convertase subtilisin/kexin type 9 (*PCSK9*), which is involved in LDLR degradation [123]. To maintain cholesterol homeostasis and prevent toxicity of excess cholesterol, reverse cholesterol transport is essential for cells [124]. The transport of cholesterol into the cell is facilitated by the TH induced apolipoprotein A1 (*APOA1*), scavenger receptor class B member 1 (*SRB1*) and cholesterol ester transfer protein (*CETP*) [125,126]. Conversion of cholesterol into bile acid is again regulated by TH induced expression of cholesterol 7 alpha-hydroxylase (*CYP7A1*) [127]. The last step of reverse cholesterol transport, the excretion of bile acids and cholesterol into the bile [124] is facilitated by the ATP-binding cassette transporters subfamily G member 5 and member 8 [128]. Their expression is regulated by LXRs and therefore, indirectly by THs [129].

Glucose metabolism

THs induce gluconeogenesis by regulation of PEPCK [130] and G6PC [131]. Additionally the regulation of PDK4, that already plays a role in lipid metabolism, leads to an indirect inhibition of pyruvate dehydrogenase (PDH) and thereby prevention of glycolysis [132]. THs have also been proposed to stimulate sirtuin 1 (SIRT1) expression [133], which in turn regulates cholesterol, lipid and glucose metabolism as well as mitochondrial activity [134]. Additionally, SIRT1 directly binds to TRβ as a coactivator [131] modulating TRβ activity and influencing insulin signaling through FOXO1 [135]. Furthermore, TRβ induces expression of ChREBP, which in the presence of insulin induces hepatic glucose production [136].

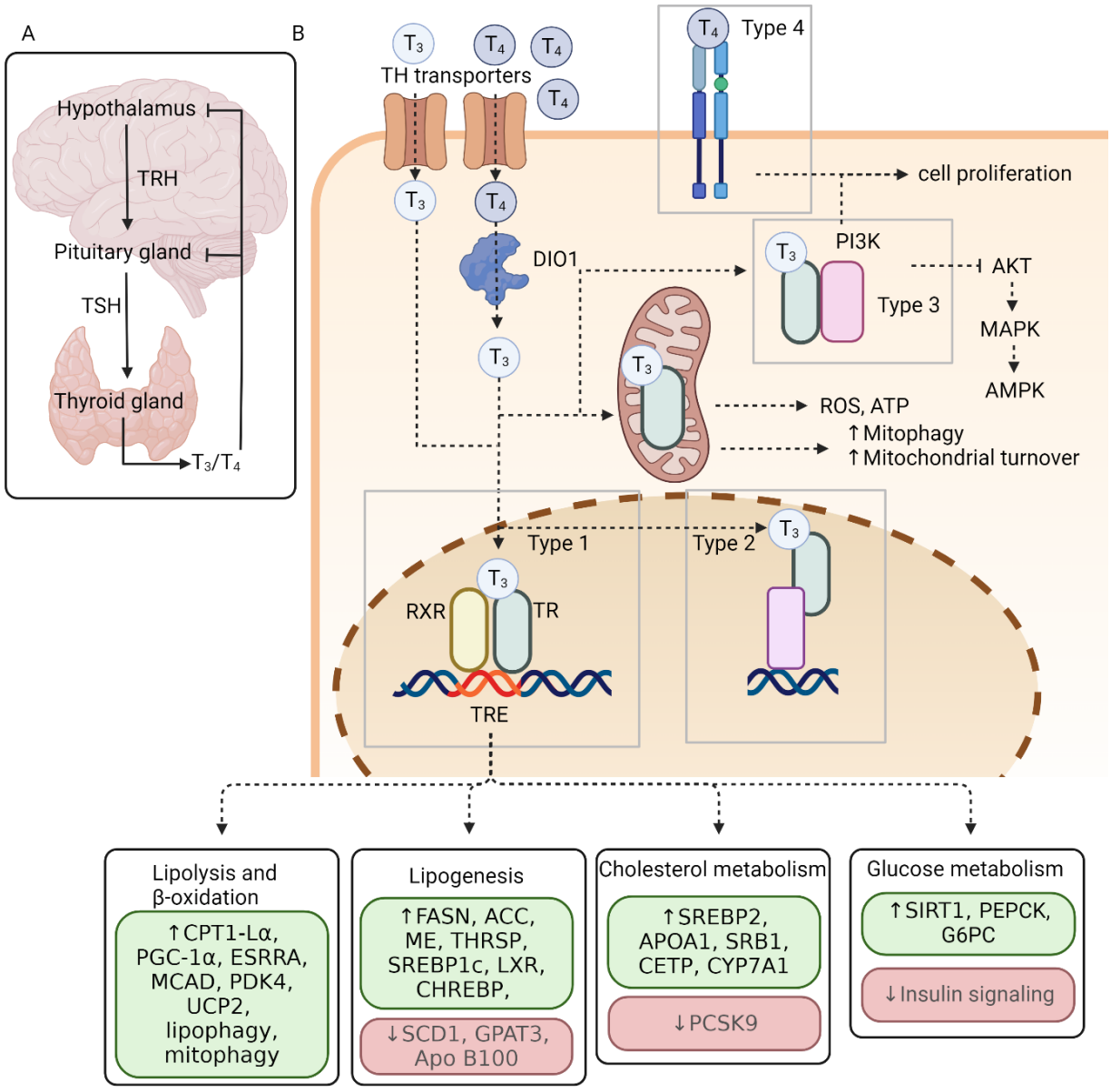

Figure 2. Thyroid hormone receptor beta signaling. A) Thyrotropin releasing hormone (TRH) is produced in the hypothalamus stimulating the release of thyroid stimulating hormone (TSH) from the pituitary. TSH in turn induces thyroid hormone production and secretion in the thyroid gland. The production of both TRH and TSH are negatively regulated by the circulating T_3 and T_4 concentration. B) Thyroid hormones (TH) are transported into the hepatocyte via transporters. Type 1: The active T_3 can directly bind to the thyroid hormone receptor beta (TRβ) while the inactive T_4 has to be transformed into T_3 by the deiodinase type I (DIO1). After activation by DIO1 the T_3 can bind to it's nuclear receptor. TRβ binds to the DNA at a thyroid hormone response element (TRE) together with another nuclear receptor, either as homodimer or with other receptors mainly RXRs. Upon T_3 binding the ratio of bound coactivators and corepressors changes, leading to a change in gene expression. TRβ regulates gene expression of lipid metabolism, both catabolism and anabolism directly on the genomic level. Similarly TRβ regulated cholesterol metabolism including synthesis, uptake and transport as well as gluconeogenesis, influencing insulin signaling. The regulation of transcription factors like ESRRA indirectly regulates further gene expression, influencing mitochondrial health. T_3 is also transported into the mitochondria binding to TRα and its isoforms directly regulating mitophagy and mitochondrial biogenesis. Type 2: T_3-bound TRβ also modulates gene expression by

binding to DNA-bound transcription factors. Type 3: Protein-protein interaction of TRβ with other proteins influences cell signaling, for example binding of TRβ to phosphoinositide 3-kinase (PI3K) suppresses the AKT/MAPK/AMPK signaling cascade which also regulates glucose and lipid metabolism. Type 4: Additionally T_3 and T_4 have the ability to bind other proteins independent of TR.

3.3.1. TH signaling in MASLD

As can be inferred from the name, metabolic dysfunction-associated steatotic liver disease, is a disease of disrupted metabolism in the liver. Considering the before mentioned importance of THs in lipid, cholesterol and glucose metabolism and mitochondria function it is of little surprise that THs play an important role in MALSD pathogenesis [107,137]. While hypothyroidism is indeed a risk factor for MASLD development [138], hyperthyroid patients show a reduction of hepatic lipid content [139]. Additionally, patients with a loss-of-function mutation in TRβ (resistance to TRβ) show hepatic steatosis [140]. Further, Bruinstroop et. al. were able to show in 2018 that treatment of euthyroid MASLD patients with T2D with Levothyroxine, an artificial form of T_4, reduced hepatic lipid content [69]. While the treatment with TH resulted in adverse events [141], a TRβ specific agonist, resmetirom was just approved by the FDA for treatment of MASH and is the first MASH medication on the market [70]. However, hypothyroidism is not the only mechanism for reduced TH signaling in MASLD. Reduced expression of the TRβ inversely correlates with MAS [32].

3.4. Epigenetics

In 1942 Waddington introduced the term epigenetics to describe the complex processes connecting genotype and phenotype [142]. This broad definition has been narrowed to the current definition: “the study of changes in gene function that are mitotically and/or meiotically heritable and that do not entail a change in DNA sequence.” [143]. These changes in gene function occur using multiple mechanisms: modification of histones, chromatin remodeling, DNA methylation and noncoding RNA (ncRNA) modulation [144]. In this thesis DNA methylation and microRNAs, a form of ncRNA, were investigated and will therefore, be described in detail.

3.4.1. Histone modifications

Histones are octamer proteins that form the nucleosomes around which the DNA wraps to give the chromosome its compact shape [145]. The organization of the DNA into chromatin fibers, which form the chromosome, influences the accessibility of the DNA for proteins. The density of packed DNA is influenced by post-translational modifications of the histones. Acetylation, phosphorylation, methylation and other modifications, which mainly occur at the N- and C-terminal ends of the histones, alter the structure and function of the chromatin enabling or repressing transcription, depending on type and place of the modification [145].

3.4.2. Chromatin remodeling

Another mechanism to regulate gene expression via density of the chromatin is chromatin remodeling. ATP-dependent chromatin remodelers regulate access of DNA by repositioning, modifying and ejecting nucleosomes [146].

3.4.3. DNA methylation

DNA methylation is the chemical modification of the DNA strand by adding a methyl group to a base, mainly the 5^{th} carbon of the cytosine ring in cytosine-guanine dinucleotides (CpG) [144,147]. This, the

5-methylcytosine (5mC), is the most thoroughly investigated form of methylation, other forms are the 5-hydroxymethylcytosine, 5-formylcytosine and 5-carboxylcytosine [148,149]. Methylation of the DNA is conducted by DNA methyltransferases (DNMTs) by transferring a methyl group from S-adenosylmethionine (SAM) onto the cytosine. While DNMT1 maintains methylation of the DNA throughout cell replication, to maintain cell identity, DNMT3a and -3b establish new methylation patterns [150]. The methylation of CpG sites changes the structure of the DNA and in turn influences the binding affinity of transcription factors, to their binding sites [151]. Whether methylation increases or decreases binding affinity depends on the transcription factor, with transcription factors like bHLH and bZIP showing reduced binding to methylated DNA while homeodomain and NFTA proteins preferred methylated binding sites [151]. So called CpG islands, which are 200-1000 bp long CpG rich section of DNA often overlap with promotor regions. CpG islands are generally un-methylated and their methylation has been associated with a reduction of gene expression [152,153]. Similarly methylation downstream of the promotor in the first intron region, which contains enhancer binding sites, is inversely correlated with gene transcription [154]. In contrast, the methylation of the remaining gene body is positively correlated with gene expression [155]. Modification of the DNA with methyl groups is very dynamic and is influenced by environmental factors like diet and exercise [156]. These changes in gene methylation have been associated with metabolic disease like T2D and obesity [147].

Detection of DNA methylation is either conducted with methods measuring changes of global methylation or to detect the methylation on the base pair level [157]. For these base-pair resolution bisulfite-based methods are considered the gold standard, where the DNA is treated with bisulfite resulting in the deamination of non-methylated cytosines into uracil, while 5mC remains as cytosines. The uracil is then translated by a uracil-tolerant polymerase into thymine during PCR amplification. The methylated cytosines can therefore, be detected during the subsequent sequencing [157,158]. Bisulfite treated DNA can be sequenced as a whole in whole genome bisulfide sequencing to generate methylation data of the complete genome, which is very cost intense or target regions can be sequenced to answer specific questions [157]. To circumvent sequencing and generate more data than a single locus detection, bisulfite treated DNA can also be utilized for hybridization based methods, for example methylation microarrays, where the treated DNA is hybridized to multiple known methylation sites [157]. A newer method to detect DNA methylation is using Oxford Nanopore Technologies sequencing, where a single molecule of DNA is sequenced. The ionic current signal from the sequencing can be used to identify modifications of the DNA [159].

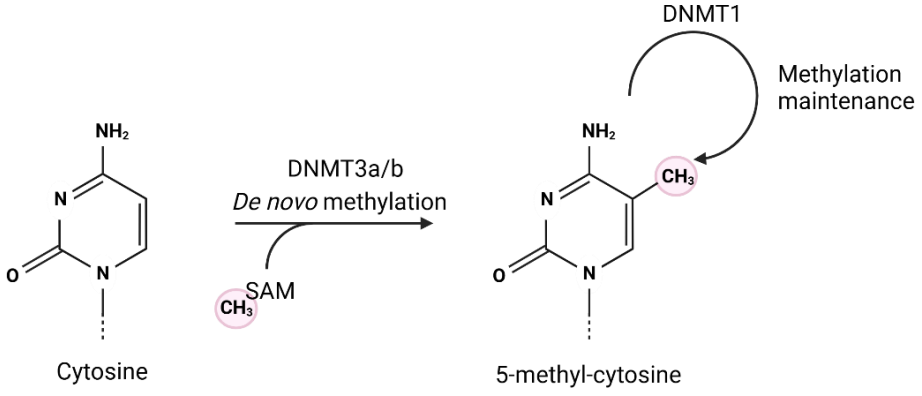

Figure 3. Mechanism of DNA methylation. The DNA methyltransferases 3a and 3b (DNMT3a/b) transfer a methyl group from S-adenosylmethionine (SAM) onto the 5th carbon of the cytosine ring for

newly synthesized DNA strands or to generate new methylation patterns upon signaling. The maintenance of the methylation of 5-methyl-cytosine is conducted by DNMT1.

3.4.4. Non-coding RNAs

Noncoding RNAs (ncRNAs) comprise the majority of the human genome and can be categorized into different categories [144]. NcRNAs are divided into circular RNA and linear RNAs which are further split in long noncoding RNAs, which typically contain more than 200 nucleotides (nt), while small ncRNAs are between 18 and 200 nt length [160,161]. Small ncRNAs are further separated into microRNAs (miRNAs), small nuclear RNAs and piwi-interacting RNAs [162]. MiRNAs are single stranded gene regulatory molecules of approx. 22 nt length [163]. They are either encoded in a transcription unit, alone or in a cluster with other miRNAs, or in an intron of a protein gene [164]. The translation of miRNAs is performed by the RNA polymerase II, the resulting transcript is polyadenylated and capped [163]. When the transcript is generated from a transcription unit it will form the pri-miRNA which contains an imperfectly matched hairpin with an length of approx. 33 base pairs (bp) and flanking segments [164]. The pri-miRNA is further processed in the nucleus by the Drosha protein, a member of the RNase III family. Drosha removes the flanking regions resulting in the pre-miRNA consisting of the stem loop [163]. For processing of miRNAs encoded in introns of host genes, the splicing machinery is used to process the mirtron into the pre-miRNA [165,166]. For further processing, the pre-miRNA is transported from the nucleus into the cytoplasm by the transporter exportin-5 [167]. After transport the terminal loop of the hairpin is cleaved off by the Dicer endonuclease [168]. The resulting mature miRNA duplex unwinds and the binding to the argonaut 2 (AGO2) protein is facilitated by TRBP to form the miRNA-induced silencing complex (miRISC). Meanwhile, the one strand is degraded the other is used in the miRISC to bind specific targets [169]. Selection of the loaded strand depends on the thermostability of the duplex ends and the identity of the 5’ nucleotide with the binding pocket of the AGO2 showing a strong affinity for uracil and adenosine [170]. The argonaut also appears to prefer binding to the less stable duplex end, which is determined by the first four nucleotides of the duplex [171,172]. While these rules promote binding of a preferred strand, both strands can be stably bound to the argonaut, with the preferred st rand often being called miRNA* strand [173]. The two strands are further differentiated by their position of either the 5’ or 3’ end of the pre-miRNA, the mature miRNA is therefore, labeled with the ending 5p or 3p. After loading of the miRNA strand into the argonaut, the miRISC binds mainly to the 3’ untranslated region (UTR) of the target messenger RNA (mRNA) [174] (Figure 4). Specific binding of miRNA to the target depends on the seed sequence, that centers around nucleotides 2-7 at the 5’ end of the miRNA [174]. There are different seed motifs, ranging from 6 nucleotides forming Watson-Crick pairs with the target to 8 nucleotides. While prediction of actual target mRNAs is more specific for 8mers, the majority of miRNAs bind their targets with 7mers. After binding to the target the miRISC regulates the translation and production of proteins, with more than 60% of protein-coding genes being targeted by miRNAs [175]. One miRNA targets multiple target genes and one mRNA often contains multiple binding sites for a variety of miRNAs [173].

Posttranscriptional repression

There are multiple mechanisms proposed by which the miRISC prevents translation. There is evidence that AGO2 contains a cap binding region, that competes with the eukaryotic translation initiation factor 4E (eIF4E) for cap binding, thereby preventing translation of capped mRNAs [176]. Binding of eIF6, which promotes binding of the 60S to the mRNA, to the Dicer-TRBP-AGO2 complex has also been associated with a reduction of translation, preventing the formation of the ribosome [169]. In addition to the prevention of the initiation of translation, miRISC promoted ribosomal drop-off has

been proposed, though a direct mechanism has not been described yet [177]. Furthermore, binding of the miRNA to the target mRNA can induce destabilization of the mRNA by promoting decapping of the mRNA or deadenylation. While there is evidence for miRISC induced degradation of mRNA, there are also mRNAs reported that are not destabilized and are only targeted by the miRNA on the translational level. The mechanisms that decide on the destabilization of only some mRNAs are not known yet [178].

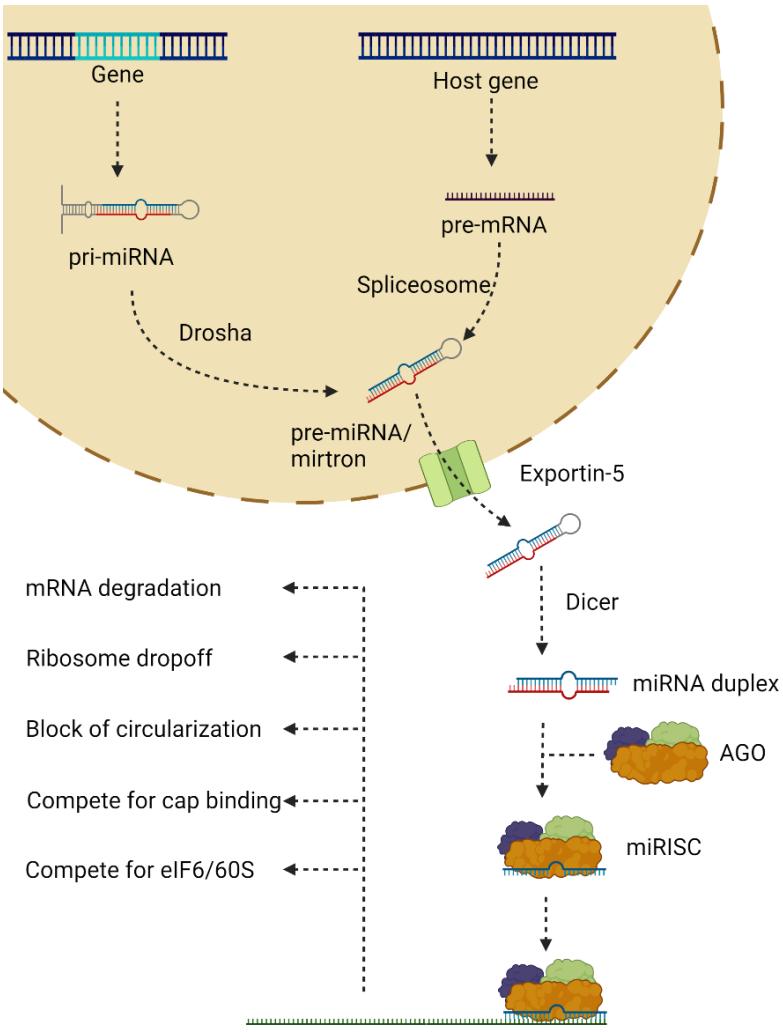

Figure 4. Biogenesis and action of miRNAs. miRNAs are either encoded in a gene or non-canonically part of a host gene. After transcription of the miRNA gene, the pri-miRNA is processed by Drosha into the shorter hairpin of the pre-miRNA, while as part of a host gene, the transformation into pre-miRNA from pre-mRNA is performed during splicing. The pre-miRNA is transported from the nucleus with exportin-5. In the cytosol Dicer removes the loop of the pre-miRNA hairpin to form the miRNA duplex. One single strand of the miRNA duplex is loaded into the argonaut protein (AGO), the miRISC can then bind to target mRNAs and interfere with translation in multiple ways. Binding of the miRISC can induce degradation of the mRNA, promote drop-off of the ribosome, prevent circularization of the mRNA and the miRISC can compete with binding of the cap and also eIF6/60S.

3.4.4.1. RNA-interacting protein immunoprecipitation-sequencing

While prediction of miRNA targets can be done with algorithms, blasting the seed sequence to 3'UTRs and evaluating predicted RNA folding to determine accessibility of potential binding sites actual binding has to be verified. Luciferase assays in which the potential target mRNA 3'UTR with the potential miRNA binding site is cloned 3' to a luciferase gene are one method of verification [179]. Using the luciferase reporter assay only allows verification of a single target mRNA at a time. Considering the high amount of potential targets, verification of all targets would be time and cost intense. Therefore, the method of RNA-interacting protein immunoprecipitation-sequencing (RIP-seq) can be used instead to potentially validate all mRNA targets at once. The expression of the miRNA of

interest is induced in cell culture to increase the ratio of miRNA of interest to other miRNAs bound to the miRISC. To only sequence miRNAs bound to the miRISC an AGO2 specific antibody mix is used for immunoprecipitation (Figure 5). The bound mRNAs are then purified and sequenced. A negative control with an IgG antibody and an input control without antibodies are used to correct for unspecific binding and background [180–185].

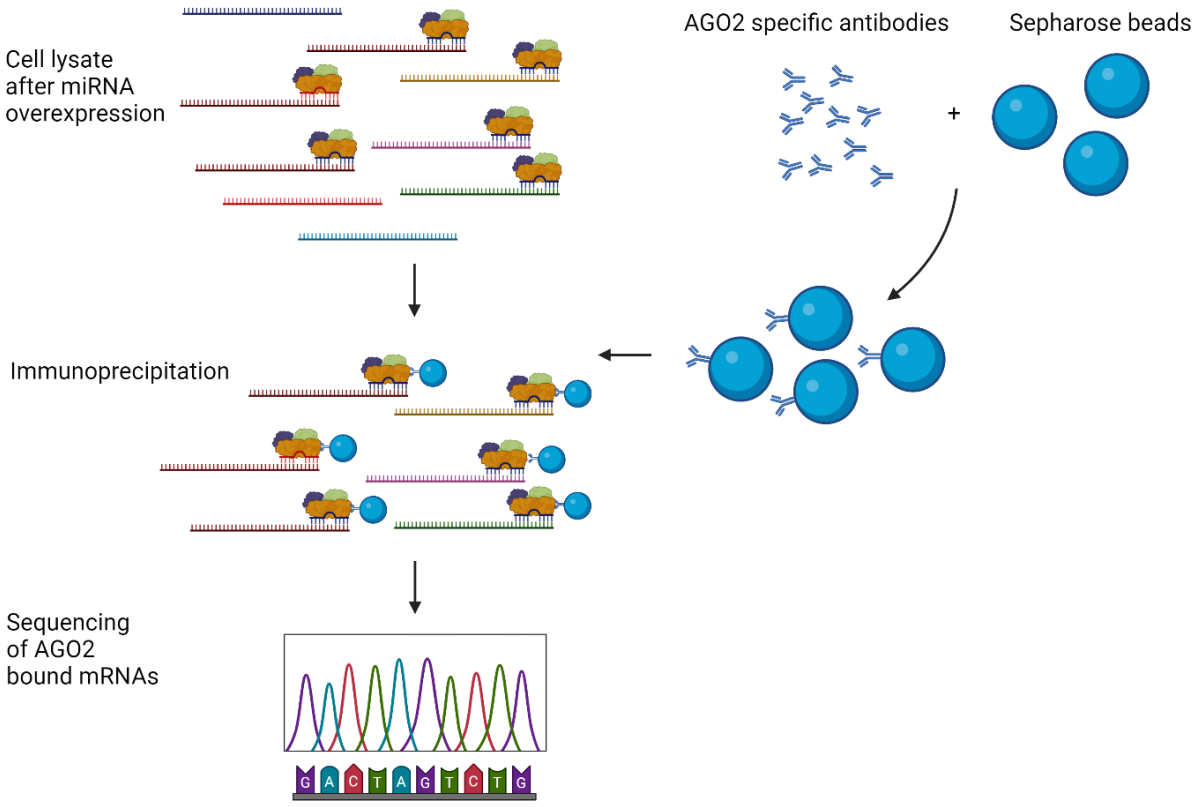

Figure 5. RNA-interacting protein immunoprecipitation-sequencing. The microRNA of interest is overexpressed in cell culture to promote binding of mainly the target miRNA to their target mRNAs. Argonaut 2 (AGO2) specific antibodies are bound to Sepharose beads and used for immunoprecipitation of mRNAs bound to the miRISC complex. The mRNAs bound to the RISC-Sepharose beads are purified and sequenced. To control for unspecific binding a control with IgG antibodies and to remove background input controls without antibodies are performed.

3.5. Epigenetics and MASLD

Metabolic diseases are highly complex and interconnected, changes in epigenetics in obesity, T2D and MASLD have been well established in different tissues, influencing each other [144,147]. In the following the effects of both changes in miRNAs, specifically miR-34a-5p and changes in methylation on the development and progression of MASLD will be discussed.

3.5.1. miRNAs and MASLD

miRNAs regulate multiple aspects of MASLD development and progression, while some of the miRNAs involved in the dysregulated signaling in the liver are produced in the liver, extracellular vesicles containing miRNAs have also been reported to contribute to the pathogenesis of the disease [186]. Here miRNAs with reported influence on different aspects of MASLD development and

progression will be reviewed. Though studies including miRNAs should ideally state whether the investigated miRNA is the 5p or the 3p, unfortunately not all publications specify the investigated miRNA, which can lead to contradicting results.

Lipid metabolism

The main expressed miRNA in the liver is miR-122, comprising 70% of miRNAs [187]. MiR-122 regulates 24 hepatocyte specific genes [188] and is involved in the regulation of lipid and cholesterol metabolism [189]. For example the upregulation of miR-122 in MASLD results in inhibition of SIRT1 and consequently in the inhibition of the LKB1/AMPK pathway which dysregulates lipogenesis [190]. Contradictory, other studies report an increase of miR-122 in the blood [191] but a decrease in the liver of individuals with MASLD [192], proposing an increased release into the circulation from the liver [193]. Meanwhile increased expression of miR-20b targets PPARα, which prevents biogenesis of mitochondria and reduces β-oxidation [194].

MiRNAs miR-33a and miR-33b have been considered as therapeutic targets for managing metabolic syndrome, as well as MASLD due to their involvement in lipid metabolism and insulin synthesis. They are co-transcribed by SREBP1 and SREBP2, which are regulators of *de novo* lipogenesis and cholesterol synthesis. Both miRNAs are involved in the repression of the, for HDL synthesis essential, ATP binding cassette transporter member 1 (ABCA1) [195]. Inhibition of both miRNAS leads to an improvement of insulin sensitivity, increases HDL circulatory levels and β-oxidation [196,197]

MiR-21 regulates the expression of 3-hydroxy-3-methylglutaryl-coenzyme A reductase (HMGCR), which in turn regulates cholesterol metabolism and triglyceride levels [198]. In addition the induction of miR-21 expression in MASLD increases fatty acid uptake, resulting in accumulation of lipids by inhibiting fatty acid-binding protein 7 (FABP7) [199]. Knockout of miR-21 in HFD fed mice improved steatosis by reduced inhibition of FOXA2, FOXO1, HNFα, STST3 and INSIG2 [200].

One miRNA that is involved in the regulation of lipid metabolism through thyroid hormone signaling is miR-451a, which regulates thyroid hormone responsive protein (THRSP) and in turn negatively regulates de novo lipogenesis [201].

MiR-155 is elevated in MCDD fed mice, both in the liver and in Kupffer cells and knock-out of miR-155 attenuates steatosis and apoptosis in MCDD mice [202]. Meanwhile there are studies that show a decrease in liver and serum expression in MASLD patient and an improve of lipid accumulation in HFD fed mice after increase of miR-155 expression, through LXRα signaling [203,204].

Table 2. Dysregulated miRNAs in the lipid and cholesterol metabolism in MASLD

miRNA	miRNA expression	Target	Reference
miR-122	Up/down	SIRT1	[188,190,192,205]
miR-20b	Up	PPARA	[194]
miR-21	Up	FOXA2, FOXO1, HNF4α, STAT3, INSIG2, HMGCR, FABP7	[198–200,205,206]
miR-33a	Up	ABCA1	[195,207]
miR-33b	Up	ABCA1	[195]

miRNA	miRNA expression	Target	Reference
miR-155	Up/down	LXRα	[202–204]
miR-451a	Down	THRSP	[201]

Inflammation and fibrosis

In addition to the involvement of miR-21 in the steatosis of MASLD, miR-21 targets PPARA which leads to the induction of inflammation as well as fibrosis [206]. Upregulated MiR-223 is alleviating inflammation as well as fibrosis by targeting TAZ, in MASLD the miRNA shows reduced expression.

miR-378 expression is increased in obese mice and patients with MASH and contributes to the progression of MASH by targeting Prkag2 which negatively regulates the NKκB-TNFα inflammatory axis leading to inflammation and fibrosis [208].

Table 3. Dysregulated miRNAs in MASLD involved in inflammation and fibrosis

miRNA	miRNA expression	Target	Reference
miR-378	Up	Prkag2	[208,209]
miR-21	Up	PPARA	[206]
miR-223	Down	TAZ	[209,210]

Insulin resistance

Additionally to the involvement of miR-122 in the regulation of the hepatic lipid metabolism, the miRNA is also involved in multiple pathways regarding insulin resistance in MASLD [211]. Gluconeogenesis essential enzymes PEPCK and G6PC are both targeted by miR-33b [212]. Insulin resistance is further induced by the upregulation of both miR-15b and miR-497 which both inhibit the expression of the insulin receptor (InsR) [213,214]. HFD mice and db/db mice show reduced miR-152 expression, which targets phosphatase and tensin homolog (PTEN). PTEN upregulation impairs glycogenesis contributing to hepatic insulin resistance [215].

Table 4. Dysregulated miRNAs in MASLD involved with insulin resistance

miRNA	miRNA expression	Target	Reference
miR-122	Up		[211]
miR-33b	Up	PEPCK, G6PC	[212]
miR-15b	Up	InsR	[214]
miR-497	Up	InsR	[213]
miR-152	Down	PTEN	[215]

Oxidative and endoplasmic reticulum stress

Oxidative and endoplasmic reticulum (ER) stress promote MASLD development and induce each other [216]. In cell lines and in mouse models the induction of miR-26a expression alleviates ER stress and lipid accumulation through the regulation of the eukaryotic initiation factor 2α. Therefore, the opposite effect is observed upon the reduced miR-26a expression during MASLD [217]. Meanwhile miR-421 is upregulated in MASLD mouse models inhibiting SIRT3, dysregulating mitochondrial function and inducing oxidative stress though the down regulation of the SIRT3/FOXO3 signaling pathway [218].

Table 5. Dysregulated miRNAs in MASLD involved in oxidative and endoplasmic reticulum stress

miRNA	miRNA expression	Target	Reference
miR-26a	Down	EIF2α	[217]
miR-421	Up	SIRT3	[218]

3.5.1.1. miR-34a and MASLD

The miR-34 family has been well established as tumor suppressor miRNAs [219]. All three miR-34 types contain the same seed-sequence and subsequently have the potential to bind to the same target mRNAs. Despite the similarities in sequence the miRNAs are encoded in different genes. MiR-34a is encoded on chromosome 1 as part of the host gene MIR34AHG in the second exon and is highly preserved in mice and in healthy tissue the prevailing miR-34 form [220]. The other two members of the miR-34 family, miR-34b and miR-34c are encoded on chromosome 11 as part of the MIR34BHG, but are generally not expressed in the liver [220].

The expression of miR-34a in patients with MASLD is increased and increases further with disease progression [209,221–224]. MiR-34a plays a role in multiple aspects of MASLD development and progression, contributing to steatosis, inflammation and fibrosis. The high degree of increased expression in MASLD patients leads to a measurable increase in miR-34a serum levels. Therefore, miR-34a has been proposed as a non-invasive marker for MASLD [224]. Similar to humans, mice also show increased miR-34a expression after being challenged with diets high in fatty acids and fructose [225,226]. Accordingly, studies in mice fed a diet high in fats and fructose show that the severity of MASLD increases proportionally with miR-34a expression and improves after miR-34a inhibitor treatment, underlining the relevance of miR-34a in MASLD [227].

The expression of miR-34a is regulated by the well-known tumor suppresser p53 which is a miR-34a activator [228,229]. Thus, p53 also alters the miR-34a expression in cancers depending on the p53 status, therefore, miR-34a might decrease in HCC. Due to the tumor suppressing effects of miR-34a, a mimic has been proposed as a cancer therapeutic [162]. Unfortunately the therapeutic MRX34 was aborted due to adverse effects on the immune system [230]. The expression of miR-34a is further regulated by the bile acid receptor FXR which inhibits miR-34a expression [228]. The expression of FXR is reduced in MASLD which contributes to the upregulation of miR-34a [231]. Indeed MASLD patients treated with a FXR agonist show improvement in liver steatosis and biomarkers [232]. In addition to regulation through transcription factors, the level of miR-34a in the liver is also regulated by inositol-requiring enzyme 1α (IRE1α) which plays an essential role in hepatic lipid homeostasis by degradation of pre-miRNAs. IRE1α is inactivated in hepatosteatosis, leading to an increase in miR-34a

levels [233]. Furthermore, there is evidence that dysbiosis of the gut microbiome has an influence on hepatic miRNA levels [234].

MiR-34a influences multiple aspects of MASLD, one of the miR-34a targets that regulate various aspects of MASLD is SIRT1 [235,236], whose inhibition leads to a dysregulation of lipogenesis, cholesterol synthesis, and a reduction of β-oxidation, mitochondrial function, induced inflammation and apoptosis [188,237,238]. SIRT1 also has been proposed to be involved in hepatic stellate cell activation and fibrosis development through a pathway involving PPARG [239,240]. Additionally, the regulation of SIRT1 indirectly contributes to the dysregulation of TH signaling due to SIRT1 acting as a coactivator of TRβ [131], which contributes to the dysregulation of the lipid metabolism. Lipogenesis is also dysregulated though miR-34a targeting of PPARA [236] and silencing of mi-R34a in mice restores SIRT1 and PPARA expression levels and improves steatosis [241]. In addition, miR-34a directly targets hepatocyte nuclear factor 4α (HNF4α), which regulates hepatic lipid and lipoprotein metabolism [209,226] and results in a reduction of VLDL secretion [226]. Finally, there is evidence that miR-34a induces fibrosis by activating hepatic stellate cells through the TGF-β pathway [242].

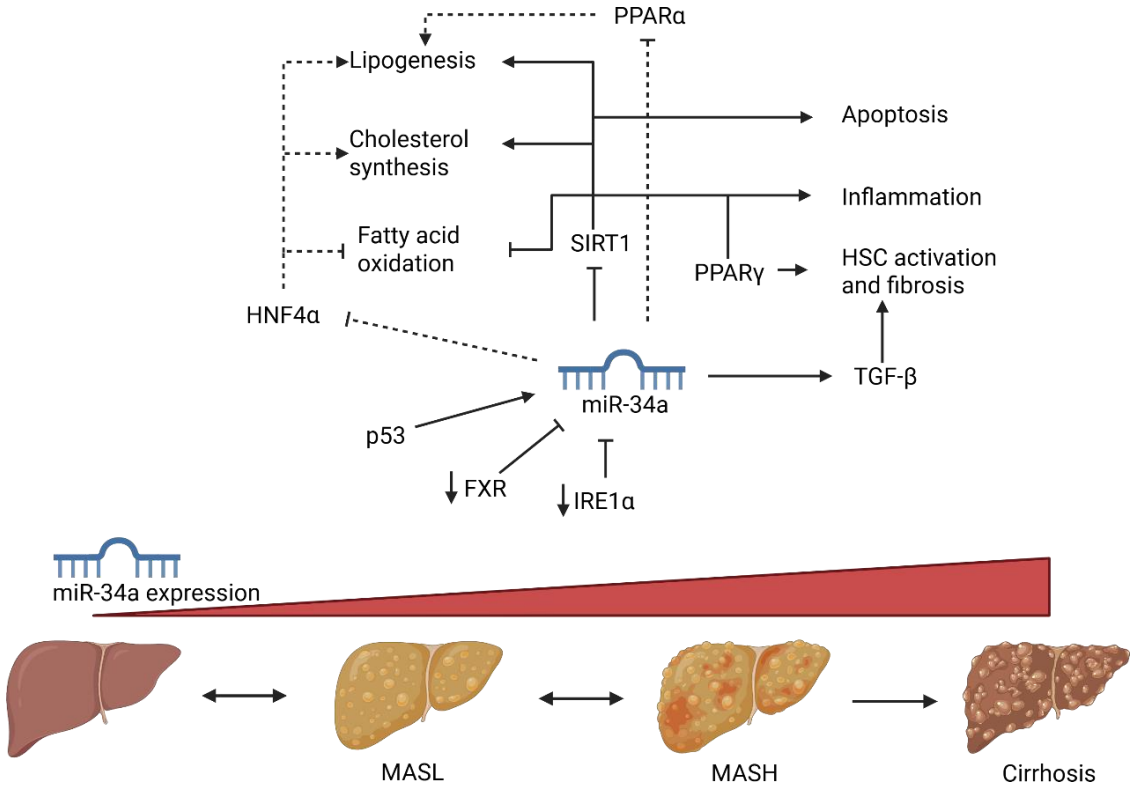

Figure 6. Function of miR-34a during MASLD. The expression of miR-34a increases during MASLD development and progression, the expression is activated by p53 and negatively regulated by farnesoid X receptor (FXR) and inositol-requiring enzyme 1α (IRE1α). Both FXR and IRE1α show reduced expression and inactivation during MASLD, resulting in the increase of miR-34a activity. The inhibition of the miR-34a target SIRT1 results in a dysregulation of the hepatic lipid metabolism by inducing lipogenesis and cholesterol synthesis and the inhibition of fatty acid oxidation which is also observed by the binding of miR-34a to hepatocyte nuclear factor 4α (HNF4α). Lipogenesis is additionally increased through PPARA inhibition by miR-34a. The reduced SIRT1 signaling also results in increased apoptosis and inflammation. SIRT1 is additionally involved in the activation of

hepatic stellate cells (HSC) and the resulting increase in fibrosis through a pathway involving PPARG. Fibrosis is also induced by the TGF-β pathway that is induced by miR-34a.

3.5.2. DNA methylation and MASLD

DNA methylation has been associated with multiple metabolic diseases and comorbidities of MASLD like T2D and obesity, with observed changes in DNA methylation in the liver [144]. Indeed, analysis of liver biopsies from MASLD patients compared to controls show significantly less global methylation and a reduction of available SAM in MASLD patients [243]. A study in mice fed an MCD diet showed changes in DNMT1 and DNMT3a expression [244]. Reduced methylation has been reported to increase dipeptidyl peptidase 4 (DPP4) expression in the liver. The increased DPP4 expression positively correlates with MASLD stages [245] and increased DPP4 activity has been associated with insulin resistance [246]. The methylation levels of NF-E2-reated factor 2 (Nfr2) are increased by a high glucose and high fat diet in mice. Increased Nfr2 methylation leads to an increase in SREBP1c and FASN expression and therefore, to an induction in lipogenesis [247]. Meanwhile the methylation of PGC-1α is increased in MASLD patients and correlates with insulin resistance. PGC-1α is also a key regulator of mitochondrial biogenesis which is reduced in the liver of MASLD patients and inversely correlates with PGC-1α promotor methylation and insulin resistance [248]. A study comparing a control group, an obese group without MASLD, a non-obese group with MASL and an obese group with MASH found 476 differentially methylated CpGs. The MASLD-related genes included enzymes important for glucose and lipid metabolism but also insulin -like signaling [249]. Additionally, changes in DNA methylation may also predict development of HCC in patients with MASLD. Differentially methylated promotor regions of tumor suppressor genes lead to an increase of oxidative DNA damage [250]. Taken together, many studies have demonstrated the relevance of changes in DNA methylation in MASLD, by influencing metabolism, insulin signaling and carcinogenesis.

4. Hypothesis

The prevalence of MASLD has dramatically increased over the last decades and is a burden to health care systems world-wide. With only one medication available for treatment, MASLD patients main options are life style changes, with limited success. It is well established that thyroid hormones regulate liver lipid metabolism and that hypothyroidism is a risk factor for disease development and progression. Our group could show that the expression of THRB negatively correlates with the MAS-Score. The down regulation of THRB during MASLD is not only well established but also the foundation of the only recently approved and first ever developed MASLD medication, resmetirom. We know that an increase of THRB activity, through increased agonist availability, either by resmetirom or LT4 [69]improves MASLD. What is still unknown is the mechanism by which the expression of TRβ is reduced during disease progression. Considering the high prevalence of epigenetic changes in metabolic disease it is hypothesized in this thesis that the changes in TRβ expression are caused by changes in the epigenetic regulation, either by miRNAs or by DNA methylation. While the involvement of epigenetic changes in metabolic diseases have been well documented the connection between epigenetic changes in thyroid hormone signaling in the liver of MASLD patients has yet to be thoroughly investigated, this study will now for the first time link both the changes in TH signaling with the changes in epigenetics during MASLD and offer a new target for therapeutics.

The subsequent aims of this thesis are therefore:

1. The identification of miRNAs with increased expression during MASLD that have the predicted ability to bind TH signaling related targets. Followed by the experimental evidence of the binding of miRNA and respective target.
2. Identification of in MASLD differentially methylated DNA regions in TH signaling associated genes.

5. Subjects, Materials and Methods

5.1. Human cohort

Table 6. Characterization of human cohort

Parameter	Unit	Non-MASH	MASH	p-value	n
Sex	m/f	6/35 14.6%	9/18 33.3%		68
Age	years	40.07 (±12.53)	49.07(±13.11)	**0.0059**	68
BMI	kg/m^2	51.97(±11.75)	54.37(±8.582)	0.3649	68
TSH	mU/L	2.015(±1.125	3.62(±8.467)	0.5669	63
Serum T_3	ng/mL	0.8872(±0.2492)	1.048(±0.1480)	**0.0057**	59
Serum T_4	µg/dL	5.183 (±1.124)	5.872 (±1.438)	**0.0448**	59
Triglycerides	mmol/L	176.8(±98.18)	255.4(±140.5)	0.0120	66
Total cholesterol	mg/dL	182.3(±35.79)	195.8(±50.84)	0.4832	66
LDL	mg/dL	102.7(±36.11)	99.67(±36.00)	0.7598	60
HbA1c	%	5.880(±1.665)	7.222(±1.934)	**0.0005**	68
Blood glucose	mg/dL	110.1(±41.86)	154.5(±72.36)	**0.0003**	68
Diabetes	Diagnose yes/no	9/32 21.9%	16/11 59.2%		68
MASLD activity	Score	0 (19)	4 (9)		68
		1 (5)	5 (10)		
		2 (10)	6 (8)		
		3 (7)			
Fibrosis	Diagnose yes/no	9/32 21.9%	21/6 77.7%		68
AST	U/L	19.78(±9.627)	37.56(±19.86)	**<0.0001**	68
ALT	U/L	24.95(±16.18)	41.74(±18.98)	**<0.0001**	68

Liver biopsies of patients with obesity were obtained from segment III during bariatric surgery at the University Hospital Eppendorf (Hamburg, Germany) [32]. The study was approved by the local ethics committee (PV4889) and all participants signed informed consent. MAFLD activity score (MAS) was determined by two pathologists according to current standards, clinical parameters were determined as described previously [32]. Cohort statistics and clinical parameters are represented in Table 1.

5.2. Material

5.2.1. Equipment

Table 7. List of Equipment

Name	Manufacturer
Bead Ruptor 24	Omni International, Kennesaw, US
Blotting chamber	Bio-Rad, Hercules, US
Cell culture clean bench Misc advanced	Thermo Fisher Scientific, Waltham, US
CellXpert®C170i	Eppendorf, Hamburg, DE
Centrifuge 5430R	Eppendorf, Hamburg, DE
Centrifuge MC 6	Sarstedt, Nümbrecht, DE
ChemiDoc™ Touch Imaging System	Bio-Rad, Hercules, US
Criterion™ Cell gel chamber	Bio-Rad, Hercules, US
Cytek Aurora Flow Cytometer	Cytek Biosciences, Fremont, US
Fixed-angle rotor	Eppendorf, Hamburg, DE
Incubator with CO2 Hera cell 150	Thermo Fisher Scientific, Waltham, US
Light microscope Axiovert 40 CFL	Zeiss, Jena, DE
Magnetic stirrer MOD 205	VWR, Radnor, US
Mastercycler Nexus Gradient	Eppendorf, Hamburg, DE
Mastercycler Nexus X2 eco	Eppendorf, Hamburg, DE
Microplate reader CLARIOstar Plus	BMG Labtech, Ortenberg, DE
Multifuge 35A Heraeus	Fisher Scientific, Schwerte, DE
Multipette E3	Eppendorf, Hamburg, DE
NanoDrop One spectrophotometer	Thermo Fisher Scientific, Waltham, US
Perfectblue gelsystem mini L,S	VWR, Radnor, US
Pipettes	Eppendorf, Hamburg, DE
Pipettus Akku	Hirschmann, Neckartenzlingen, DE
Powerpack basic power supply	Bio-Rad, Hercules, US
PyroMark Q48 Autoprep pyrosequencer	Qiagen, Venlo, NL
”Quenzy” and cartridges	
QuantStudio 5 Real-Time PCR System	Applied Biosystems, Foster City, US
Rotator RS-24	Kisker Biotech, Steinfurt, DE
Rotor A-2-MTP	Eppendorf, Hamburg, DE
Scales Kern PCB 1000-1	KERN & SOHN GmbH, Balingen, DE

Name	Manufacturer
ThermoMixer C	Eppendorf, Hamburg, DE
Trans-Blot® Turbo™	Bio-Rad, Hercules, US
Vortex mixer 7-2020	neoLab Migge, Heidelberg, DE
Vortex mixer orbit	Fisher Scientific, Schwerte, DE
Water bath Grant OLS 200	Grant Instruments, Cambridge, UK

5.2.2. Consumables

Table 8. List of consumables

Name	Manufacturer
0.2 µm Nitrocellulose membrane Trans-Blot turbo	Bio-Rad, Hercules, US
Aluminium foil (0.03 mm x 300 mm x 1ßß m), Labsolute	Th.Geyer GmbH & Co. KG, Renningen, Germany
Biosphere Filter Tip 1000 µl, 300 µl, 200 µl, 100 µl, 20 µl, 10 µl, 2.5 µl	Sarstedt, Nümbrecht, Germany
Bulk beads 1.4 mm Zirconium oxide beads	Precellys, Bertin Technologies, Montigny-le-Bretonneux, France
Cell culture flask T75, standard, ventilated cap	Sarstedt, Nümbrecht, Germany
Cell culture plate, 6 well, 12 well, 96 well	Sarstedt, Nümbrecht, Germany
Cell scraper	Sarstedt, Nümbrecht, Germany
Combitips advanced/Plus Biopur R 0.2, 0.5, 2.5, 5.0 and 10 ml	Eppendorf, Hamburg, Germany
Criterion™ TGX Stain-free™ Precast Gels 10%	Bio-Rad, Hercules, US
Cryo tubes 2 mL	Sarstedt, Nümbrecht, Germany
Falcon tubes, 15 mL, 50 mL	Sarstedt, Nümbrecht, Germany
Filter paper, extra thick	Bio-Rad, Hercules, US
Filtropur V25 250 mL, 0.2 µm	Sarstedt, Nümbrecht, Germany
Gelloader pipette tips, 200 µL	Sarstedt, Nümbrecht, Germany
MicroAmp™ optical adhesive film	Applied Biosystems, Foster City, US
Microplate, 96-well, F, transparent	Sarstedt, Nümbrecht, Germany
Microtubes low binding, 1.5 ml, 2 ml	Sarstedt, Nümbrecht, Germany
Millipore membrane filters 0.1 µM	Merck, Darmstadt, Germany
Multiply Strip 0.2 mL	Sarstedt, Nümbrecht, Germany
Pasteur pipettes	Th.Geyer GmbH & Co. KG, Renningen, Germany

Name	Manufacturer
PCP Plate half skirt HP white	Sarstedt, Nümbrecht, Germany
PCR cover chain	Sarstedt, Nümbrecht, Germany
PCR plates, HP, 0.2 ml	Th.Geyer GmbH & Co. KG, Renningen, Germany
Petri dish w/ cams, 100 mm	Sarstedt, Nümbrecht, Germany
Pipettes, serological, 5 mL, 10 mL, 25 mL	Sarstedt, Nümbrecht, Germany
Plating spatula	Sarstedt, Nümbrecht, Germany
Pleated filter	Whatman, GE Healthcare, Chicago, US
PyroMark Q48 absorber stripes	Qiagen, Venlo, Netherlands
PyroMark Q48 discs	Qiagen, Venlo, Netherlands
PyroMark Q48 magnetic beads	Qiagen, Venlo, Netherlands
Qubit Assay tubes, 0.5 ml	Life Technologies, Carlsbad, US
RNaseZAP™	Sigma-Aldrich, St. Louis, US
Safe Seal reactiontube, 1.5 mL, 2 mL, 5 mL	Sarstedt, Nümbrecht, Germany
Scalpel, disposable	Feather Safety Razor, Osaka, Japan
Screw cap micro tubes, 2 mL	Sarstedt, Nümbrecht, Germany
Serological pipettes, 1 ml, 2 ml, 5 ml, 10 ml, 25 ml	Sarstedt, Nümbrecht, Germany
Syringe filter, Filtropur S 0.2 µM	Sarstedt, Nümbrecht, Germany
Syringes 1 ml, 20 ml	Becton Dickinson, Franklin Lakes, US
Syringes, insulin 0.5 ml	Becton Dickinson, Franklin Lakes, US

5.2.3. Chemicals

Table 9. List of chemicals

Reagent	Manufacturer
Agarose Broad Range	Carl Roth, Karlsruhe, Germany
B27 supplement	Thermo Fisher Scientific, Waltham, US
Bovine Serum Albumin (BSA)	Sigma Aldrich, St. Louis, US
Charcoal stripped FBS	Life Technologies, Carlsbad, US
Chloroform	Carl Roth, Karlsruhe, Germany
D (+) Glucose, 99.5%	Carl Roth, Karlsruhe, Germany
D(-)Fructose	Sigma Aldrich, St. Louis, US
D(+)Glucose	Carl Roth, Karlsruhe, Germany

Reagent	Manufacturer
DEPC treated water	Life Technologies, Carlsbad, US
Dimethyl sulfoxide (DMSO)	AppliChem GmbH, Darmstadt, Germany
DNA Away	Thermo Fisher Scientific, Waltham, US
DTT	New England Biolabs, Ipswich, US
Ethanol 70%, denatured	Carl Roth, Karlsruhe, Germany
Ethanol 99.8%, denatured	Carl Roth, Karlsruhe, Germany
Ethanol 99.8%, pure	Carl Roth, Karlsruhe, Germany
Ethylenediaminetetraacetic acid (EDTA) solution 0.5 M, pH 8.0	AppliChem GmbH, Darmstadt, Germany
Fetal Bovine Serum (FBS), heat-inactivated One Shot	Life Technologies, Carlsbad, US
Geltrex	Thermo Fisher Scientific, Waltham, US
GeneRuler 100 bp DNA Ladder	Life Technologies, Carlsbad, US
GlutaMax	Life Technologies, Carlsbad, US
HEPES	Carl Roth, Karlsruhe, Germany
IGEPAL® CA-630 (NP-40 sub)	Sigma Aldrich, St. Louis, US
Insulin Humalog 100 IE/ml	Eli Lilly and Company, Indianapolis, US
Isopropanol, pure	Thermo Fisher Scientific, Waltham, US
KCl	Merck, Darmstadt, Germany
KO-Serum replacement	Life Technologies, Carlsbad, US
Lipofectamin 2000	Life Technologies, Carlsbad, US
Lipofectamin 3000	Life Technologies, Carlsbad, US
Loading buffer, 6x	Life Technologies, Carlsbad, US
MgCl2	Carl Roth, Karlsruhe, Germany
Milk powder	Carl Roth, Karlsruhe, Germany
NaBut	Sigma Aldrich, St. Louis, US
NEAA	Life Technologies, Carlsbad, US
Penicillin/Streptomycin	Life Technologies, Carlsbad, US
Protein G Sepharose Fast Flow	Sigma Aldrich, St. Louis, US
Proteinase inhibitor cocktail (PIC)	Merck, Darmstadt, Germany
QIAzol Lysis Reagent	Quiagen, Venlo, Netherlands
Recombinant Human Hepatocyte Growth Factor (HGF)	PeproTech, Cranbury, US

Reagent	Manufacturer
Recombinant Human Oncostatin-M (OSM)	PeproTech, Cranbury, US
Recombinant Human/Mouse/Rat Activin A	R&D systems, Minneapolis, US
Recombinant Murine Wnt-3a	PeproTech, Cranbury, US
Restore™ PLUS Western Blot Stripping Buffer	Bio-Rad, Hercules, US
RNAiMax	Life Technologies, Carlsbad, US
RNase Inhibitor, 2000 U	Life Technologies, Carlsbad, US
Rock inhibitor Y-27632	StemCell Technologies
SDS	Sigma Aldrich, St. Louis, US
Sodium butyrate	Sigma Aldrich, St. Louis, US
Sodium chloride (NaCl), pure, solid	AppliChem, Darmstadt, Germany
Sodium oleate, O7501	Sigma Aldrich, St. Louis, US
Sodium palmitate, P9767	Sigma Aldrich, St. Louis, US
Sodium pyruvate, 100 mM	biowest, Nuaill´e, France
Sodium selenite	Sigma Aldrich, St. Louis, US
SYBR™ Safe DNA gel stain	Thermo Fisher Scientific, Waltham, US
T_3 [T6397-100mg]	Sigma Aldrich, St. Louis, US
Tris-HCl	Carl Roth, Karlsruhe, Germany
Trizma Base, 2-Amino-2-(hydroxymethyl)-1,3-propanediol	Sigma Aldrich, St. Louis, US
Trypan Blue Solution, 0.4%	Sigma Aldrich, St. Louis, US
Vanadyl ribonucleoside (VRC)	New England Biolabs, Ipswich, US
β-mercaptoethanol	Life Technologies, Carlsbad, US

5.2.4. Solutions, media and buffers

Table 10. List of solutions, media and buffers

Name	Ingredients	Manufacturer/description
Dulbecco's Modified Eagle Medium (DMEM)	w/o glucose, sodium, HEPES	Life Technologies, Carlsbad, US. Basic cell culture medium
Dulbecco's Modified Eagle Medium (DMEM) high glucose (4.5 g/L)	GlutaMAX Supplement	Life Technologies, Carlsbad, US. Basic cell culture medium
HepG2 maintenance medium	Mixture of DMEM high glucose and w/o glucose (1.5 g/L), 10% (v/v) FBS, 200 mM glutamine, 1 mM sodium pyruvate, 1% penicillin/streptomycin	For maintenance of HepG2 cells
HepG2 stripped maintenance medium	Mixture of DMEM high glucose and w/o glucose (1.5 g/L), 10% (v/v) charcoal stripped FBS, 200 mM glutamine, 1 mM sodium pyruvate, 1% penicillin/streptomycin	For maintenance of HepG2 cells
HepG2 transfection medium	Mixture of DMEM high glucose and w/o glucose (1.5 g/L), 10% (v/v) FBS, 200 mM glutamine, 1 mM sodium pyruvate	For transfection of HepG2 cells
HepG2 stripped transfection medium	Mixture of DMEM high glucose and w/o glucose (1.5 g/L), 10% (v/v) charcoal stripped FBS, 200 mM glutamine, 1 mM sodium pyruvate	For transfection of HepG2 cells
HEK298T maintenance medium	DMEM high glucose (4.5 g/L), 10% (v/v) FBS, 200 mM glutamine, 1 mM sodium pyruvate, 1% penicillin/streptomycin	For maintenance of HEK298T cells
HEK298T transfection medium	DMEM high glucose (4.5 g/L), 10% (v/v) FBS, 200 mM glutamine, 1 mM sodium pyruvate	For transfection of HEK298T cells

Name	Ingredients	Manufacturer/description
Huh-7 maintenance medium	Mixture of DMEM high glucose and w/o glucose (1.0 g/L), 10% (v/v) FBS, 200 mM glutamine, 1 mM sodium pyruvate, 1% penicillin/streptomycin	For maintenance of Huh-7 cells
Huh-7 transfection medium	Mixture of DMEM high glucose and w/o glucose (1.0 g/L), 10% (v/v) FBS, 200 mM glutamine, 1 mM sodium pyruvate	For transfection of Huh-7 cells
Huh-7 stripped transfection medium	Mixture of DMEM high glucose and w/o glucose (1.0 g/L), 10% (v/v) charcoal stripped FBS, 200 mM glutamine, 1 mM sodium pyruvate	For transfection of Huh-7 cells
Fast Media Amp Agar solid medium	1 pouch in 200 mL water, w/ ampicillin	InvivoGen, San Diego, US. Selection of bacteria containing plasmids with ampicillin resistance
Fast Media Amp (Lysogency Broth) LB liquid medium	1 pouch in 200 mL water, w/ ampicillin	InvivoGen, San Diego, US. Growth of bacteria containing plasmids with ampicillin resistance
HepG2 freezing medium	DMEM low glucose medium + DMSO 10% (v/v)	Self-diluted. For freezing of cells
Opti-MEM		Life Technologies, Carlsbad, US. Reduced serum media for transfection
S.O.C. medium	S.O.B. (super optimal broth) medium with glucose supple-ment: 2% tryptone, 0.5% yeast extract, 10 mM NaCl, 2.5 mM KCl, 10 mM MgCl 2, 10 mM MgSO4, 20 mM glucose.	Invitrogen, Carlsbad, US. For final step in bacteria transformation

Name	Ingredients	Manufacturer/description
TAE buffer	242 g tris (Trisma baze), 57.1 mL acetic acid, 100 mL 0.5 M EDTA (pH 8) ad 1000 mL water for 50X TAE, dilute 1:50 for 1X TAE	Self-diluted. For agarose gel electrophoresis
TrypLE Express	Trypsin, EDTA	Life Technologies, Carlsbad, US. Basic cell culture enzyme for passaging of cells
NT2	50 mM Tris pH 7.4, 150 mM NaCl, 1 mM MgCl2, 0.5% NP-40 sub, 0.5% VRC, 1mM DTT, 15 mM ETDA	RIP seq washing buffer
Polysome lysis buffer (PolyLB)	5 mM MgCl2, 100 mM KCl, 10 mM Hepes pH 7, 0.5% NP-40 sub, 1 mM DTT, 100 U/ml RNase OUT, 1x PIC	RIP seq lysis buffer
RPMI/B27 media	RPMI, 2% 50 x B27 (v/v), 1% penicillin/streptomycin	Gibco Base media for definite endoderm induction
DE-induction media day 6	RPMI/B27 media, 100 ng/ml activin A, 50 ng/ml Wnt3a, 0.5 mM NaBut	Differentiation medium for definite endoderm
KO-media	KO-DMEM, 20% KO-serum replacement, 1x NEAA, 1x GlutaMax, 0.1 mM b-mercaptoethanol, 1% DMSO, 1% penicillin/streptomycin	Life Technologies, Carlsbad, US. Hepatocyte differentiation
HBM-media	HBM, 20 ng/ml HGF, 20 ng/ml OSM, 1% penicillin/streptomycin	Lonza, Basel, Switzerland. Hepatocyte differentiation
HBM Bullet Kit	HBM, 5 nM T_3, 100 nM sodium selenite, 1% penicillin/streptomycin, insulin, transferrin, ascorbic acid, BSA (fatty acid free), hyrdocortistone, HEGF, GA-1000	Lonza, Basel, Switzerland. Maturation of hepatocytes
Western blot running buffer 10X	0.25 M Tris, 1.92 M glycine, 1% SDS	1X buffer is used for SDS-gel electrophoresis
DE-induction media days 1-5	RPMI/B27 media, 100 ng/ml activin A, 50 ng/ml Wnt3a	Medium for differentiation into definite endoderm

Name	Ingredients	Manufacturer/description
Western blot TBS buffer pH 7.4 10X	100 mM Tris, 1.5 M NaCl	For washing buffer after dilution to 1X 0.1% Tween is added (TBST), for blocking 5% milk powder is added to TBS

5.2.5. Enzymes and master mixes

Table 11. List of enzymes and master mixes

Name	Manufacturer
Cut Smart	New England Biolabs, Ipswich, US
DNase I	Qiagen, Venlo, Netherlands
DpnI	New England Biolabs, Ipswich, US
FastStart Universal SYBR Green Master (ROX)	Roche, Basel, Swiss
GoTaq G2 Green Master Mix	Promega, Madison, US
NotI-HF	New England Biolabs, Ipswich, US
PerfeCta® Universal Primer	QuantaBio, Beverly, US
Phusion Hotstart II Mastermix (Pfu)	Thermo Fisher Scientifc, Waltham, US
Proteinase K	Qiagen, Venlo, Netherlands
PyroMark PCR Kit	Qiagen, Venlo, Netherlands
Pyrophosphatase, inorganic (0.1 U/µL)	Life Technologies, Carlsbad, US
qScript miRNA cDNA Synthesis Set	Quantabio, Beverly, US
Quick CIP	New England Biolabs, Ipswich, US
RNase A	Qiagen, Venlo, Netherlands
RNaseOUT™	Life Technologies, Carlsbad, US
StemPro Accutase	Life Technologies, Carlsbad, US
TaqMan® Fast Advanced Master Mix (2X)	Thermo Fisher Scientifc, Waltham, US
Trypsin TrypLE Exp.Enzyme (1X) no phenol red	Life Technologies, Carlsbad, US
XhoI	New England Biolabs, Ipswich, US

5.2.6. Kits

Table 12. List of kits

Name	Manufacturer and usage
Bio-Plex®Cell lysis Kit	Bio-Rad laboratories, Hercules, US. Cell lysis kit used for protein isolation.
Clarity Max™ Western ECL substrates	Bio-Rad laboratories, Hercules, US
Dual-Luciferase Reporter Assay System	Promega, Madison, US. Luminescence assay for gene expression measurement with Firefly and Renilla luciferase.
High Capacity cDNA reverse transcriptase Kit	Life Technologies, Carlsbad, US. cDNA synthesis for mRNA analysis.
miRNeasy Mini Kit	Qiagen, Venlo, NL. Extraction of whole cell RNA from mammalian cells.
Pierce™BCA Protein Assay Kit	Life Technologies, Carlsbad, US. Photometric assay to determine protein concentration in a suspension. A serial dilution of BSA suspension is used as standard
PyroMark Q48 advanced CpG Reagents	Qiagen, Venlo, NL. Contains buffer solutions, nucleic acids and enzymes for pyrosequencing.
Qiagen Plasmid Midi Kit	Qiagen, Venlo, NL. Extraction of plasmid DNA from 50 mL over-night bacteria culture
QIAprep spin Miniprep Kit	Qiagen, Venlo, NL. Extraction of plasmid DNA from 5 mL over-night bacteria culture.
qScript miRNA cDNA Synthesis Set	Quantabio, Beverly, US
Qubit dsDNA BR Assay	Thermo Fisher Scientifc Inc., Waltham, US
Qubit dsDNA HS Assay	Thermo Fisher Scientifc Inc., Waltham, US
Quick Ligation Kit	New England Biolabs, Ipswich, US. Contains buffer and ligase for ligation of inserts into vectors.
RiboCop	Lexogen, Vienna, AUT. rRNA depletion kit used for RIP-seq input control
RNase-Free DNase Set	Qiagen, Venlo, NL. On-column digestion od DNA during RNA extraction.
TaqMan advanced miRNA cDNA Synthesis Kit	Life Technologies, Carlsbad, US. cDNA synthesis for miRNA analysis.
Wizard SV Gel and PCR clean up System	Promega, Madison, US. Column-based system for clean-up of PCR products from reaction solution or agarose gel.

5.2.7. Antibodies

Table 13. List of antibodies

Name	Manufacturer and description
11A9	Sigma Aldrich, S. Louis, US
Anti-6X His tag® antibody (ab9108)	Abcam, Cambridge, United Kingdom
Mouse IgG1 kappa isotype Control	Life Technologies, Carlsbad, US
Polyclonal Goat Anti-Rabbit immunoglobulins/HRP	Agilent Dako, Santa Clara, US
Recombinant Anti-DDDDK tag antibody (ab205606)	Abcam, Cambridge, United Kingdom
HSP90 (C45G5) Rabbit mAb	Cell Signaling Technology, Danvers, US
2E12-1C9	Abnova, Taipeh, Taiwan

5.2.8. Primers and TaqMan assays

SYBR green primer were acquired from IDT (Coralville, US), TaqMan Assay were purchased from Thermo Fisher Scientific (Waltham, US).

Table 14. Genomic primer designed for luciferase reporter assays

Name	Sequence	Melting temperature [°C]	Product size
THRA-34a-2F	5′ATCTCTCGAGCCCATCACTCATAACACACATACC	60.0	224 bp
THRA-34a-2R	5′TGCGGCCGCCGGTCCCACCCCTCCCTGGGGAA	60.0	
34a-5pTHRB_F2	5′ATCTCTCGAGTAACTTTCCTGCCCAACCTG	60.1	358 bp
34a-5pTHRB_R2	5′TGCGGCCGCGACCTAGAATTACAAATCTA	59.4	
DIO1_34a_F	5′ATCTCTCGAGTGGCTTTTACCCTTGACCTG	60.1	381 bp
DIO1_34a_R	5′TGCGGCCGCTTAGTGTCTTAAATGATCAATT	59.2	
SLC10A1_34a_F	5′ATCTCTCGAGCCTTCCCTTTTGACATTATTGG	59.7	358 bp
SLC10A1_34a_R	5′TGCGGCCGCTAAATTTTATTAGAGACAATTTGAAAT	58.6	
pmirGLO_Seq_F	5′CGAGGTGCCTAAAGGACTGA	60.3	-
pmirGLO_Seq_R	5′GTTGTGGTTTGTCCAAACTCATCAA	95.2	-

NotI and XhoI cutting sites are depicted in red.

Table 15. Primer designed for QuickChange PCR of luciferase assays

Name	Sequence
THRB_miR34a-5p_qc_F	5′CCTTTGCCTTTGCCTACCTTTTACT**T**CCTTATCCTGGAAATATTG
THRB_miR34a-5p_qc_R	5′CAATATTTCCAGGATAAGG**A**AGTAAAAGGTAGGCAAAGGCAAAGG

The seed binding site is depicted in red, the point mutation is bold.

Table 16. Primer designed for bisulfite sequencing

Name	Sequence
BS_THRB_P1_F2	5′GTTTTATTGGAAAGGAAGGATTAGG
BS_THRB_P1_R2	5′AACCAACAAATCTACAAAACAACTTC-biotin
BS_THRB_P1_S2	5′ATTAATAAATTATATGGGTTTTTGG
BS_THRB_P2_F1	5′AAGATAGAAGAGAGTTGGAAGTTAAG
BS_THRB_P2_R1	5′TATTACATTTCCATCCTACCTCTAACC-biotin
BS_THRB_P2_S	5′AGTTTGTTTATTTAAGAGGTT
THRB P3_2 F1	5′GGTTAGGTTTAGAGGAAAGTTAAAAAGTA-biotin
THRB P3_2 R1	5′TACACCACTCTACATTCCTCATAATCTC
BS_THRB_P3_S3	5′TTTAGAAAAGGATGATTTAGTTTAT
BS_MIR34AHG_P2_F1	5′GGGTTGTAGGGGTGATTTGGT
BS_MIR34AHG_P2_R1	5′TACCCCATACTCCCCCCTATA-biotin
BS_MIR34AHG_P2_S2	5′GGTGGGAAGGGATAT

Table 17. List of primer for measuring of mRNA expression levels using SYBR green

Name	Sequence	Species
hTHRA_qPCR_f	5′AGGTCACCAGATGGAAAGCG	Human
hTHRA_qPCR_r	5′AGTGATAACCAGTTGCCTTGTC	
HsTHRB_FcDNA	5′TGGGACAAACCGAAGCACTG	Human
HsTHRB2_RcDNA	5′TGGCTCTTCCTATGTAGGCAG	
HsDIO1_FcDNA	5′GTCGTGGGTAAAGTGCTTCTG	Human
HsDIO1_RcDNA	5′GTTCCGCTTGACTCTGTCTGG	
hSLC10A1_qPCR_f	5′AAGGACAAGGTGCCCTATAAAGG	Human
hSLC10A1_qPCR_r	5′TTGAGGACGATCCCTATGGTG	
HsSLC16A2_FcDNA	5′CCACGCCTACGGTAGAGAC	Human

Name	Sequence	Species
HsSLC16A2_RcDNA	5′CAGAGTTATGGATGCCGAAGATG	
HsCASC3_FcDNA	5′ACCTCGGAAAGGGCTCTTCTT	Human
HsCASC3_RcDNA	5′CGACCCTCATCCTTCCATAGC	
CYP7A1_qPCR_F	5′AGCATTGACCCGATGGATGG	Human
CYP7A1_qPCR_R	5′TCCGTGAGGGAATTCAAGGC	
hCYP27A1_F	5′CAGCACGACCTGACCTATGG	Human
hCYP27A1_R	5′TGGTCCAGTCGAGTCATAAAGT	
hTHRSP_F	5′CAGGTGCTAACCAAGCGTTAC	Human
hTHRSP_R	5′CAGAAGGCTGGGGATCATCA	
hFASN	5′AAGGACCTGTCTAGGTTTGATGC	Human
hFASN	5′TGGCTTCATAGGTGACTTCCA	
Malic enzyme 1 F	5′GAAAGAGGTGTTTGCCCATGA	Human
Malic enzyme 1 R	5′AATTGCAGCAACTCCTATGAGG	
TRa1 fwd	5′GTGACTGACCTCCGCATGAT	Mouse
TRa1 rev	5′ATCCTCAAAGACCTCCAGGAA	
TRa2 fwd	5′GTCTCTGACGCCATCTTTGA	Mouse
TRa2 rev	5′ACAACATGCATTCCGAGAAG	
TRb1 fwd	5′ACACCTTATCCAGGCCACTT	Mouse
TRb 1 rev	5′GTGGTACCCTGTGGCTTTGT	
B2m_F	5′CCCCACTGAGACTGATACATACG	Mouse
B2m_R	5′CGATCCCAGTAGACGGTCTTG	
Dio1_frw	5′GCTGAAGCGGCTTGTGATATT	Mouse
Dio1_rev	5′GTTGTCAGGGGCGAATCGG	
Slc10a1 frw	5′CAAACCTCAGAAGGACCAAACA	Mouse
Slc10a1 rev	5′GTAGGAGGATTATTCCCGTTGTG	
Slc16a2 frw	5′CGGCTGGATAGTGGTGTTTG	Mouse
Slc16a2 rev	5′CAGAGTTATGGATGCCGAAGATG	
Acc frw (Acaca)	5′ATGGGCGGAATGGTCTCTTTC	Mouse
Acc rev (Acaca)	5′TGGGGACCTTGTCTTCATCAT	
Actb_frw	5′ACTGAGCTGCGTTTTACACCC	Mouse
Actb_rev	5′TGCTCCAACCAACTGCTGTC	

Table 18. List of primers used for miRNA expression measurement

Name	Sequence
hsa-miR-34a-5p	5′GGCAGTGTCTTAGCTGGTTGTAAAA
hsa-miR-155-5p	5′TGCTAATTGTGATAGGGGTAAAAA
hsa-miR-224-3p	5′TGGTGCCCTAGTGACTACAAAA
hsa-miR-24-3p	5′TGGCTCAGTTCAGCAGGAACA

Table 19. List of TaqMan Advanced Assays used for miRNA expression measuring

ID	Gene	Dye
478048_mir	miR-34a-5p	FAM
478050_mir	miR-34b-5p	FAM
478052_mir	miR-34c-5p	FAM
477992_mir	miR-24-3p	FAM
483064_mir	miR-155-5p	FAM
478780_mir	miR-224-3p	FAM
477855_mir	miR-122-5p	FAM

5.2.9. Mimics and inhibitors

MicroRNA mimics and inhibitors were purchased from Life Technologies, Carlsbas, US.

Table 20. List of miRNA mimics and inhibitors

ID	Mature miRNA
MC11030	hsa-miR-34a-5p
MH11030	miR-34a-5p inhibitor
MC15149	miR-224-3p
MC28440	miR-155-5p
MH28440	miR-155-5p inhibitor

5.2.10. Vectors and plasmids

For Luciferase assays the pmirGLO vector from Promega (Madison, US) was used, which is specifically designed for qualitative measurement of miRNA activity. The plasmid contains the firefly luciferase gene with a multiple cloning site at the 3’ untranslated region (UTR) to insert the potential

miRNA binding site. Firefly luciferase is used to measure miRNA binding while the *Renilla* luciferase is used for normalization.

For testing of possible tags at the C-terminus of the THRB gene plasmids were designed using VectorBuilder (Chicago, US). The vector contained a human cytomegalovirus immediate early enhancer/promotor (CMV) region, followed by the Kozak translation initiation sequence, which is immediately followed by the THRB sequence [NM_001128176.3]. For the THRB-6xHis and the THRB-3xFLAG plasmids His-Tags and FLAG-Tags were added respectively, before the stop codon of the THRB sequence.

Table 21. List of luciferase plasmids

Name	Contents
pmirGLO-THRA-34a-2	pmirGLO vector with insert of THRA 3'UTR of potential miR-34a-5p binding site 2
pmirGLO-THRB-6mer-34a	pmirGLO vector with insert of THRB 3'UTR at potential miR-34a-5p 6mer seed binding site
pmirGLO-DIO1-7mer-34a	pmirGLO vector with insert of DIO1 3'UTR of potential miR-34a-5p
pmirGLO-SLC10A1-7mer-34a	pmirGLO vector with insert of SLC10A1 3'-UTR at possible miR-34a-5p 7mer seed binding site
pmirGLO-THRB-6mer-34a-QC	pmirGLO-THRB-6mer-34a vector with point mutation in seed sequence

5.2.11. Mouse models

5.2.11.1. Metformin treated high-fat diet mouse model

The metformin mouse experiment was performed by Natalie Taege [251]. Male C57BL/6N mice were randomized into a chow diet and a high-fat diet (HFD) for 12 weeks. The HFD mice were again randomized into two groups and fed HFD for an additional 6 weeks during which one HFD group was treated with metformin (250 mg/kgBW/day). Mice were sacrificed after 18 weeks, anesthesia with isoflurane followed by decapitation, tissue was removed, snap-frozen and stored at -80°C.

5.2.11.2. Choline deficient high-fat diet (CD-HFD) mouse model

The mouse model was conducted in the lab of Rubén Nogueiras at the University of Santiago de Compostela in Spain. Eight week old male C57 BL/6J mice had *ad libitum* access to standard diet (STD) or choline-deficient and high fat diet (D05010402, Research diet, containing 45% fat). Mice were sacrificed after 6 weeks (standard diet n = 6, CD-HFD n = 7), after 16 weeks (standard diet n = 8, CD-HFD n = 10) and after a total of 52 weeks (standard diet n = 8, CD-HFD n = 9) [252–255]. The model was used to mimic MASLD progression from steatosis to steatohepatitis.

5.2.11.3. Methionine choline deficient diet (MCDD) mouse model

The mouse model was conducted in the lab of Rubén Nogueiras at the University of Santiago de Compostela in Spain [252–255]. Eight week old male C57 BL/6J mice were fed an STD (n = 5) or methionine-choline deficient diet (A02082002BR, Research diets) for 6 weeks to detect fibrosis.

5.2.11.4. Carbon tetrachloride (CCl_4) treated mouse model

The mouse model was conducted in the lab of Rubén Nogueiras at the University of Santiago de Compostela in Spain [253–255]. Eight week old male C57 BL/6J mice had *ad libitum* access to STD and injected with either 0.6 mL/kg carbon tetrachloride (CCl_4) (n = 6) or only the vehicle corn oil (VEH) (n = 6) one a week for 6 weeks to induce liver fibrosis.

5.2.12. Bacteria

For transformations NEB5α competent *E.coli* (high efficiency), a derivate of *E.coli* K12, from New England Biolabs, Ipswich, US were used.

Genotype: *fhuA2Δ(argF-lacZ)U169 phoA glnV44 Φ80Δ(lacZ)M15 gyrA96 recA1 relA1 endA1 thi-1 hsdR17.*

5.2.13. Cell lines

Cell line	Manufacturer	Description
BIHi005-A	Berlin Institute of Health, Berlin, Germany	Epithelial derived stem cells from male donor
BIHi001-B	Berlin Institute of Health, Berlin, Germany	Epithelial derived stem cells from male donor
HepG2	American Type Culture Collection, Manassas, US	Hepatoblastoma cells of a 15 year old male Caucasian patient.
HEK298T	American Type Culture Collection, Manassas, US	Human embryonic kidney cells derived from a female fetus.
Huh-7	CLS Cell line Service, Eppelheim, Germany	Hepatocyte carcinoma cells from a 57 year old Japanese male.

5.2.14. Hardware

Analysis, statistics and assay designs were performed on Dell Inspiron 15 700 (Intel® Core™ i7-10750H CPU 2.60GHz, 16 GB RAM)

5.2.15. Software

Name	Manufacturer	Version
BioRender	BioRender, Toronto, CA	
GraphPad Prism 10	GraphPad Software Inc, US	v10.2.1
Office 365	Microsoft Corporation, Redmond, US	
PyroMark Q48 Autoprep	Qiagen, Venlo, NL	v2.4.2
PyroMark Assay Design	Qiagen, Venlo, NL	v2.0.1.15

Name	Manufacturer	Version
QuantStudio Desktop qPCR	Applied Biosystems, Foster City, US	v1.3.1
RStudio, statistic and modeling	RStudio, Inc, Boston, US	v4.3.1
Unipro UGENE, molceular biology	(Okonechnikov et al., 2012) and NCIT	V41.0
	UNIPRO, LLC, Novosibirsk, RU	
Jamovi	Open source	v.1.8.1

5.3. Methods

5.3.1. Target gene prediction of miRNAs and RNA folding of 3'UTRs

Target genes for miR-34a-5p were predicted as described previously [256].

For prediction of RNA secondary structure for analysis of 3'UTR binding of miRNAs CentroidFold was used [257,258]

5.3.2. RNA extraction from liver tissue

RNA was extracted from approximately 15 mg frozen liver tissue using the miRNeasy mini Kit as indicated by the manufacturer. The liver sample was transferred into a 2 ml screw cap microtube with 5 ceramic beads and 700 µl QIAzol Lysis Reagent added. The samples were homogenized using the Bead Ruptor 24 shaking on intensity 5, twice for 20 seconds and placed at room temperature for 5 minutes. 120 µl Chloroform was added to the tubes and the samples vigorously shaken for 15 seconds before pacing the samples for 3 min at room temperature. For phase separation the samples were centrifuged for 15 min at 4 °C and 12 000 x g. Afterwards, the aqueous phase was transferred to a new microtube and 1.5 volumes of ethanol were added and mixed. The samples were transferred to a column, washed and the flow-through was discarded. The RNase-Free DNase Set was used for on-column DNA digestion of the liver samples, which was performed as per manufacturer instructions. 10 µl of DNase I were diluted with 70 µL RDD buffer, gently mixed and pipetted directly onto the column membrane. Digestion was performed at room temperature for 15 min, afterwards, the samples were washed and the flow-through discarded. Elution of purified RNA was done using 50 µL of RNase-free water. The concentration of the samples was measured using the NanoDrop, the 260/280 and 260/230 ratios were utilized to ascertain RNA quality. All RNA samples were stored at -80 °C until further use.

RNA extraction of human liver samples was performed by Christin Krause.

5.3.3. RNA extraction from cell culture

For RNA extraction from cells, the miRNeasy mini Kit was used to the specifications of the manufacturer. Cells from a 6-well plate were washed with 1 mL PBS and then lysed using 700 µL QIAzol Lysis Reagent. The cell lysate was transferred to a microtube and 120 µL chloroform was added. The RNA extraction and DNA digestion was further performed as described above (5.3.1). The RNA was eluted in 30 µL RNase-free water and stored at -80 °C until further use.

5.3.4. Synthesis of mRNA-cDNA

For analysis of mRNA expression levels, the RNA first has to be reverse transcribed into complementary DNA (cDNA). To prevent RNA degradation, due to the unstable nature of RNA, the protocol is performed on ice and the workplace and tools were treated with RNaseZAP™ to create a RNase free environment. For cDNA synthesis the High Capacity cDNA Synthesis Kit was used as indicated by the manufacturer. For each reaction 1 µg of RNA was used in a total reaction volume of 20 µL. Each reaction furthermore contained 2 µl 10x RT Buffer, 0,8 µL 25x dNTPS Mix (100 mM), 2 µL 10x Random Primers, 1 µL Multiscribe RT, 1 µL RNase Inhibitor and nuclease-free water. The reverse transcription (RT) was performed in a thermal cycler for 10 min at 25 °C, 120 min at 27 °C and the reverse transcriptase was heat inactivated at 85 °C for 5 min. Each experiment included a no enzyme (NoRT) and a no template control (NTC). The stock cDNA concentration was 50 ng/µL, which was diluted 1:10 to a final concentration of 5 ng/µL for gene expression analysis using quantitative real time Polymerase chain reaction (qRT-PCR). The cDNA was stored at -20 °C until further use.

5.3.5. Synthesis of miRNA-cDNA

For analysis of miRNA expression, the miRNAs have to be reverse transcribed into cDNA. Due to the small nature of miRNAs they have to be elongated which can be achieved by polyadenylation and adapters. Two methods were used for miRNA-cDNA synthesis, the TaqMan® Advanced miRNA cDNA synthesis kit which uses polyadenylation and adapters and the Quanta Biosciences qScript miRNA cDNA synthesis Set which uses polyadenylation.

The TaqMan® Advanced miRNA cDNA Synthesis Kit was used according to manufacturer specifications. The RNA samples were diluted to a concentration of 5 ng/µL to, 2 µL were utilized for a final RNA amount of 10 ng for the first step, where a poly(A) tail is added to the miRNA 3'end. The RNA is added to the reaction mix (Table 22) and incubated in the thermo cycler according to Table 23. To add the adaptor, which functions as forward primer binding site adaptor ligation reaction mix (Table 24) is added to the polyadenylated RNA, the ligation takes place in a thermal cycler as described in Table 25. For reverse transcription of RNA into DNA the reverse transcription reaction mix (Table 26) was added to the RNA and the reaction was run on a thermal cycler with the program described in Table 27. In the final step the cDNA is amplified (miR-Amp), 5 µL of the reverse transcription product was used in the reaction and mixed with the miR-Amp reaction mix (Table 28) and incubated in a thermo cycler as described in Table 29. After amplification the cDNA is diluted 1:10 in RNase-free water for TaqMan® Advanced qPCR, cDNA was stored at -20°C.

Table 22. Reaction mix for TaqMan® polyadenylation

Component	Volume
10X Poly(A) Buffer	0.5 µL
ATP	0.5 µL
Poly(A) Enzyme	0.3 µL
RNase-free water	1.7 µL
Total volume	**3.0 µL**

Table 23. Program for TaqMan® polyadenylation

Step	Temperature	Time
Polyadenylation	37°C	45 minutes
Stop reaction	65°C	10 minutes
Hold	4°C	Hold

Table 24. Reaction mix for TaqMan® adaptor ligation

Component	Volume
5X DNA Ligase Buffer	3.0 µL
50% PEG 8000	4.5 µL
25X Ligation Adaptor	0.6 µL
RNA Ligase	1.5 µL
RNase-free water	0.4 µL
Total volume	**10 µL**

Table 25. Program for TaqMan® adaptor ligation

Step	Temperature	Time
Ligation	16°C	60 minutes
Hold	4°C	Hold

Table 26. Reaction mix for TaqMan® reverse transcription

Component	Volume
5X RT Buffer	6.0 µL
dNTP Mix (25 mM each)	1.2 µL
20X Universal RT Primer	1.5 µL
10X RT Enzyme Mix	3.0 µL
RNase-free water	3.3 µL
Total volume	**15 µL**

Table 27. Program for TaqMan® reverse transcription

Step	Temperature	Time
Reverse transcription	42°C	15 minutes
Stop reaction	85°C	5 minutes
Hold	4°C	Hold

Table 28. reaction mix for TaqMan® miR-Amp reaction

Component	Volume
2X miR-Amp Master Mix	25 µL
20X miR-Amp Primer Mix	2.5 µL
RNase-free water	17.5 µL
Total Volume	**45 µL**

Table 29. Program for TaqMan(R) miR-Amp reaction

Step	Temperature	Time	Cycles
Enzyme activation	95°C	5 minutes	1
Denature	95°C	3 seconds	14
Anneal/Extend	60°C	30 seconds	
Stop reaction	99°C	10 minutes	1
Hold	4°C	Hold	1

The Quanta Bioscience qScript miRNA cDNA Synthesis Set was used according to manufacturer's specification. 1 µg of RNA was utilized for the polyadenylation reaction (Table 30) and incubated as described in Table 31. For reverse transcription the reaction mix as described in Table 32 and the incubation program in Table 33 were used. The resulting cDNA was stored at -20°C and diluted 1:10 in RNase-free water for qPCRs.

For both cDNA synthesis methods, each experiment contained a no reverse transcriptase and a no template control.

Table 30. Reaction mix for Quanta Bioscience qScript polyadenylation reaction

Component	Volume
5x Poly-A Buffer	2 µL
RNA (1 µg)	x µL
Nuclease-free water	x µL add to end volume
Poly-A Polymerase	1 µL
Total Volume	**10 µL**

Table 31. Program for Quanta Bioscience qScript polyadenylation reaction

Step	Temperature	Time
Polyadenylation	37°C	60 minutes
Stop reaction	70°C	5 minutes
Hold	4°C	Hold

Table 32. Reaction mix for Quanta Bioscience reverse transcription

Component	Volume
Polyadenylated RNA	10 µL
miRNA cDNA Reaction Mix	9 µL
qScript RT	1 µL
Total Volume	**20 µL**

Table 33. Program for Quanta Bioscience reverse transcription

Step	Temperature	Time
Reverse transcription	42°C	20 minutes
Heat deactivation	85°C	5 minutes
Hold	4°C	Hold

5.3.6. qRT-PCR

Quantitative real time PCR (qRT-PCR) was used to measure expression levels of miRNAs and mRNAs. The SYBR green system was used to measure relative mRNA expression(Table 34, Table 35), while both the SYBR Green system (Table 38,Table 39) and TaqMan® assays (Table 36,Table 37) were utilized for quantitative analysis of miRNAs. For normalization of mRNA expression CASC3 was used as a housekeeper for human derived samples and ActinA/B2m for mouse samples. Expression of miRNA was normalized to miR-24-3p in human and mice. Analysis was performed using the Pfaffl method [259].

Human cohort miRNAs were measured by Veronika Hartman and mRNAs by Christin Krause.

Table 34. Reaction mix for mRNA-cDNA SYBR green qRT-PCR

Component	Volume
Forward Primer (10 µM)	0.5 µL
Reverse Primer (10 µM)	0.5 µL
FastStart Universal SYBR Green Master (ROX)	5.0 µL
cDNA (5 ng/µl)	4.0 µL
Total Volume	**10 µL**

Table 35. Program for mRNA-cDNA qRT-PCR with melt curve analysis

Step	Temperature	Time	Cycle
Initial denaturation	95°c	10 minutes	1
Denaturation	95°C	15 seconds	40
Elongation	60°C	1 minute	
Melt Curve Stage			
Denaturation	95°C	15 seconds	1
Elongation	60°C	1 minute	
Denaturation	95°C	1 second	

Table 36. Reaction mix for TaqMan® qRT-PCR

Component	Volume
TaqMan® Fast Advanced Master Mix (2X)	5 µL
TaqMan® Advanced miRNA Assay (20X)	0.5 µL
RNase-free water	0.5 µL
Diluted cDNA sample	4.0 µL
Total Volume	**6 µL**

Table 37. Program for TaqMan® qRT-PCR

Step	Temperature	Time	Cycle
Enzyme activation	95°C	20 seconds	1
Denature	95°C	3 seconds	40
Anneal/Extend	60°C	30 seconds	

Table 38. Reaction mix for miRNA-cDNA SYBR green qRT-PCR

Component	Volume
Specific miRNA Assay Primer (10µM)	0.2 µL
PerfeCta Universal Primer (10 µM)	0.2 µL
Roche SYBR Green	5.0 µL
Nuclease-free water	0.6 µL
miRNA-DNA (2.5 ng/µl)	4.0 µL
Total volume	**10 µL**

Table 39. Program for miRNA-cDNA SYBR green qRT-PCR

Step	Temperature	Time	Cycle
Activation	95°C	2 minutes	1
Denature	95°C	5 seconds	40
Annealing	60°C	15 seconds	
Extension	70°C	15 seconds	
Melt curve			

5.3.7. Cultivation of cells

All immortalized cancer cell lines were kept at 37°C with 5% CO_2 and 90% humidity. Cells were thawed by transferring the cells from a cryotube into 9 ml of their respective pre-warmed maintenance medium, followed by centrifugation for 5 min at 300 xg. The old medium was discarded and the cell pellet was resuspended in 12 ml maintenance medium and transferred into a T75 cell culture flask. Medium was changed three times a week and cells were sub cultivated 1:10 after reaching 80% confluency. Detachment of cells was reached by cultivating with trypsin for 5-20 min at 37°C, depending on cell line and then diluted in maintenance medium

5.3.8. Differentiation of iPSC derived hepatocytes

The human pluripotent stem cells were acquired from Katarzyna Ludwik from Charite, Berlin, Germany. The protocol for differentiation into hepatocytes was developed by Ludwik et al. (unpublished). To prevent spontaneous differentiation and increase efficiency of definite endoderm (DE) differentiation, iPSCs were first adapted to ROCK inhibitor (ROCKi). Frozen aliquots of ROCKi adapted iPSCs, containing $1.5x10^6$ cells/mL, were thawed in a water bath at 37°C, the cells were then transferred into 10 ml of prewarmed mTeSR medium with ROCKi and centrifuged for 5 minutes at 300 xg. For expansion of the cells the pellet was resuspended in 10 ml mTeSR+ROCKi medium and plated on a Geltrex coated 10 cm tissue culture dish. The cells were cultivated until they reached 70-80% confluence and then passaged using accutase. Medium was changed daily, except on Saturday the cells were given double the amount of medium, negating the feeding on Sunday. On day 0 of the differentiation scheme (Table 40) the cells were replated onto a 6 well plate with $1.3x10^3$ cells/well. For differentiation the medium was changed daily according to schedule with different media used for differentiation into endoderm and mature hepatocyte-like cells. At day 7 of the differentiation the cells were tested for their differentiation status using flow cytometry. The marker CXCR4 was used to check for definite endoderm, the differentiation was continued if more than 90% of cells contained CXCR4. After the differentiation completed on day 28 the cells were directly used for experiments.

Table 40. Feeding schedule for iPSC differentiation

Day	Weekday	Media	Action	Additional Steps
-5	Thursday	mTeSR+Ri	Thawing	
-4	Friday	mTeSR+Ri	Media Change	
-3	Saturday	mTeSR+Ri	Media Change	Double feeding
-2	Sunday	mTeSR+Ri		
-1	Monday	mTeSR+Ri	Media Change	
0	Tuesday	mTeSR+Ri	Replating	
1	Wednesday	DE-in.media +NaBut	Media Change	
2	Thursday	DE-in.media +NaBut	Media Change	
3	Friday	DE-in.media +NaBut	Media Change	
4	Saturday	DE-in.media +NaBut	Media Change	Double feeding
5	Sunday	DE-in.media +NaBut		
6	Monday	DE-in.media **-NaBut**	Media Change	

Day	Weekday	Media	Action	Additional Steps
7	Tuesday	KO-media	Media Change	FACS d7
8	Wednesday	KO-media	Media Change	
9	Thursday	KO-media	Media Change	
10	Friday	KO-media	Media Change	
11	Saturday	KO-media	Media Change	Double feeding
12	Sunday	KO-media		
13	Monday	KO-media	Media Change	
14	Tuesday	HBM-Media	Media Change	
15	Wednesday	HBM-Media	Media Change	
16	Thursday	HBM-Media	Media Change	
17	Friday	HBM-Media	Media Change	
18	Saturday	HBM-Media	Media Change	Double feeding
19	Sunday	HBM-Media		
20	Monday	HBM-Media	Media Change	
21	Tuesday	Bullet Kit	Media Change	
22	Wednesday	Bullet Kit	Media Change	
23	Thursday	Bullet Kit	Media Change	
24	Friday	Bullet Kit	Media Change	
25	Saturday	Bullet Kit	Media Change	Double feeding
26	Sunday	Bullet Kit		
27	Monday	Bullet Kit	Media Change	
28	Tuesday	Bullet Kit	Harvest/Experiment	

5.3.9. Metabolomic treatment of cells

Cells were treated with different concentrations of fructose over different time periods. Fructose was dissolved in either cell line specific maintenance medium or transfection medium, if cells were simultaneously transfected with miRNA mimic or inhibitor.

For treatment with oleate palmitate a 10% BSA solution was prepared over night. All materials were prewarmed to 50°C and palmitate and oleate salts were each weighed in 1.5 ml microtubes and dissolved in 0.1 M NaOH at 50°C for approximately 10 minutes. Dissolved palmitate and oleate were each transferred to prewarmed BSA solution for a final concentration of 5 mM in 7.5% BSA. For control a 7.5% BSA solution was prepared with 0.1 M NaOH. Cells were treated with a total oleate and palmitate concentration of 0.5 mM with 0.167 mM palmitate and 0.33 mM oleate for different time durations. The fatty acids were added to the cell specific maintenance medium.

For high glucose treatment DMEM high glucose medium 4.5 g/L was used without further dilution.

Insulin treatment was performed with Humalog (Eli Lilly) and was freshly added daily to the treated wells. A final concentration of 100 nM and 500 nM was used in the experiments, though iPSC derived hepatocyte-like cell experiments used an estimated insulin concentration due to the unknown insulin concentration in the Bullet Kit™ medium.

All experiments were conducted with cell passages between P10-25.

5.3.10. Transfection of miRNA mimics

For transfection of cells with miRNA mimics and inhibitors, 200.000 cells were seeded per well on a 6-well plate. Transfection was performed on day of cell seeding. MiRNA mimics and inhibitors were diluted to a concentration of 10 µM. For the transfection reaction 2.5 µL RNAiMAX were mixed with 250 µL Opti-MEM, the mixture was incubated at room temperature for 5 minutes. In the meantime 2.5 µL of mimic/inhibitor were used per reaction and mixed with 250 µL Opti-MEM. Both reactions were mixed and incubated another 20 minutes at room temperature. After incubation 500 µL reaction mixture were added to the cells and incubated for 24 or 48 hours, depending on the experiment

For experiments with additional T_3 stimulation HepG2 cells were kept in FBS stripped medium for 48 hours before transfection and after. T_3 was added daily with fresh medium with an end concentration of 10 nM or 50 nM, NaOH was used for 0 nM control.

5.3.11. Polymerase chain reaction (PCR)

For amplification of genomic DNA two different polymerases were used. For amplification of inserts (Table 41, Table 42) and QuickChange PCR (Table 43, Table 44) the Pfu (Phusion Hotstart II) polymerase was used, due to the proofreading function. Purification of inserts was done using a 1% agarose gel SYBR Safe (1:10.000) and the Wizard SV Gel and PCR clean up System, while plasmids were directly purified with the clean-up System. The purification was done according to manufacturer's instructions.

Colony PCRs, for selection of positive bacteria clones for sequencing, were done using Taq polymerase (GoTaq). For the colony PCR, bacteria colonies were picked and transferred into 15 µL 1xTE buffer and lysed for 5 min at 95 °C. The lysate was centrifuged at full speed for 10 minutes and 8 µl of the supernatant transferred to a new tube. The colony PCR was performed as described in Table 45 and Table 46.

Table 41. Reaction mix for amplification of inserts

Components	Volume
2X Pfu Master Mix	25 µL
Forward primer (10 µM)	1 µL
Reverse primer (10 µM)	1 µL
DNA (50 ng/µL)	2.5 µL
Nuclease-free water	20.5 µL
Total volume	50 µL

Table 42. Program for amplification of inserts

Step	Temperature	Time	Cycle
Initial denaturation	98 °C	30 seconds	1
Denaturation	98 °C	10 seconds	35
Annealing	x °C	10 seconds	
Elongation	72 °C	15 s/kb	
Final elongation	72 °C	5 minutes	1
Hold	4 °C		

15-30 s/kb Annealing depending on primer

Table 43. Reaction mix for QuickChange PCR

Components	Volume
Pfu Master Mix	25 µL
Forward primer (10 µM)	1 µL
Reverse primer (10 µM)	1 µL
Plasmid (10 ng/µL)	1 µL
Nuclease-free water	22 µL
Total volume	50 µl

Table 44. Program for QuickChange PCR

Step	Temperature	Time	Cycle
Initial denaturation	98 °C	30 seconds	1
Denaturation	98 °C	30 seconds	12
Annealing	55 °C	1 minute	
Elongation	72 °C	1 min/kb	
Final elongation	72 °C	10 minutes	1
Hold	4 °C	Hold	

Table 45. Reaction mix for colony PCR

Component	Volume
GoTaq Master Mix	5 µL
Forward primer (10 µM)	0.4 µL
Reverse primer (10 µM)	0.4 µL
Nuclease-free water	2.2 µL
Supernatant	2 µL
Total volume	10 µL

Table 46. Program for colony PCR

Step	Temperature	Time	Cycle
Initial denaturation	95 °C	2 minutes	1
Denaturation	95 °C	3 seconds	30
Annealing	x °C	30 seconds	
Elongation	72 °C	1 minute	
Final elongation	72 °C	5 minutes	1
Hold	4 °C	Hold	

5.3.12. Ligation and restriction digestion

To prepare inserts and vectors for ligation both were digested with the restriction enzymes NotI and XhoI according to Table 47 and Table 48. After digestion 0.25 µL of Quick CIP enzyme was added to the reaction mix containing the vector and incubated first for 10 min at 37°C and heat activated at 80 °C for 20 min to dephosphorylate the vector and prevent relegation without insert. Insert and vector were purified after digestion on Millipore membranes.

Table 47. Reaction mix for vector and insert digestion

Component	Volume
NotI	1 µL
XhoI	1 µL
Cut Smart	5 µL
Nuclease-free water	x
Insert (200 ng) or vector (1 µg)	x
Total volume	50 µL

Table 48. Program for vector and insert digestion

Step	Temperature	Time
Digestion	37 °C	15 minutes
Deactivation	65 °C	20 minutes

For ligation the Quick Ligation Kit was used, vector and insert were added to the reaction mix (Table 49) in a 1:3 ratio and incubated for 15 minutes at room temperature. The plasmids were then stored at -20°C or directly used for transformation (see 5.3.12)

Table 49. Reaction mix for ligation

Component	Volume
Quick ligation buffer	10 µL
Quick ligase	1 µL
Vector (50 ng)	x µL
Insert (x ng)	x µL
Nuclease-free water	x µL
Total volume	20 µL

5.3.13. Transformation and cloning

Transformation was carried out using 50 µL NEB5α competent *E. Coli* with 5 µL of ligation mix, after 30 min incubation on ice heat shock was performed for 30 s at 42°C on a heat block. After heat shock the bacteria were placed on ice for 5 min. 250 µL room temperature SOC medium was added and the bacteria incubated 1.5 h at 37°C shaking at 300 rpm. After incubation 100 and 200 µL bacteria were spread on agar plates containing ampicillin and incubated at 37°C overnight.

Transformation was confirmed using sanger sequencing and colony PCR (see 5.3.10). Agar plates were stored at 4°C up to six weeks.

5.3.14. Mini and Midi plasmid preparation

Miniprep was performed using the QIAprep® Spin Miniprep Kit according to manufacturer's instructions for centrifuge processing. The midiprep was performed using the Qiagen Plasmid Midi Kit was performed according to the manufacturer's centrifugation instructions, with the following deviations. Samples were centrifuged at 7197 xg instead of 20,000 xg for 30 min at 4°C, after centrifugation the supernatant was filtered using a pleated Whatman filter instead of a second centrifugation step, before the supernatant was added to the column.

5.3.15. Transfection of plasmids

For Luciferase assays HEK298T cells were seeded in 96-well plates (20.000 cells/well) in HEK298T transfection medium and incubated for 24 h at 37 °C, 5% CO_2 and 90% humidity. Per well 0.25 µL of lipofectamine 2000 was mixed with 4.74 µL of Opti-MEM and incubated for 5-10 minutes. In addition 100 ng plasmid were mixed with miR-34a-5p mimic (end concentration 10 nM) in Opti-MEM in a total volume of 5 µL. Both reaction mixes were combined and incubated for 15 minutes at room temperature and 10 µL transfection mix were added to the cells. Cells were incubated for 48 h after transformation and luciferase activity was measured directly after.

To test the suitability of tags to the THRB gene Huh-7 and HEK298T cells were transfected with the respective plasmids. Cell were seeded in 6-well plates (200.000 cells/well) in transfection medium and incubated for 24 h at 37 °C, 5% CO_2 and 90% humidity. The transfection mix contained 2 µL Lipofectamin 3000 and 123 µL Opti-MEM per well and was incubated for 5-10 minutes. The plasmid mix contained 100 ng plasmid in Opti-MEM in a total volume of 125 µL per well. Transfection and plasmid mixtures were mixed together and incubated for 15 minutes at room temperature. 250 µL of reaction mix were added to each well already containing 2 ml transfection medium. To test the efficiency of the tag-antibodies the cells were incubated for 72 h before harvesting in PBS. To test the effect of the tags on the mRNA expression of downstream genes the cells were kept in Huh-7 stripped transfection medium after seeding for 24 h and additionally stimulated with 0, 10 and 50 nM T_3 directly after transfection. Medium was changed after 24 hours and T_3 added, after a total of 48 h after transfection the cells were harvested for RNA extraction in QIAzol.

5.3.16. Luciferase reporter assays

After transfection and incubation for 48 h (see 5.3.14) luciferase activity was measured using the Dual-Luciferase Reporter Assay in the CLARIO Star Microplate reader. Plasmids (50 ng end concentration) were transfected with either nc#1 or miR-34a-5p mimic (10 nM end concentration) into HEK298T cells as described in 5.3.15. The cells were incubated for 48 h after transfection, then the medium was removed and the cells lysed with 50 µL 1X passive lysis buffer for 15 min while gently shaking. 20 µL of lysate are used for the luciferase reaction with 50 µL LAR II and 50 µL Stop & Glo® reagent. A mock transfection was used as additional background control.

5.3.17. RNA interacting protein immunoprecipitation sequencing (RIP-seq)

For RIP-seq 1×10^6 HepG2 cells were seeded per 6-well plate well and transfected with 10 nM miR-34a-5p mimic miRVana™ as described in 5.3.10. 24 h after transfection three wells were pooled while harvesting for each experiment. The protocol of Meier et al. [180] was followed except for the following modifications: lysate and beads were incubated at 4 °C over night and protein degradation was carried out in NT2 buffer. 5 µg of both argonaut 2 (AGO2) antibodies (Abnova, clone 2E12-1C9 LOT M9221-S2 and Sigma Aldrich, clone 11A9 LOT3894983) were used. The experiment was repeated three times to generate a biological triplicate. RNA isolation was performed as described in

5.3.3. Input control samples were rRNA depleted using the RiboCop rRNA depletion Kit from Lexogen. Library prep, RNA sequencing and analysis of data was performed by Novogene (China).

5.3.18. RNA-sequencing

RNA sequencing was performed by Nathalie Kruse at the Institute of Human Genetics. The RNA was extracted as described in 5.3.3. The library was prepared using the QuantSeq 3'mRNA Seq V2 Library Prep Kit after manufacturer's instructions with the add on PCR. The quality of the RNA was verified using the Qubit 1X dsDNA HS Assay Kit according to manufacturer's protocol using the Qubit fluorometer 2.0 and the 2100 Bioanalyzer Instrument. For quantification of the library the NEBNext Library Quant Kit for Illumina was used according to manufacturer's instruction, qPCRs were performed on the Real Time PCR System and calculations were performed using the NEBbioCalculator. The NextSeq 2000 System was used for sequencing. Analysis of the RNA sequencing was performed using PathfindR [260].

5.3.19. Bisulfite pyrosequencing

DNA extraction of human liver samples and bisulfite conversion of genomic DNA was performed by Christin Krause. Genomic DNA was extracted from 25 mg frozen liver using the QIAmp DNA Mini Kit according to manufacturer's instructions with minor changes. Frozen liver tissue was homogenized in 2 ml screw cap micro tubes with ceramic beads in 80 mL ice cold DPBS with the Bead Ruptor for two times 20 sec. After shaking 180 µL ALT buffer and 20 µL Proteinase K were added and incubated for 15 to 60 min at 56°C. Digested liver samples were stored at room temperature up to 2 month before final DNA extraction. DNA extraction was performed according to manufacturer. The DNA concentrations were measured with QuantiFluor ONE dsDNA System, after manufacturer instructions. DNA was stored at -20°C until further use.

For bisulfite conversion the EpiTect Fast DNA Bisulfite Kit was used. 20 µL extracted DNA (100 to 2000 ng input) was added to 140 µL bisulfite conversion reaction according to manufacturers specifications. After preparation the DNA was denatured at 95°C for 5 min, followed by an incubation time of 30 min at 60°C, a second denaturation step at 95°C for 5 min and the final incubation at 60°C for 10 min. The converted DNA was stored at 4°C until clean-up over columns according to the instructions. Bisulfite converted DNA (BisDNA) was stored at -20°C.

To measure DNA methylation at specific CpG sites, primer were designed for bisulfite PCR using the PyroMark Assay Design 2.0 software. For each investigated CpG site three primers were designed. A forward and reverse primer pair for amplification, with one of those biotinylated and a sequencing primer. The refence genome used for primer design was human genome hg19. The PCR was conducted with the PyroMark Q48 advanced CpG PCR Reagents (Table 50) using 1 µL of bisDNA (10-20 ng) and the program in Table 51.

Table 50. Reaction mix for bisulfite PCR

Component	Volume
2X PyroMark PCR MasterMix	12.5 µL
10X CoralLoad Concentrate	2.5 µL
RNase-free water	8 µL
Forward primer 10 µM	0.5 µL
Reverse primer 10 µM	0.5 µL
Total volume	24 µL

Table 51. Program for bisulfite PCR

Step	Temperature	Time	Cycles
Initial activation	95°C	15 minutes	1
Denaturation	94°C	30 seconds	40
Annealing	56°C	30 seconds	
Extension	72°C	30 seconds	
Hold	4°C	Hold	1

5.3.20. Western blot

The HEK298T cells transfected with THRB tag plasmids were harvested in PBS (5.3.14), the pellets were lysed using the Bio-Plex®Cell lysis Kit according to manufacturer's instruction. Protein concentration was measured using the Pierce™BCA Protein Assay Kit. 20 µg of protein were loaded on a 10% SDS gel and run for 40 min at 200 V. The stain-free gel was then activated and blotted on a nitrocellulose membrane using the turbo blotter for 7 min. The blot was blocked with TBS containing 5% milk powder for 1 h at room temperature. Primary antibodies were diluted 1:500 and 1:1000 in 5% milk powder solution and incubated with the blot over night at 4°C. After incubation the blot was washed three times for 20 min with TBST buffer. The secondary antibody was diluted 1:5000 in 5% milk powder solution and incubated fir 1 h at room temperature. Afterwards, the blot was washed three times for 20 min in TBST buffer. Chemiluminescence was measured with ECL and ClarityMax. After measurement the blot was washed for 5 min in TBST and incubated for 15 min with stripping buffer at room temperature. Then the blot was washed three times for 15 min in TBST buffer at and blocked with 5% milk powder solution for 1 h at room temperature. The protocol was then repeated with housekeeper protein HSP90.

5.3.21. Statistical analysis

Human data is depicted with standard deviation (SD), mouse and cell culture data with standard error of mean (SEM). Correlations were calculated using Pearson correlations. Human hepatic expression analysis was not corrected for multiple testing and considered independent from each other due to differences in time point of measurement, assay and plate. Data was tested for normality and statistical test was selected accordingly, except methylation analysis, which was performed using Mann-Whitney test. qPCRs were analyzed using unpaired t-tests, one-way ANOVA or two-way ANOVA depending on experiment. Data was corrected for multiple testing using the false discovery rate after Benjamini-Hochberg.

6. Results

The following part of this thesis contains the results of the investigation on epigenetic changes in humans with MASH and a variety cell and mouse MASH models. This thesis concentrates on changes in microRNA (miRNA) expression and DNA methylation to unravel novel mechanisms in the MASLD pathogenesis.

6.1. microRNA

Due to the dysregulation of thyroid hormone (TH) metabolism and reduction of thyroid hormone receptor β (*THRB)* expression in patients with MASH miRNAs were identified that could potentially bind to *THRB* via their seed-sequence and correlated negatively with the *THRB* expression.

6.1.1. Hepatic expression of THRB targeting miRNAs in humans with MASH and correlation of clinical parameters

For identification of potential miRNAs a microRNA microarray 4.0 [256] was utilized to identify miRNAs that potentially bind to THRB in a sub-cohort of the human obese cohort. The expression of potential miRNAs of interest was verified using qRT-PCR (Figure 7) in the presented cohort (Table 6). Four of the measured miRNAs showed significant changes in expression, though miRNA-103-3p was not further investigated due to the reduction of miRNA expression in MASH patients. The three miRNAs with increased expression miR-34a-5p (fold change (FC) = 1.66, p-value = 0,00016), miR-224-3p (FC = 1.42, p-value = 0.037) and miR-155-5p (FC = 1.32, p-value = 0.037) were further analyzed. The results of the miR-34a-5p were previously published and figures are adapted accordingly [261].

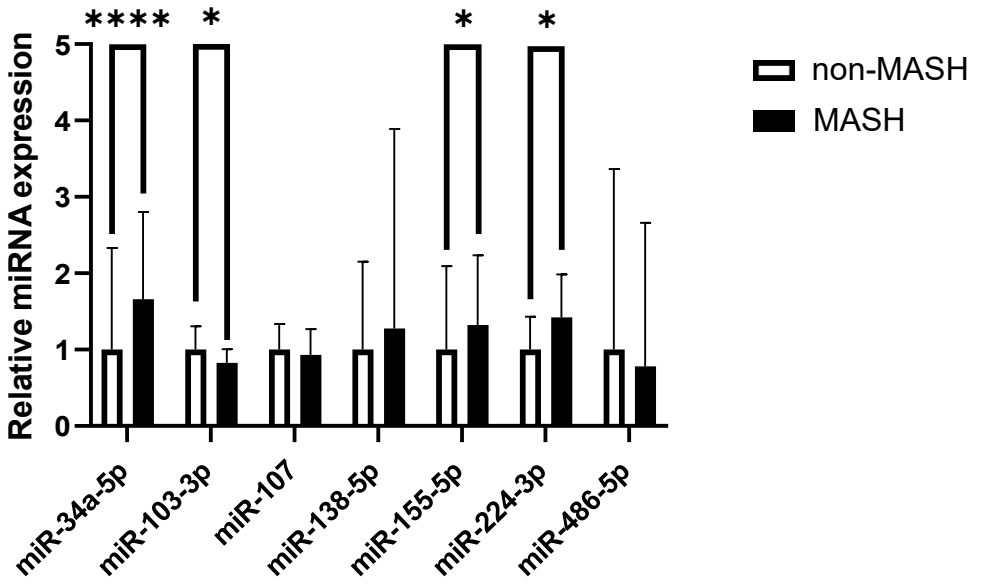

*Figure 7. Expression of potentially THRB binding miRNAs in complete cohort of humans with and without MASH. Expression normalized to miR-24-3p and control normalized to 1. Multiple t-tests. ***<0.001, *<0.05 SD. miR-34a-5p, miR-107, miR-224-3p $n_{non\text{-}MASH}$ = 41, n_{MASH} = 27, miR-103-3p $n_{non\text{-}MASH}$ = 40, n_{MASH} = 27, miR-138-5p $n_{non\text{-}MASH}$ = 32, n_{MASH} = 24, miR-155-5p $n_{non\text{-}MASH}$ = 36, n_{MASH} = 26, miR-486-5p $n_{non\text{-}MASH}$ = 20, n_{MASH} = 16. The expression of miR-34a-5p was published previously and the figure adapted to include all potential THRB targeting miRNAs* [261].

Target prediction of the three identified miRNAs proposed binding of miR-34a-5p to multiple TH metabolism related genes (*THRA, THRB, DIO1, SLC10A1, SCL16A2*), potentially master regulating the TH signaling with one miRNA. Figure 8A compares the potential binding sited of each predicted target gene with the miRNA, showing multiple potential binding sited in the *THRA*, *THRB* and *SLC16A2* genes. Target prediction proposes three binding sites for miR-224-3p in the THRB gene (Figure 8B) and multiple binding sites for the miR-155-5p in THRB and SLC16A2 each (Figure 8C).

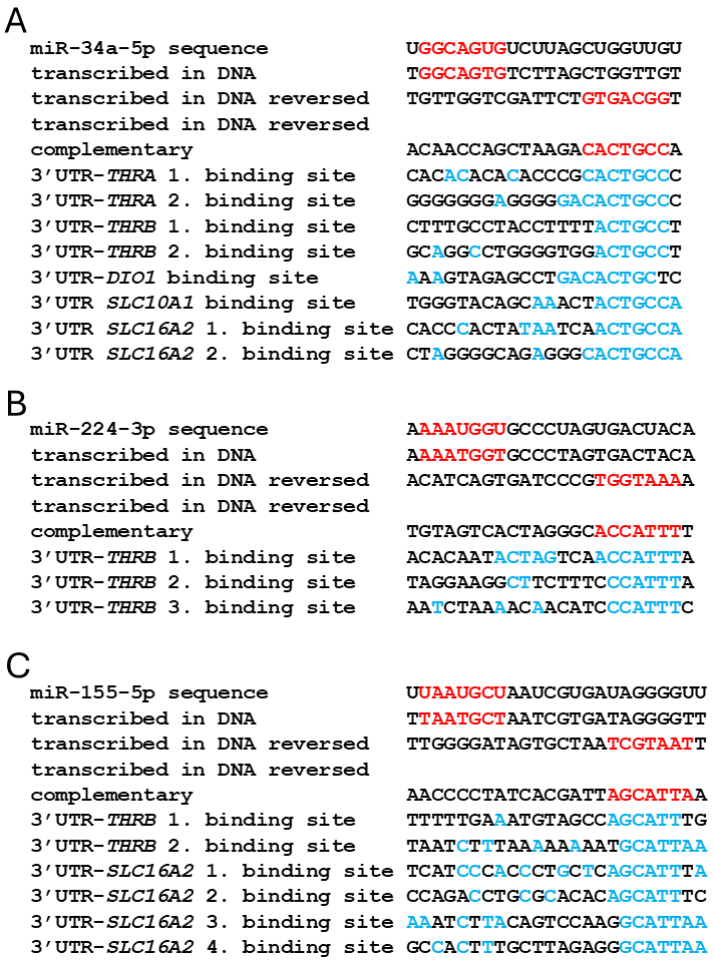

Figure 8. Potential miRNA binding sites. A) miR-34a-5p sequence compared to predicted binding sites, B) miR-224-3p sequence compared to predicted binding sites. C) miR-155-5p sequence compares to predicted binding sites.

To determine possible effects of increased miRNA expression on thyroid hormone signaling miRNA expression was correlated with TH metabolism gene expression and MASLD clinical parameter. Further, due to the association of MASLD with type 2 diabetes glucose and HbA1c were also correlated with miRNA expression. To account for confounding factors age, gender and BMI partial correlations were performed when necessary. Expression of TH genes was performed by Christin Krause [32]. MiR-34a-5p correlated negatively with *SLC10A1* (r = -0.263, p-value = 0.01) and *SLC16A2* (r = -0.419, p-value <0.001) and showed positive correlations with HbA1c (r = 0.563, p-value = 0.007), glucose (r = 0.591, p-value = 0.001), liver fat content (r = 0.565, p-value = <0.001) and MAS (r = 0.484, p-value = 0.006). Meanwhile miR-155-5p correlates with miR-224-3p expression (r = 0.397, p-value = 0.011) and miR-244-3p further correlates positively with MAS (r = 0.307, p-value = 0.009) and liver fat content (r = 0.283, p-value <0.001).

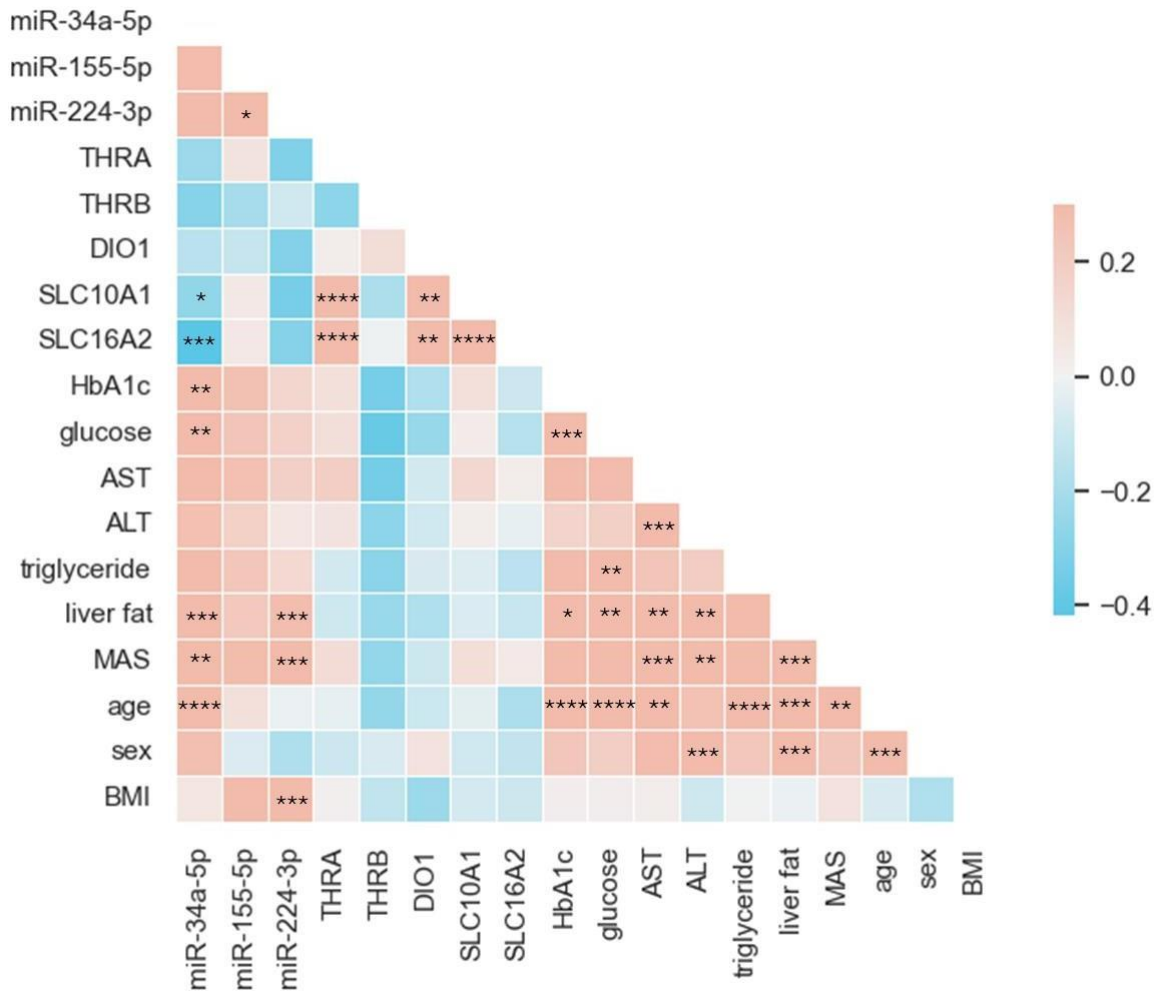

*Figure 9. Pearson correlation matrix of miR-34a-5p, miR-115-5p, miR-224-3p, TH genes and clinical parameters in human cohort. *<0.05, **<0.01, ***<0.001, ****<0.0001, adapted from* [261].

6.1.2. Mouse models

To verify the results of the results of the human cohort we utilized multiple MASLD mouse models.

In 6.1.1 the miRNAs miR-34a-5p, miR-155-5p and miR-224-3p are proposed as potential THRB binding. Since miR-224-4p is not expressed in mice liver only the other two miRNAs were investigated in the following part of this thesis.

6.1.2.1. CD-HFD mouse model

The CD-HFD mouse model was utilized to mimic the development of steatosis and steatohepatitis over a long period of time. The mice were held for 6, 16 and 52 weeks on an *ad libitum* CD-HFD or STD before sacrifice. The CD-HFD mice showed a MASH phenotype after 52 weeks [253,255].

After 16 weeks miR-34a-5p is significantly higher expressed (FC = 2.06, q-value = 0,0184) and week 52 (FC = 1.96, q-value = 0,0294) in the CD-HFD mice compared to the STD mice, while the expression of miR-155-5p significantly decreases after 16 weeks of treatment (FC = 0.26, q-value = 0.0369), before the expression increases again (Figure 10A-B). On the mRNA level expression of *Thra1* changes after 52 weeks on CD-HFD (FC = 2.33, q-value = 0,0004). The expression of *Dio1*

changes in the CD-HFD mice over the course of the treatment, after an initial induction of *Dio1* expression in week 6 (FC = 1.78, p-value = 0,003), the expression reduces back to STD level at week 16 and shows a further trend of reduction at week 52 (FC = 0.76) (Figure 10C).

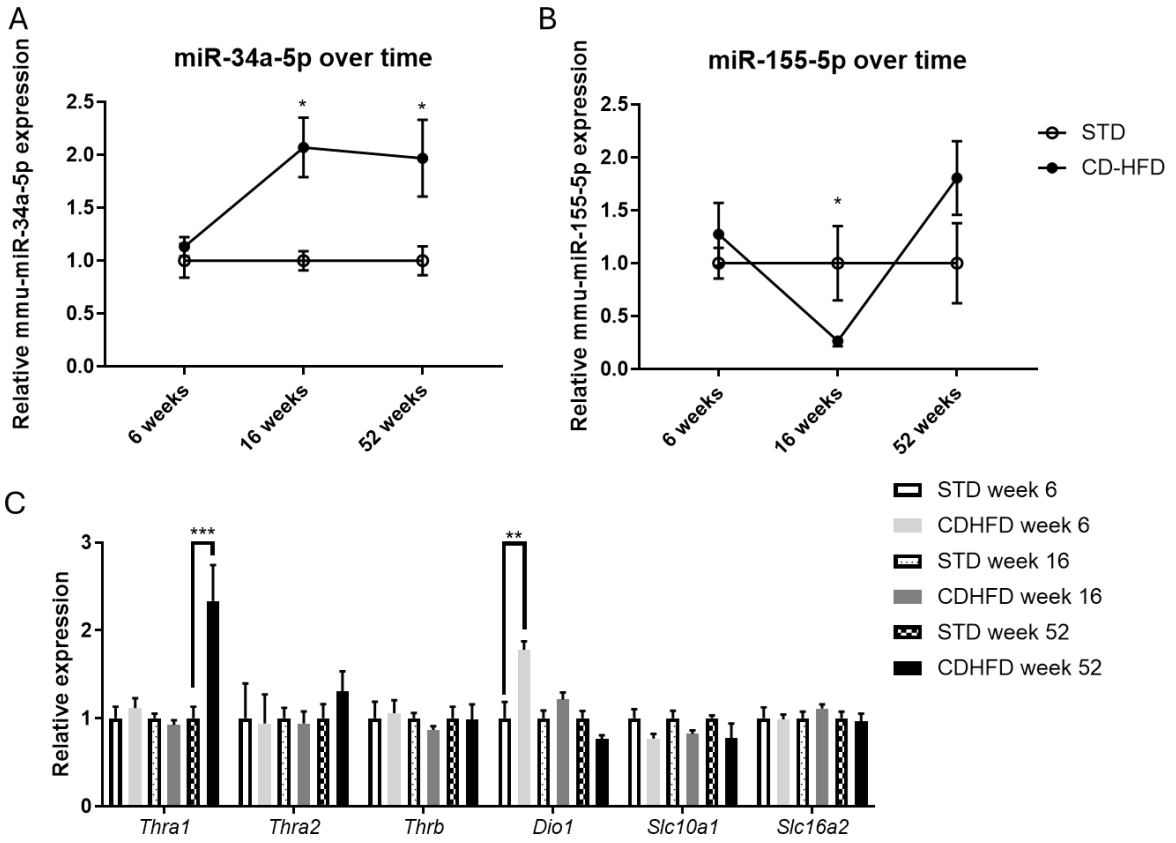

*Figure 10. Expression of miRNAs and potential target genes in CD-HFD treated mice. A) expression of miR-34a-5p measured using SYBR green and normalized to miR-24-3p. B) Expression of miR-155-5p measured using TaqMan Advanced Assay and normalized to miR-24-3p. C) Expression of TH metabolism genes normalized to actin beta. Data was analyzed using two-way ANOVA and correcting for multiple test of RNAs with Benjamini-Hochberg. Depicted is the mean with SEM. *<0.05, **<0.01, ***<0.001, ****<0.0001.*

6.1.2.2. MCDD mouse model

The MCDD mouse model was utilized as a rapid MASH onset mouse model. In contrast to other MASLD models MCDD induces impairment of liver metabolism by reduction of methionine and choline and is only suitable to study the hepatic aspect of MASLD, since other aspects of the disease e.g. metabolic syndrome do not manifest. After 6 weeks the mice exhibit a MASH phenotype (steatosis, hepatocyte ballooning, inflammation and fibrosis) [255].

Surprisingly there is no change in miR-34a-5p expression, though miR-155-5p expression is significantly increased after 6 weeks of MCDD (FC = 1.75, q-value = 0.023) (Figure 11A). Similarly expression of Thra2 is increased (FC = 2.30, q-value = 0,0004) while Slc10a1 is down regulated (FC = 0.49, q-value = 0,0078) (Figure 11B).

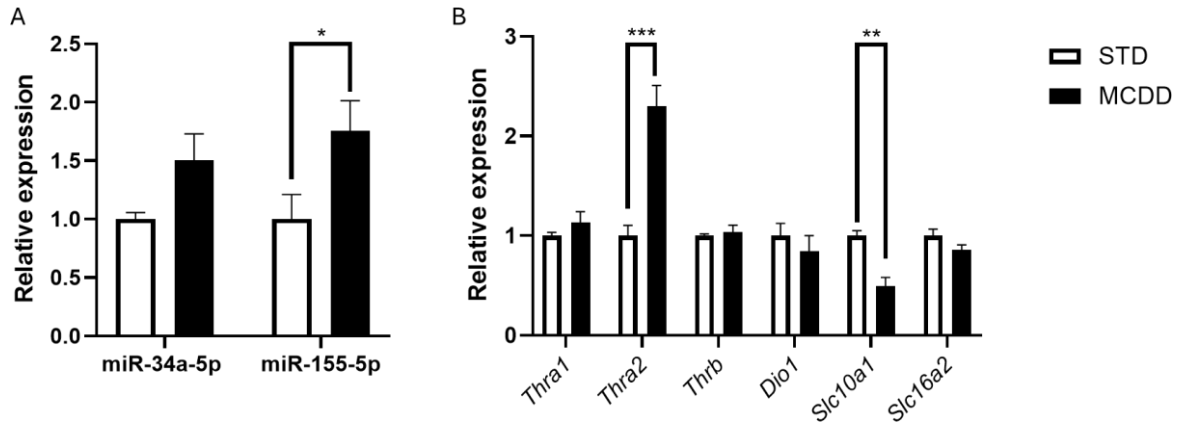

*Figure 11. Expression of miRNAs and TH metabolism genes in MCDD mice. A) Expression of miRNAs miR-34a-5p and miR-155-5p. B) Expression of potential target genes. MiRNAs were normalized to housekeeper miR-24-3p and mRNAs to beta-2-microglobulin (B2m). Data was analyzed using multiple t-tests with Benjamini-Hochberg correction. The mean with SEM are depicted. *<0.05, **<0.01, ***<0.001, ****<0.0001.*

6.1.2.3. CCl_4 mouse model

While the other mouse models are commonly used to mimic MASLD in mice, the treatment of mice with CCl_4 is used to generate acute liver injury with fibrosis, without accumulation of lipids in the liver. While the TH metabolism genes remained unchanged in their expression, miR-34a-5p was significantly induced (FC = 2.60, q-value = 0,0001) (Figure 12A). Verifying the role of miR-34a-5p not only in MASLD but generally in liver injury.

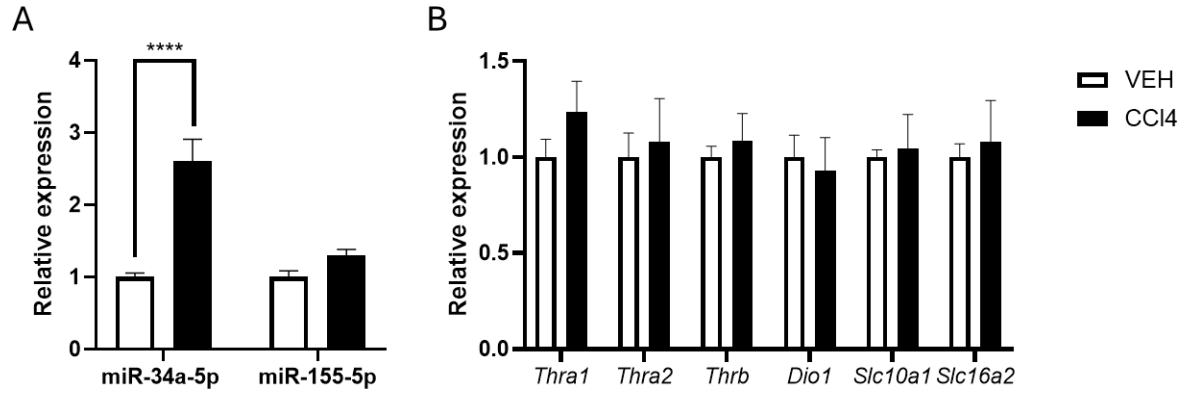

*Figure 12. Expression of miRNA and TH metabolism genes in mice treated with CCl_4. A) Expression of miRNAs, B) expression of potential miRNA target genes. MiRNAs were normalized to housekeeper miR-24-3p and mRNAs to actin beta. Data was analyzed using multiple t-tests with Benjamini-Hochberg correction. The mean with SEM are depicted. ****<0.0001.*

6.1.2.4. HFD mouse model treated with metformin

Metformin is the first line drug for type 2 diabetes treatment and acts in the liver, the reduction of liver fat is a common side effect. Therefore mice treated with a HFD and metformin were used to ascertain the effect of a common medical intervention on miRNA expression and MASH gene expression. Both HFD groups gained more weight compared to the chow control and while the increased liver triglyceride levels reduced after metformin treatment the body weight did not decrease [251].

As expected, miR-34a-5p increases under HFD significantly in both HFD groups (FC_{HFD} = 5.64, q-$value_{HFD}$ = 0.0003; $FC_{HFD\ metformin}$ = 5.72, q-$value_{HFD\ metformin}$ = 0.0003) (Figure 13A). After six weeks the untreated HFD group shows unchanged increased expression of miR-34a-5p (FC_{HFD} = 6.08, q-$value_{HFD}$ = 0.0003) while the metformin treatment group expression of miR-34a-5p is only 3.29 fold-change increased compared to chow diet fed mice (q-$value_{HFD\ metformin}$ = 0.0003). Meanwhile miR-155-5p expression slightly increases after 12 weeks of HFD in the HFD group, but not in the HFD metformin group and at week 18 miRNA levels are comparable to chow group (Figure 13A). *Thra1* and *Thra2* show a tendency of reduced expression after 12 and 18 weeks of HFD in both HFD groups ($FC_{HFD\ Thra1}$ = 0.53; $FC_{HFD\ Thra2}$ = 0.54; $FC_{HFD\ metformin\ Thra1}$ = 0.57; $FC_{HFD\ metformin\ Thra2}$ = 0.63), though *Thra1* ($FC_{HFD\ Thra1}$ = 0.60; $FC_{HFD\ metformin\ Thra1}$ = 0.69) and *Thra2* ($FC_{HFD\ Thra2}$ = 0.57; $FC_{HFD\ metformin\ Thra1}$ = 0.69) expression seems to recover slightly after 6 weeks of metformin treatment. Similar observations can be made for the expression of *Thrb* which reduces in the first 12 weeks of HFD in both groups ($FC_{HFD\ Thrb\ 12\ weeks}$ = 0.79; $FC_{HFD\ metformin\ Thrb\ 12\ weeks}$ = 0.86). While the expression of the HFD group remains lowered ($FC_{HFD\ Thrb\ 18\ weeks}$ = 0.83) the expression in the metformin treated group recovers to control levels ($FC_{HFD\ metformin\ Thrb\ 18\ weeks}$ = 1.04). In contrast the expression of *Dio1* is significantly upregulated upon HFD treatment in both HFD groups compared to chow mice after 12 weeks ($FC_{HFD\ Dio1\ 12\ weeks}$ = 1.71, q-$value_{HFD\ Dio1\ 12\ weeks}$ = 0,0143; $FC_{HFD\ metformin\ Dio1\ 12\ weeks}$ = 2.21, q-$value_{HFD\ metformin\ Dio1\ 12\ weeks}$ = 0,0143). *Dio1* expression after 18 weeks is still increased in the HFD group with a fold change of 1.82 but only significantly increased in the HFD metformin group ($FC_{HFD\ metformin\ Dio1\ 18\ weeks}$ = 2.16, q-$value_{HFD\ metformin\ Dio1\ 18\ weeks}$ = 0,0143). The HFD treatment additionally led to a trend of reduced expression of *Slc10a1* 12 weeks in both HFD groups ($FC_{HFD\ Slc10a1\ week\ 12}$ = 0.68; $FC_{HFD\ metformin\ Slc10a1\ 12\ weeks}$ = 0.80), the reduction was significant in the HFD group after 18 weeks of treatment ($FC_{HFD\ Slc10a1\ 18\ weeks}$ = 0.71, q-$value_{HFD\ Slc10a1\ 18\ weeks}$ = 0.0444), while the metformin treated group recovered *Slc10a1* expression back to control levels ($FC_{HFD\ metformin\ Slc10a1\ 18\ weeks}$ = 0.97) (Figure 13B).

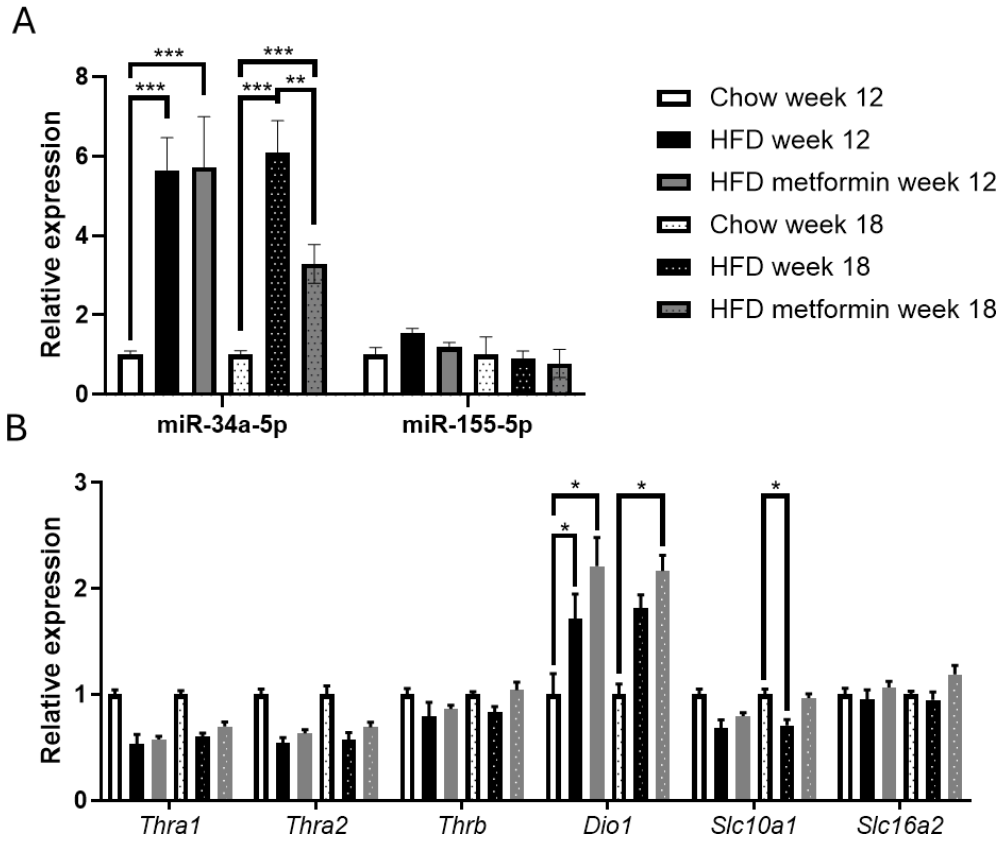

*Figure 13. Expression of miRNAs and TH metabolism genes after HFD and treatment with metformin. A) Expression of miRNAs, B) expression of potential miRNA target genes. MiRNAs were normalized to housekeeper miR-24-3p and mRNAs to actin beta. Data was analyzed using 2-way ANOVA with Benjamini-Hochberg correction. Depicted are the mean with SEM.. *<0.05, **<0.01, ***<0.001, ****<0.0001.*

Summarizing the results of the mouse models, the expression of miR-34a-5p is increased in mice fed different high fat diets and upon liver injury by CCl_4, while there is an increase in mice fed an MCDD diet, the change is not significant. Expression of miR-155-5p is also increase in high fat diet animals, as well as MCDD mice, but not in the CCl_4 mice, indicating that liver injury through non-metabolic means does not affect miR-155-5p.

6.1.3. Cell metabolic stimulation

MASLD development is marked by excess of sugars and fatty acids. To mimic the condition in the liver and potentially stimulate miRNA expression and influence TH metabolism different hepatocyte cell models were stimulated with different sugar and lipid concentrations. In 6.1.1 three miRNAs are proposed to bind *THRB*, miRNA-155-5p is not expressed in HepG2 cells, the main cell culture model used for this part of the thesis and therefore was therefore not investigated in this part of the thesis.

6.1.3.1. Fructose

Due to the important role of fructose in MASLD with the ability of increased fructose levels to disrupt hepatic lipid metabolism and the induction of insulin resistance, we treated HepG2 cells with 5 mM fructose for 24 h, this did not result in an increase of miR-34a-5p and had no significant effects on the potential miRNA target genes

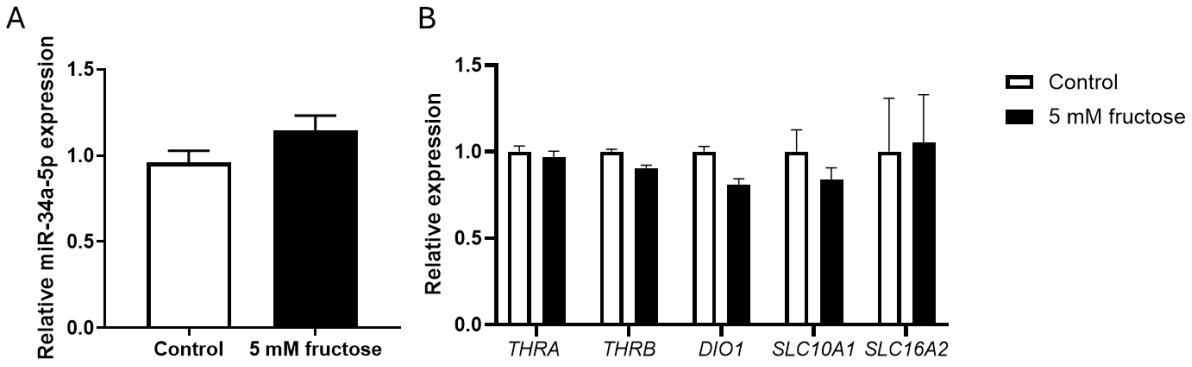

Figure 14. Treatment of HepG2 cells with 5 mM fructose for 24 hours. MicroRNA-34a-5p was normalized to miR-24-3p and for normalization of mRNAs CASC3 was used. Data is depicted as mean with SEM.

6.1.3.2. Fructose Insulin

To further simulate the high fructose aspect of a western diet with insulin resistance different liver cell lines were stimulated with high levels of fructose and insulin for 6h to 14 days.

Stimulation of HepG2 cells with high fructose (50 mM) and high insulin (100 nM or 500 nM) over 6 h did not result in significant changes of target gene expression, though *THRA*, *DIO1* and *SLC10A1* show tendencies of reduced expression (Figure 15A). While increasing the stimulation over 24 h did not result in significant changes in expression miR-34a-5p and *SLC16A2* show an increase ($FC_{\text{miR-34a-5p 24h 100 nM}} = 1.30$, $FC_{\text{miR-34a-5p 24h 500 nM}} = 1.11$, $FC_{\textit{SLC16A2}\ \text{24 h 100 nM}} = 1.40$, $FC_{\textit{SLC16A2}\ \text{24 h 500 nM}} = 1.69$) while all other target genes showed potential reduction of expression ($FC_{\textit{THRA}\ \text{24h 100 nM}} = 0.82$, $FC_{\textit{THRA}\ \text{24 h 500 nM}} = 0.79$, $FC_{\textit{THRB}\ \text{24 h 100 nM}} = 0.85$. $FC_{\textit{THRB}\ \text{24 h 500 nM}} = 0.85$, $FC_{\textit{DIO1}\ \text{24 h 100 nM}} = 0.60$, $FC_{\textit{DIO1}\ \text{24 h 500 nM}} = 0.53$, $FC_{\textit{SLC10A1}\ \text{24 h 100 nM}} = 0.64$. $FC_{\textit{SLC16A2}\ \text{24 h 500 nM}} = 0.62$) (Figure 15B). Similarly, treatment of HepG2 cells for 48 h did only result in a slight increase of miR-34a-5p expression with 100 nM insulin stimulation ($FC_{\text{miR-34a-5p 48 h 100 nM}} = 1.21$). While not significant the expression of *SLC16A2* increase upon stimulation ($FC_{\textit{SLC16A2}\ \text{48 h 100 nM}} = 1.39$, $FC_{\textit{SLC16A2}\ \text{48 h 500 nM}} = 1.73$) and *DIO1* expression decreased ($FC_{\textit{DIO1}\ \text{48 h 100 nM}} = 0.63$, $FC_{\textit{DIO1}\ \text{48 h 500 nM}} = 0.54$). Meanwhile expression of *THRA*, *THRB* and *SLC10A1* were significantly reduced upon stimulation ($FC_{\textit{THRA}\ \text{48h 100 nM}} = 0.80$, $\text{q-value}_{\textit{THRA}\ \text{48 h 100 nM}} = 0{,}0118$; $FC_{\textit{THRA}\ \text{48 h 500 nM}} = 0.80$, $\text{q-value}_{\textit{THRA}\ \text{48 h 500 nM}} = 0{,}0118$; $FC_{\textit{THRB}\ \text{48 h 100 nM}} = 0.73$, $\text{q-value}_{\textit{THRB}\ \text{48 h 100 nM}} = 0{,}0056$; $FC_{\textit{THRB}\ \text{48 h 500 nM}} = 0.66$, $\text{q-value}_{\textit{THRB}\ \text{48 h 500 nM}} = 0{,}003$; $FC_{\textit{SLC10A1}\ \text{48 h 100 nM}} = 0.66$, $\text{q-value}_{\textit{SLC10A1}\ \text{48 h 100 nM}} = 0{,}003$; $FC_{\textit{SLC10A1}\ \text{48 h 500 nM}} = 0.63$, $\text{q-value}_{\textit{SLC10A1}\ \text{48 h 500 nM}} = 0{,}003$) (Figure 15C). Stimulation over 14 days was only done in one preliminary experiment, though gene expression did not reduce as expected in the experiments over a shorter time period (Figure 15D). Treatment with increased insulin dosage did not significantly change gene expression compared to the smaller dosage, though a tendency to an increased treatment response can be observed with higher insulin levels in the target genes.

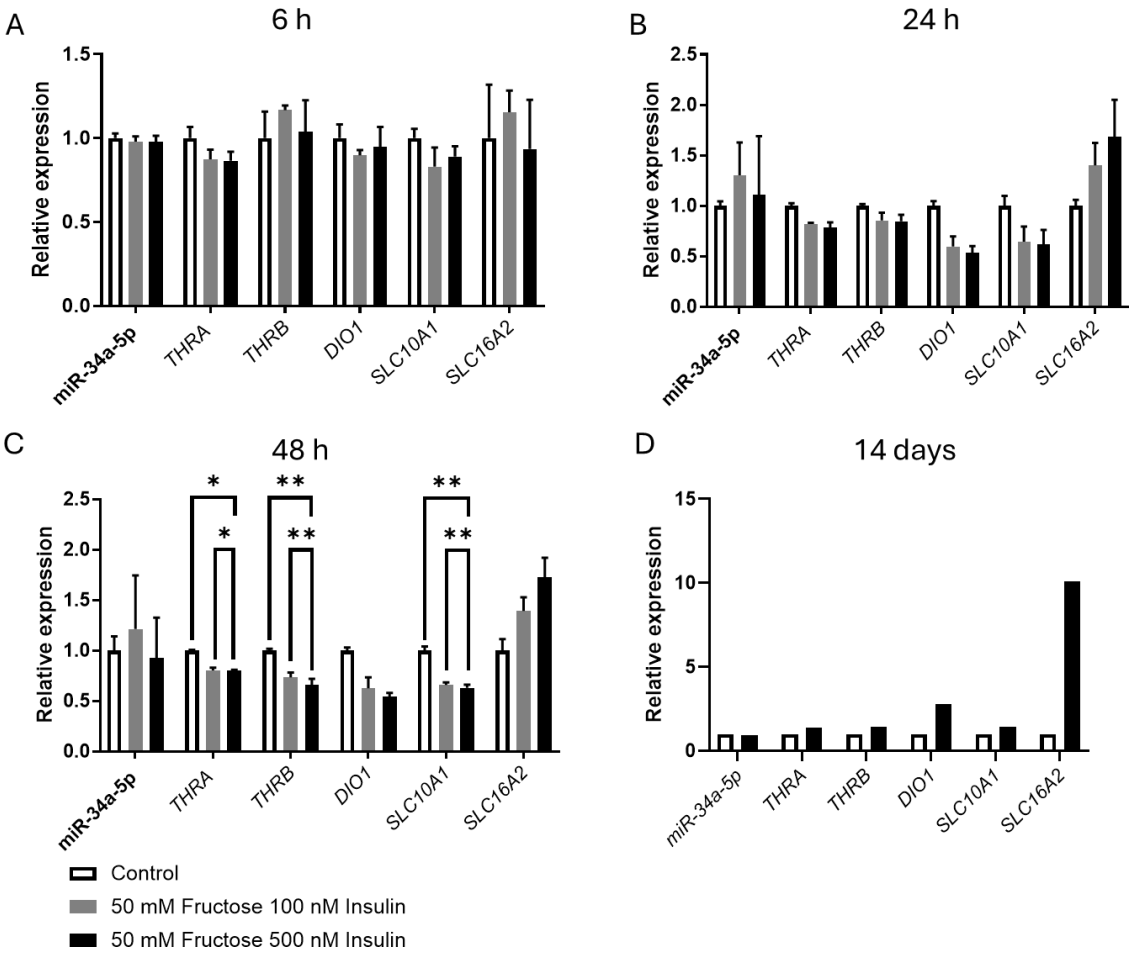

*Figure 15. Stimulation of HepG2 cells with fructose and insulin. Treatment with 50 mM fructose and 100 or 500 nM insulin A) for 6 h, B) for 24 h, C) for 48 h.. One way ANOVA, n=3, *<0.05, **<0.01, ***<0.001, ****<0.0001, Depicted as mean with SEM. D) Treatment with 50 mM fructose and 500 nM insulin for 14 days, n= 1. MiRNA-34a-5p was normalized to miR-24-3p and mRNAs to CASC3.*

To verify the results of metabolic stimulation with fructose and insulin in HepG2 cells the experiment was repeated in Huh-7 cells, another hepatocyte cancer cell line. The expression of *SLC16A2* was not measured, due to a low baseline expression in Huh-7 cells [262,263]. Since the stimulation over 6 and 24 h did not result in significant changes in expression levels only stimulation over 48 h and a preliminary experiment over 14 days was performed. The stimulation over 48 h did not result in significant changes in expression of mRNAs in Huh-7 cells (Figure 16A). Since the target genes showed either no change in expression or a tendency to increased expression miR-34a-5p expression was not measured. The stimulation over 14 days was only performed with the higher dose of insulin and only done once. While miR-34a-5p expression does seem to be induced so do all potential miR-34a-5p target genes ($FC_{\text{miR-34a-5p 14 days}}$ = 1.50, $FC_{THRA\ 14\ days}$ = 1.36, $FC_{THRB\ 14}$ days = 1.51, $FC_{DIO1\ 14\ days}$ = 2.41, $FC_{SLC10A1\ 14\ days}$ = 1.21) (Figure 16B).

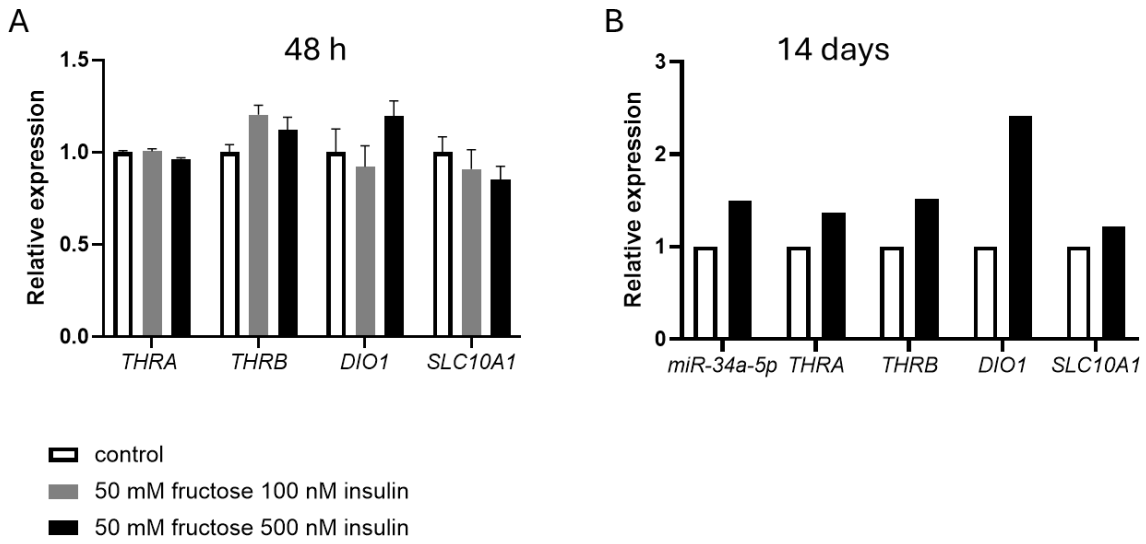

Figure 16. Stimulation of Huh-7 cells with high fructose and high insulin. A) Stimulation of Huh-7 cells with 50 mM fructose and 100 or 500 nM insulin for 48 h. One-way ANOVA, data is depicted as mean with SEM. B) Stimulation of Huh-7 cells for 14 days with 50 mM fructose and 500 nM insulin, preliminary data with n = 1. Data of miR-34a-5p was normalized to miR-24-3p and mRNAs to CASC3.

Since the results of the HepG2 experiments could not be reproduced in the Huh-7 cells iPSC derived hepatocyte like cells were used as another hepatocyte model to verify the results. The experiment was performed in iPSC derived hepatocyte-like cells of cell line BIHi001-B, the differentiation is described in 5.3.8 The experiment was conducted using 500 nM insulin, though the differentiation medium contains unknown amounts of insulin, therefore the concentration of insulin is only an approximation. The preliminary experiment was repeated twice and the protocol has to be fully established and optimized for further investigations. As Figure 17 A-F shows there is response of miR-34a-5p, *THRA*, *THRB* and *SLC16A2* expression to the metabolic stimulation, meanwhile *DIO1* and *SLC10A1* show a tendency of reduced expression, though there is a high variation between repeats.

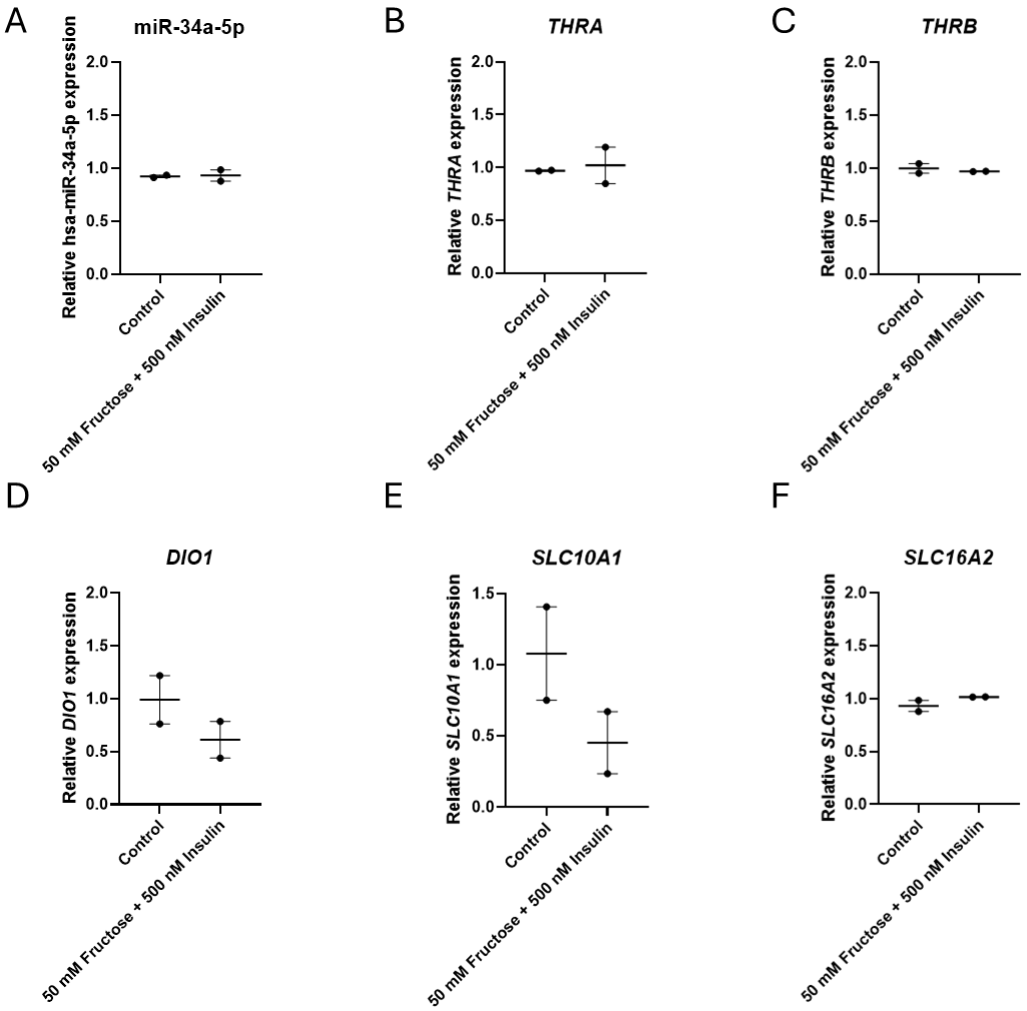

Figure 17. Stimulation of iPSC derived hepatocyte like cells with 50 mM fructose and insulin for 48 hours. Data is depicted as mean with SEM, preliminary data with n = 2. MicroRNA-34a-5p was normalized to miR-24-3p and mRNAs to CASC3.

6.1.3.3 Fructose and glucose

To test further metabolic stimulants HepG2 cells were treated with 25 mM glucose and 50 mM fructose for 72 h to simulate a high glucose and fructose rich diet over a longer time period. The expression of mIR-34a-5p was not changed and only *THRA* (FC = 0.90, q-value = 0,003655) and *SLC16A2* (FC = 2.36, q-value = 0,011359) show similar expression changes as seen with high fructose and insulin stimulation of the cells for 48 h (Figure 18).

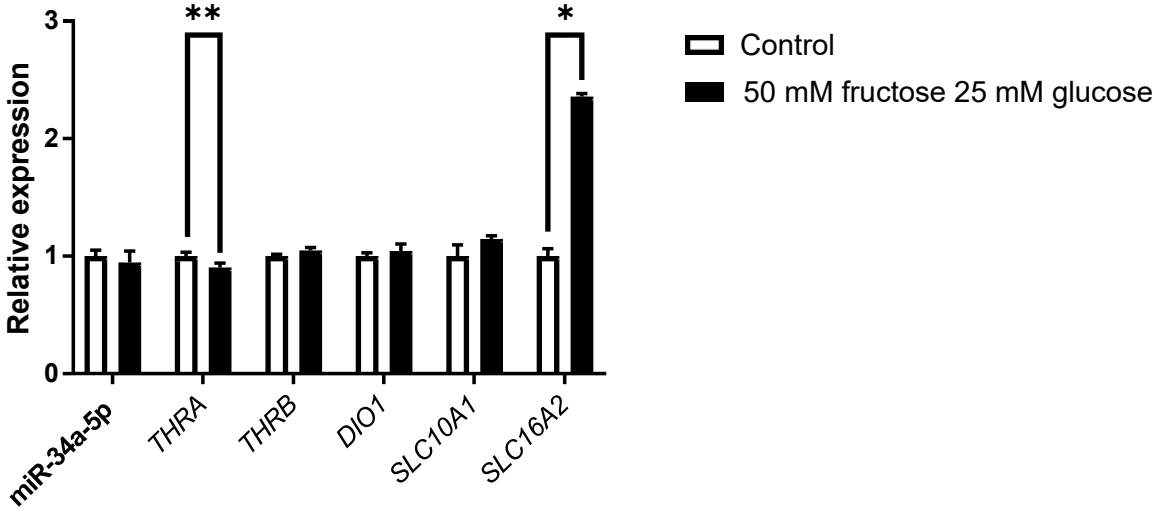

*Figure 18. Stimulation of HepG2 cells with high fructose and glucose for 72 hours. HepG2 cells were treated with 25 mM glucose and 50 nM fructose. miRNA expression was normalized to miR-24-3p and mRNAs to CASC3, multiple t-tests, *<0.05, **<0.01, mean depicted with SEM.*

6.1.3.4. Oleate/palmitate

Since the western diet not only contains high sugars but also high fat content treatment of the HepG2 cells with 0.5 mM oleate and palmitate in a 2:1 ratio was used to induce lipid accumulation in cells. After 48 h of oleate and palmitate treatment miR-34a-5p expression significantly increased (FC = 1.15, p-value = 0.040). Nevertheless, the majority of the potential target genes react to the induction of miR-34a-5p expression and show a tendency of increased expression ($FC_{THRA\ 48\ h}$ = 1.01, $FC_{THRB\ 48\ h}$ = 1.15, $FC_{DIO1\ 458\ h}$ = 1.15, $FC_{SLC10A1\ 48\ h}$ = 1.19, $FC_{SLC16A2\ 48\ h}$ = 0.90) (Figure 19A). After 72 h of treatment the increase in miR-34a-5p expression was no longer significant and only SLC10A1 showed significant reduction of expression ($FC_{SLC10A1\ 72\ h}$ = 0.86, q-$value_{SLC10A1\ 72\ h}$ = 0,045069) while the expression of other target genes remained unchanged.

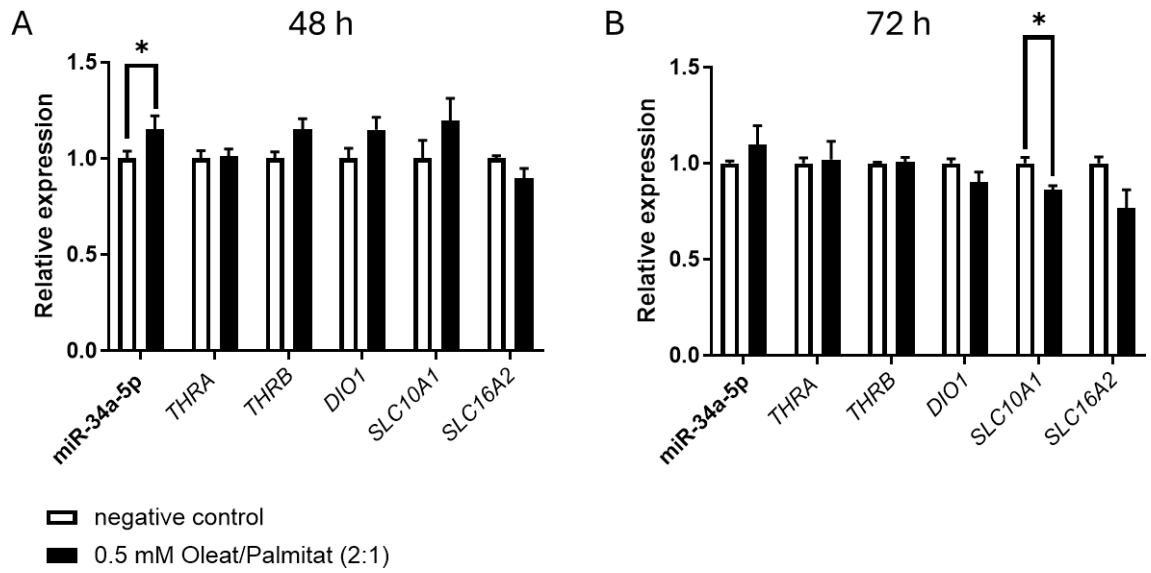

*Figure 19. Stimulation of HepG2 cells with oleate palmitate (2:1). HepG2 cells were stimulated with 0.5 mM oleate and palmitate mixture (2:1) for A) 48 h and B) 72 h. Data was analyzed with multiple t-tests, miRNA expression was normalized to miR-24-3p and mRNAs to CASC3. * > 0.05.*

6.1.3.5. RNA-seq

Due to the observed dysregulation of TH metabolism genes in HepG2 cells after treatment with fructose and insulin (6.1.3.2), but only slight non-significant increase of miR-34a-5p expression, HepG2 cells were again stimulated with fructose and insulin for 48 h but in addition transfected with miR-34a-5p inhibitor to ascertain whether the observed effect is due to the slight change in miR-34a-5p expression. To verify that inhibition of miR-34a-5p does not result in a compensatory increased expression of miR-34b-5p or miR-34c-5p both miRNAs were measured as well. As expected the treatment with miR-34a-5p inhibitor does reduce the expression of miR-34a-5p compared to both control samples ($FC_{\text{miR-34a-5p inhibitor}} = 0.24$, $\text{q-value}_{\text{miR-34a-5p inhibitor vs nc\#1}} = 0{,}0005$, $\text{q-value}_{\text{miR-34a-5p inhibitor vs nc\#1 fructose insulin}} = 0{,}0005$) and TH metabolism expression reduces upon stimulation with fructose and insulin except for the expected increase in *SLC16A2* expression ($FC_{THRA\ \text{nc\#1 fructose insulin}} = 0.84$, $\text{q-value}_{THRA\ \text{nc\#1 fructose insulin}} = 0{,}0483$; $FC_{THRB\ \text{nc\#1 fructose insulin}} = 0.82$, $\text{q-value}_{THRB\ \text{nc\#1 fructose insulin}} = 0{,}013$; $FC_{DIO1\ \text{nc\#1 fructose insulin}} = 0.57$, $\text{q-value}_{DIO1\ \text{nc\#1 fructose insulin}} = 0{,}0015$; $FC_{SLC10A1\ \text{nc\#1 fructose insulin}} = 0.67$, $\text{q-value}_{SLC10A1\ \text{nc\#1 fructose insulin}} = 0{,}012$; $FC_{SLC16A2\ \text{nc\#1 fructose insulin}} = 2.06$, $\text{q-value}_{SLC16A2\ \text{nc\#1 fructose insulin}} = 0{,}0216$). Contrary to what was expected the inhibition of miR-34a-5p did not result in a normalization of TH metabolism gene expression. Gene expression compared to the only nc#1 treated group were significant and similar to the results of the nc#1 fructose insulin group ($FC_{THRA\ \text{inhibitor}} = 0.81$, $\text{q-value}_{THRA\ \text{inhibitor}} = 0{,}0483$; $FC_{THRB\ \text{inhibitor}} = 0.80$, $\text{q-value}_{THRB\ \text{inhibitor}} = 0{,}013$; $FC_{DIO1\ \text{inhibitor}} = 0.55$; $\text{q-value}_{DIO1\ \text{inhibitor}} = 0{,}0015$, $FC_{SLC10A1\ \text{inhibitor}} = 0.66$, $\text{q-value}_{SLC10A1\ \text{inhibitor}} = 0{,}012$; $FC_{SLC16A2\ \text{inhibitor}} = 2.41$, $\text{q-value}_{SLC16A2\ \text{inhibitor}} = 0{,}0195$) (Figure 20A). The expression of miR-34c-5p was not affected by inhibition of miR-34a-5p and miR-34b-5p was significantly reduced by the inhibitor ($FC_{\text{miR-34b-5p}} = 0.54$, $\text{q-value}_{\text{miR-34b-5p inhibitor vs nc\#1}} = 0{,}0099$, $\text{q-value}_{\text{miR-34b-5p inhibitor vs nc\#1 fructose insulin}} = 0{,}0099$) (Figure 20B). Therefore, reduced miR-34a-5p expression was not compensated by other members of the miR-34 family.

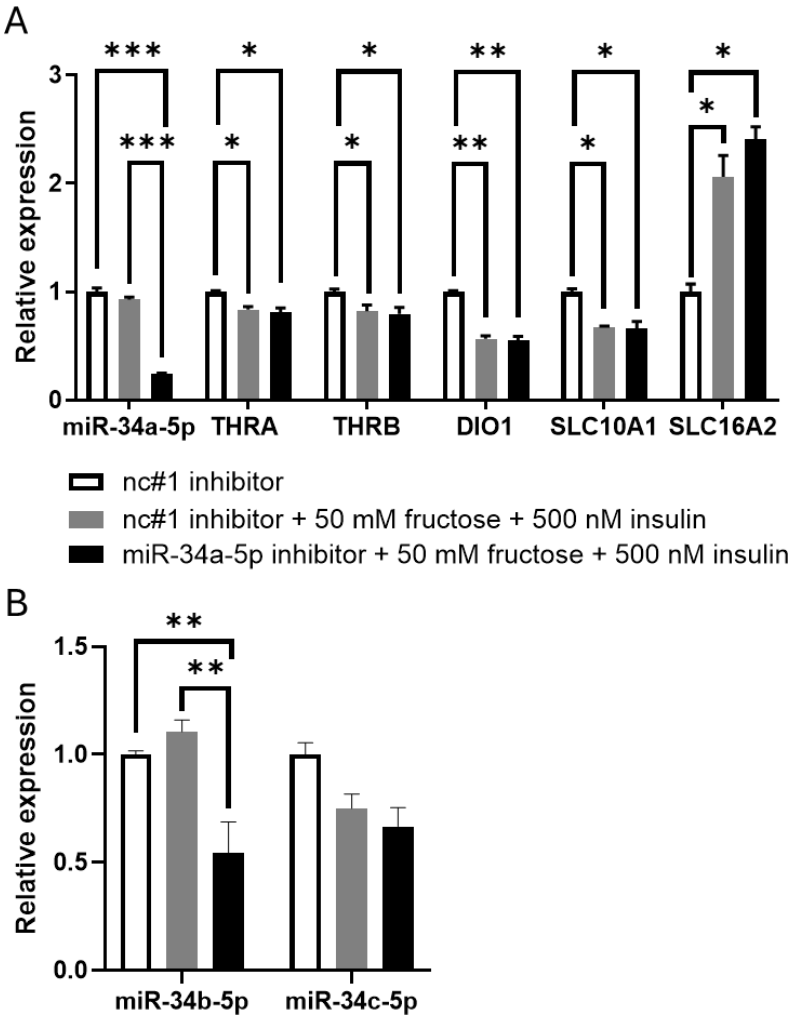

*Figure 20. Stimulation of HepG2 cells with fructose and insulin with miR-34a-5p inhibitor treatment. Expression of miR-34b-5p and miR-34c-5p after stimulation with fructose and insulin and treatment with miR-34a-5p inhibitor. One way ANOVA, n=3, *<0.05, **<0.01, ***<0.001, depicted as mean with SEM. miRNA expression was normalized to miR-24-3p and mRNAs to CASC3*

To get a better understanding of the mechanism behind the reduction of TH metabolism genes after fructose and insulin treatment the samples were used for RNA sequencing. KEGG pathway analysis shows some overlap in detected pathways and detects metabolism pathways in both. Pathways relevant for cell cycle, DNA replication and cellular senescence are enriched after both treatments as is the MAPK signaling pathway. The transfection with miR-34a-5p inhibitor additionally to the stimulation with fructose and insulin lead to an enrichment in liver injury pathways observed in hepatitis c infection and hepatocellular carcinoma while the treatment only with fructose and insulin lead to an enrichment in the AGE-RAGE signaling pathway in diabetic complications.

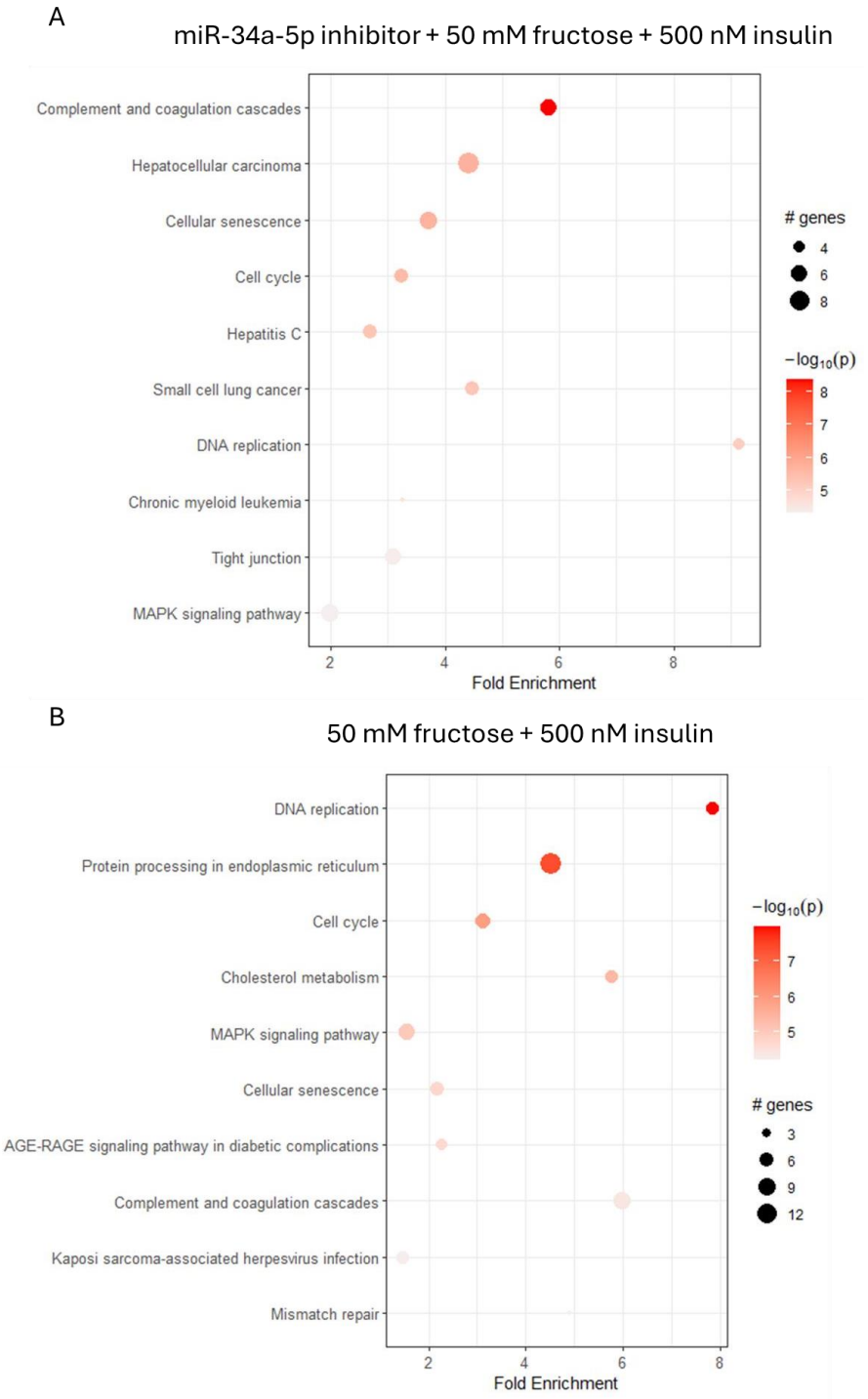

Figure 21. RNA sequencing of metabolic stimulation of HepG2 cells with 50 mM fructose, 500 nM insulin and 10 nM miR-34a-5p inhibitor or control A) KEGG pathway analysis of miR-34a-5p inhibitor with 50 mM fructose and 500 nM insulin stimulation. B) KEGG pathway analysis of nc#1 inhibitor with 50 mM fructose and 500 nM insulin stimulation.

6.1.4. Mechanistic studies

In this part of the thesis the binding of the target miRNAs to their respective predicted targets were investigated in cell culture based experiments.

6.1.4.1. Overexpression of miRNAs in HepG2 cells

6.1.4.1.1. MiRNA-34a-5p

To simulate the increased expression of miR-34a-5p we transfected HepG2 cells with miR-34a-5p mimic. The following data were published in the European Thyroid Journal [261].

To investigate the effect of increased expression of miR-34a-5p, as observed in patients and mouse models with MASLD on the TH metabolism HepG2 cells were first transfected with a miR-34a-5p mimic. After 48 h incubation the overexpression of miR-34a-5p (Figure 22A) resulted in significant reduction of *THRA* (FC = 0.65, p = 0.0227), *THRB* (FC = 0.45, p = 0.0014), *DIO1* (FC = 0.19, p = 0.0014) and *SLC10A1* (FC = 0.44, p = 0.0017), while *SLC16A2* (FC = 3.33, p = 0.0014) was upregulated (Figure 22B). To ascertain the effect on reduced miR-34a-5p expression a miR-34a-5p inhibitor was transfected into HepG2 cells which resulted in the expected significant reduction of miR-34a-5p expression (Figure 22C) as well as an induction of *THRB* (FC = 1.11, p = 0.0187) (Figure 22D). To verify that the changes in TH metabolism genes indeed affect TH signaling in HepG2 cells were next stimulated with T_3 in addition to transfection with miR-34a-5p mimic and inhibitor and THRB downstream regulated genes were measured. The transfection with inhibitor and T_3 did not result in significant changes (data not shown) while the transfection with the miR-34a-5p mimic significantly changed T_3 response in *THRB* regulated genes *DIO1* and *CYP7A1*. Upon stimulation with 10 nM T_3 *CYP7A1* increased 2.41 fold while the expression remained at a fold change of 1.07 after transfection with miR-34a-5p ($q\text{-value}_{CYP7A1\ 10\ nM\ T3\ nc\#1\ vs\ 10\ nM\ T3\ miR\text{-}34a\text{-}5p}$ = 0.0170) and also after stimulation with 50 nM T_3 did the expression of CYP7A1 increase significantly more in the nc#1 group (FC = 2.63) than in the miR-34a-5p treated group (FC = 1.04, q-value = 0,0113). The DIO1 expression reacted similar to the stimulation with T_3 and additional transfection with miR-34a-5p mimic ($FC_{DIO1\ 10\ nM\ T3\ nc\#1}$ = 3.64, $FC_{DIO1\ 10\ nM\ T3\ miR\text{-}34a\text{-}5p}$ = 1.84, q-value = 0,0003; $FC_{DIO1\ 50\ nM\ nc\#1}$ = 3.82, $FC_{DIO1\ 50\ nM\ miR\text{-}34a\text{-}5p}$ = 1.84, q-value = 0,0003) (Figure 22E-F).

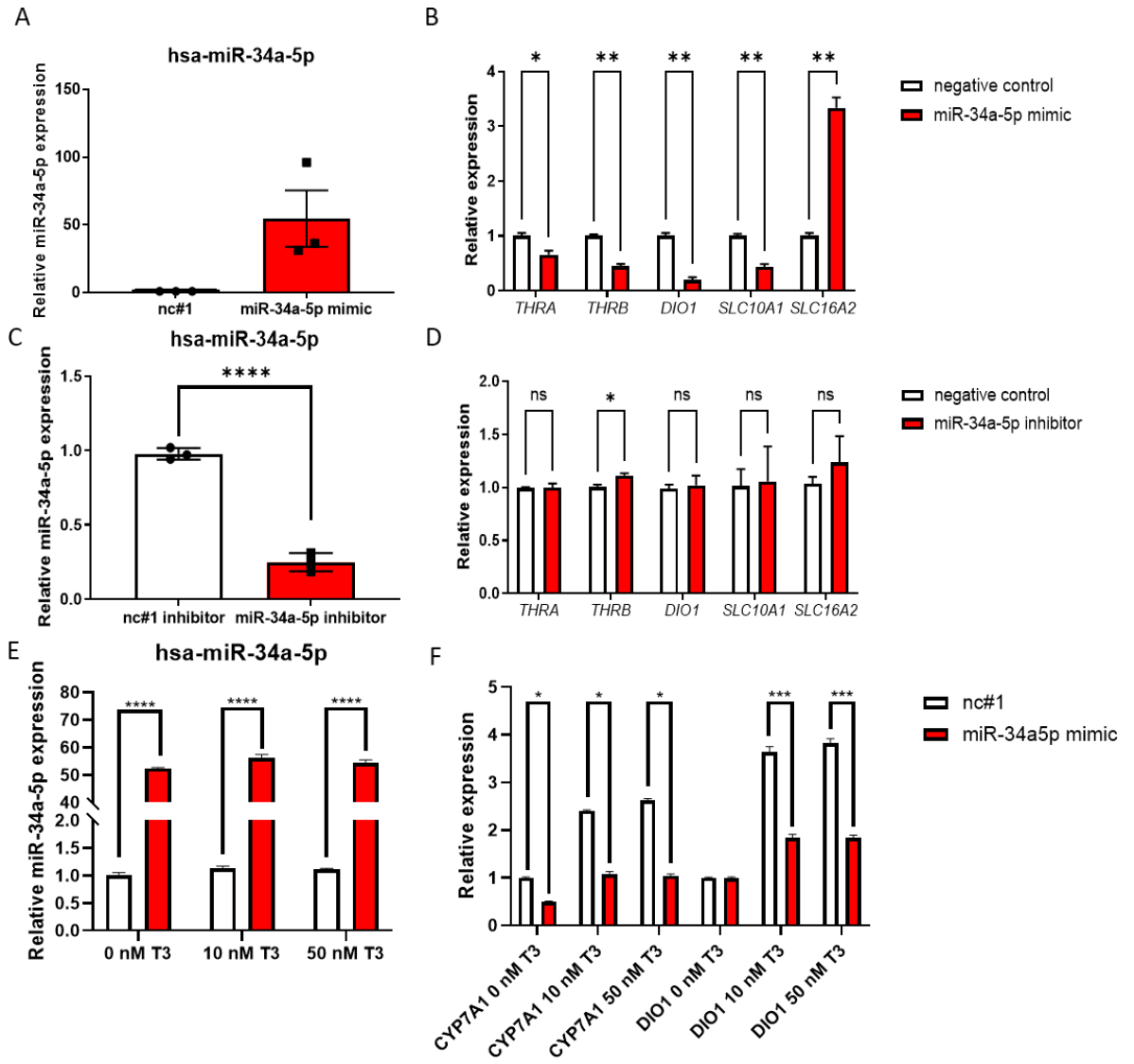

*Figure 22. Transfection of HepG2 cells with 10 nM miR-34a-5p mimic and inhibitor for 48 hours. A) Relative expression of miR-34a-5p B) Relative expression of TH genes after miR-34a-5p transfection. C) Relative expression of miR-34a-5p and D) relative expression of TH metabolism genes after transfection with miR-34a-5p inhibitor. miRNA expression was normalized to miR-24-3p and mRNA expression to CASC3. Multiple t-test and one-way ANOVA, *<0.05, **<0.01, ****<0.0001* [261]

6.1.3.1.2. MiRNA-224-3p

Transfection of miR-224-3p mimic resulted in a 7702-fold change (p-value < 0.0001) (Figure 23A). The expected reduction of *THRB* did not occur upon induction of miR-224-5p over expression, instead the expression of *DIO1* and *SLC10A1* are induced (FC_{DIO1} = 1.08,$q\text{-value}_{DIO1}$ = 0.0018; $FC_{SCL10A1}$ = 1.59, $q\text{-value}_{SLC10A1}$ = 0.0027while the expression of *SLC16A2* is significantly reduced ($FC_{SLC16A2}$ = 0.64, $q\text{-value}_{SLC16A2}$ = 0.0028) (Figure 23B). Because miR-224-5p does not seem to have any influence of *THRB*, it was not further investigated.

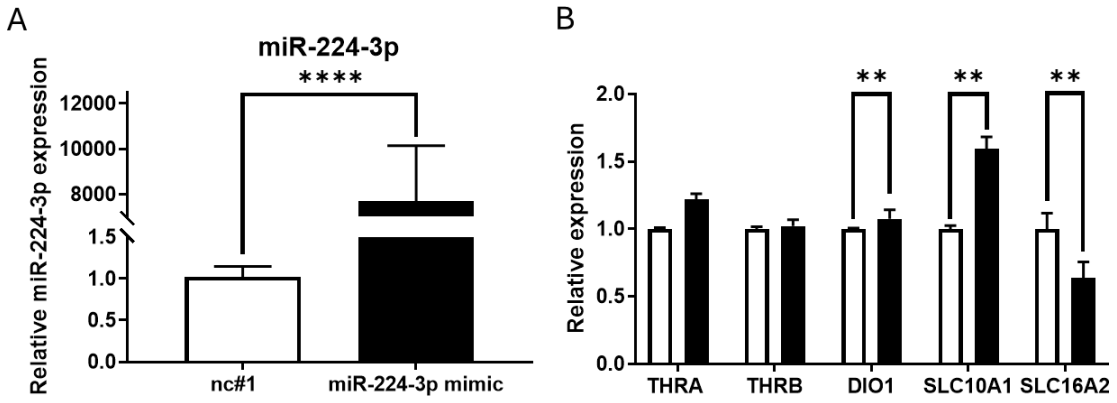

*Figure 23.Transfection of HepG2 cells with miR-224-3p mimic. A) Relative miR-224-5p expression normalized to miR-24-3p. B) Relative expression of TH metabolism genes normalized to CASC3. Data were analyzed using multiple t-test and are depicted as mean with SEM. ** < 0.01, **** < 0.0001*

Since the overexpression of miR-224-3p did not result in any expected changes in expression of potential target genes it was not further investigated.

6.1.3.1.3. MiRNA-155-5p

According to target prediction miR-155-5p potentially regulated expression of THRB and SLC16A2.

MiR-155-5p is not expressed in HepG2 cells, nevertheless to determine a possible effect of the miRNA on potential target genes HepG2 cells were transfected with miR-155-5p mimic and inhibitor. Since the baseline expression of the miRNA was not detectable with qPCR analysis or miRNA changes proved difficult. After transfection of miR-155-5p mimic the dCt changed from not detectable to a value of 15, as expected after transfection with miR-155-5p inhibitor no miR-155-5p was detectable. After transfection with miR-155-5p mimic the expression of *THRB* and *SLC10A1* was significantly reduced (FC_{THRB} = 0.57, q-$value_{THRB}$ = 0,018382; $FC_{SLC10A1}$ = 0.61, q-$value_{SLC10A1}$ = 0,018382) (Figure 24A). Unsurprisingly the inhibition of the already low base line expression of miR-155-5p in the HEpG2 cells did no lead to any significant changes in the expression of potential target genes *THRB* and *SLC16A2*, though there is a notable increase in SLC16A2 expression ($FC_{SLC16A2}$ = 2.16) (Figure 24B).

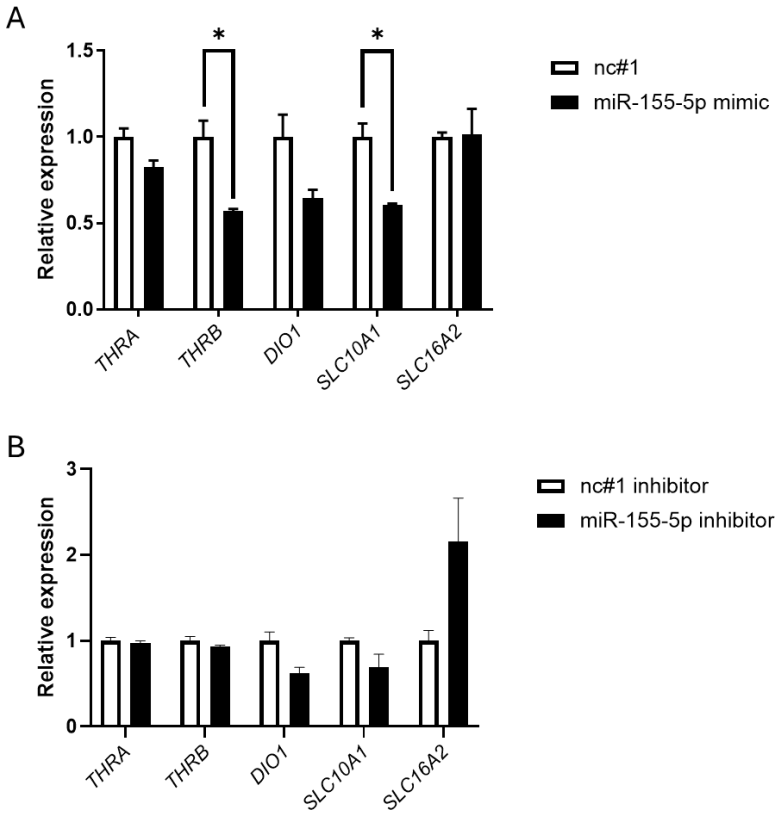

*Figure 24. Transfection of HepG2 cells with 10 nM miR-155-5p mimic or inhibitor for 48 h. A) Expression of TH metabolism related genes after overexpression of miR-155-5p with 10 nM mimic for 48 h. B) Expression of TH metabolism genes after inhibition of miR-155-5p function using 10 nM inhibitor for 48 h. Results were analyzed using multiple t-tests and are depicted as mean with SEM. Gene expression was normalized against CASC3. * < 0.05.*

6.1.4.2. Luciferase reporter assays

Target gene prediction of miR-34a-5p detected potential binding sited in the TH metabolism genes thyroid hormone receptor α (*THRA*), *THRB,* deiodinase type I (*DIO1*), solute carrier family 10 member 1 (*SLC10A1*) and solute carrier family 16 member 2 (*SLC16A2*) (Figure 8). To estimate the accessibility of the potential binding sites for actual miR-34a-5p binding CentroidFold was used to predict secondary RNA structure of approximately ± 200 bp from the potential binding site (Figure 25). While *THRA* binding site one seemed slightly more accessible than binding site 2, the second binding site had longer complementary sequence to the 3'UTR and was chosen for the experiment. The potential binding sites of the *THRB* binding sites were the same length and due to the slightly less predicted accessibility of binding site 2, the first was investigated. Both the binding sites for DIO1 and SLC10A1 show low probability of binding, though both are depicted in stems.

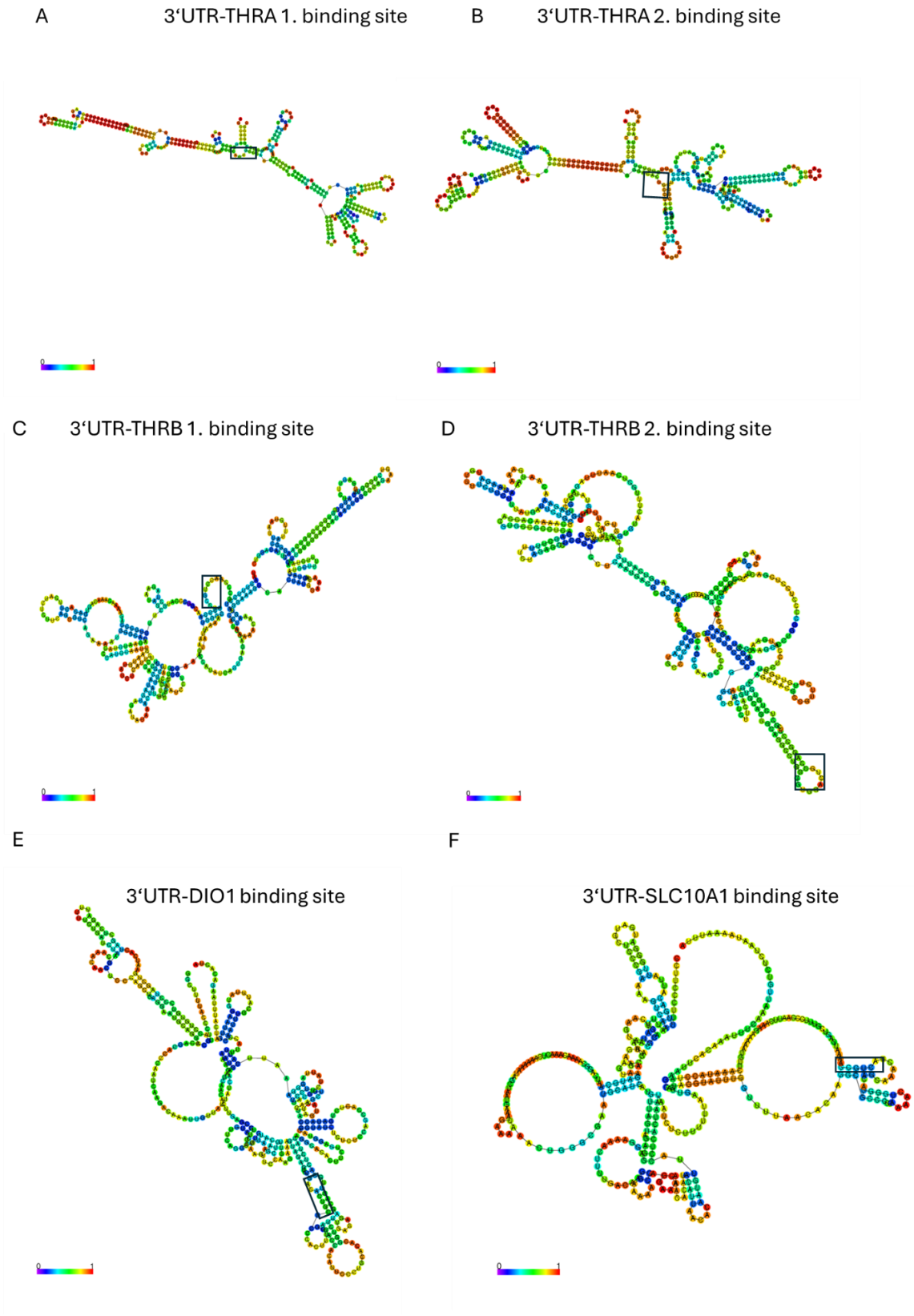

Figure 25. Prediction of 3'UTR secondary structure using CentroidFold. A) Predicted structure around THRA-3’UTR binding site 1. B) Predicted structure around THRA-3’UTR binding site 2. C) Predicted structure around THRB-3’UTR binding site 1. D) Predicted structure around THRB 3’UTR binding

site 2. E) Predicted structure around DIO1-3'UTR binding site. F) Predicted structure around SLC10A1-3'UTR binding site. The color indicates binding probability.

The selected potential miR-34a-5p binding sites were cloned into the pmirGLO vector at the 3' end of the firefly luciferase reporter gene (*luc2*) (see vector card in 11.1). The humanized *Renilla* luciferase (*hRluc*) functions as internal control for normalization. The plasmids were transfected into HEK293T cells either with nc#1 or with miR-34a-5p mimic to determine binding or miR-34a-5p to the binding site. While there were no significant differences in the luciferase reporter assays of *THRA* and *SLC10A1* the firefly expression significantly reduced after miR-34a-5p treatment in both the assay with the THRB 3'UTR (FC = 0.72, p-value 0.0005) (Figure 26. Luciferase reporter assay. Transfection of 100 ng pmirGLO plasmid containing 3'UTR of A) THRB and B) DIO1 with 10 nM miR-34a-5p mimic for 48 h measured using the Dual-Luciferase Reporter Assay System. Two-way ANOVA and t-test, ** < 0.01, *** < 0.001. (Adapted from [261])A) and the DIO1'UTR (FC = 0.79, p-value = 0.0031) (Figure 26B). To verify the results the binding site in the THRB 3'UTR was mutated using QuickChange PCR with one point mutation. After mutation of the seed sequence the firefly expression was no longer affected by miR-34a-5p transfection.

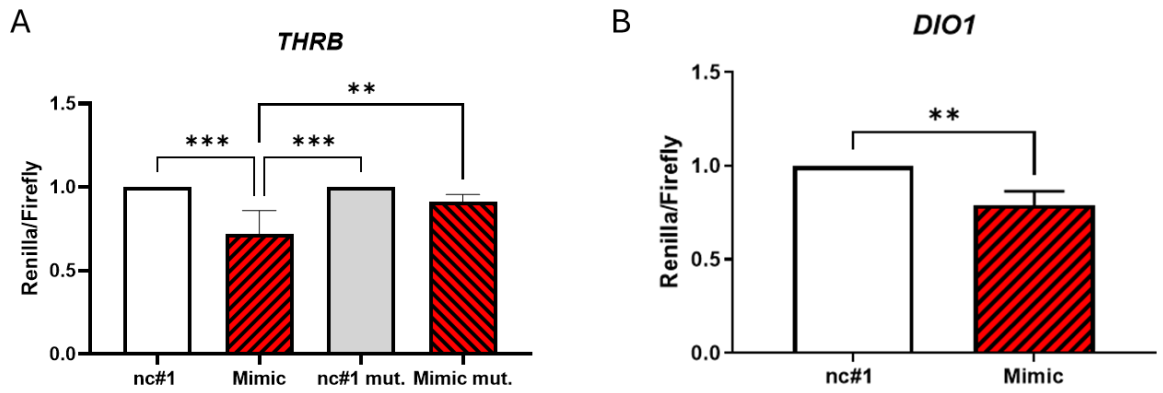

*Figure 26. Luciferase reporter assay. Transfection of 100 ng pmirGLO plasmid containing 3'UTR of A) THRB and B) DIO1 with 10 nM miR-34a-5p mimic for 48 h measured using the Dual-Luciferase Reporter Assay System. Two-way ANOVA and t-test, ** < 0.01, *** < 0.001. (Adapted from* [261]*).*

6.1.4.3. RNA-interacting protein immunoprecipitation-sequencing

As another method to verify binding of miR-34a-5p to the proposed target genes RIP-sequencing was performed. To increase the amount of detected mRNAs that are targeted by miR-34a-5p the miRNA was overexpressed in HepG2 cells using the miR-34a-5p mimic, the cells were harvested 24 h after transfection to maximize the amount of mRNAs bound to the RISC complex. After correction for unspecific binding, detected also in control samples, all detected mRNAs with a log2fold change of at least 1 were considered bound to AGO2. In total 544 gene products were bound to AGO2 with 265 *in silico* predicted miR-34a-5p targets (full list in chapter 10) (Figure 27A). This includes *THRB*, which was two-fold increased compared to the AGO2-nc#1 control. Kyoto Encyclopedia of Genes and Genomes (KEGG) pathway analysis shows significant enrichment of metabolic pathways including genes, like carbohydrate-responsive element-binding protein (*ChREBP)* or adiponectin receptor 1 (*ADIPOR1*), involved in MASLD (Figure 27B) and Gene Ontology (GO) enrichment analysis also shows upregulation of metabolism pathways (Figure 27C). A more detailed brake down of the affected metabolic pathways are depicted in Figure 28.

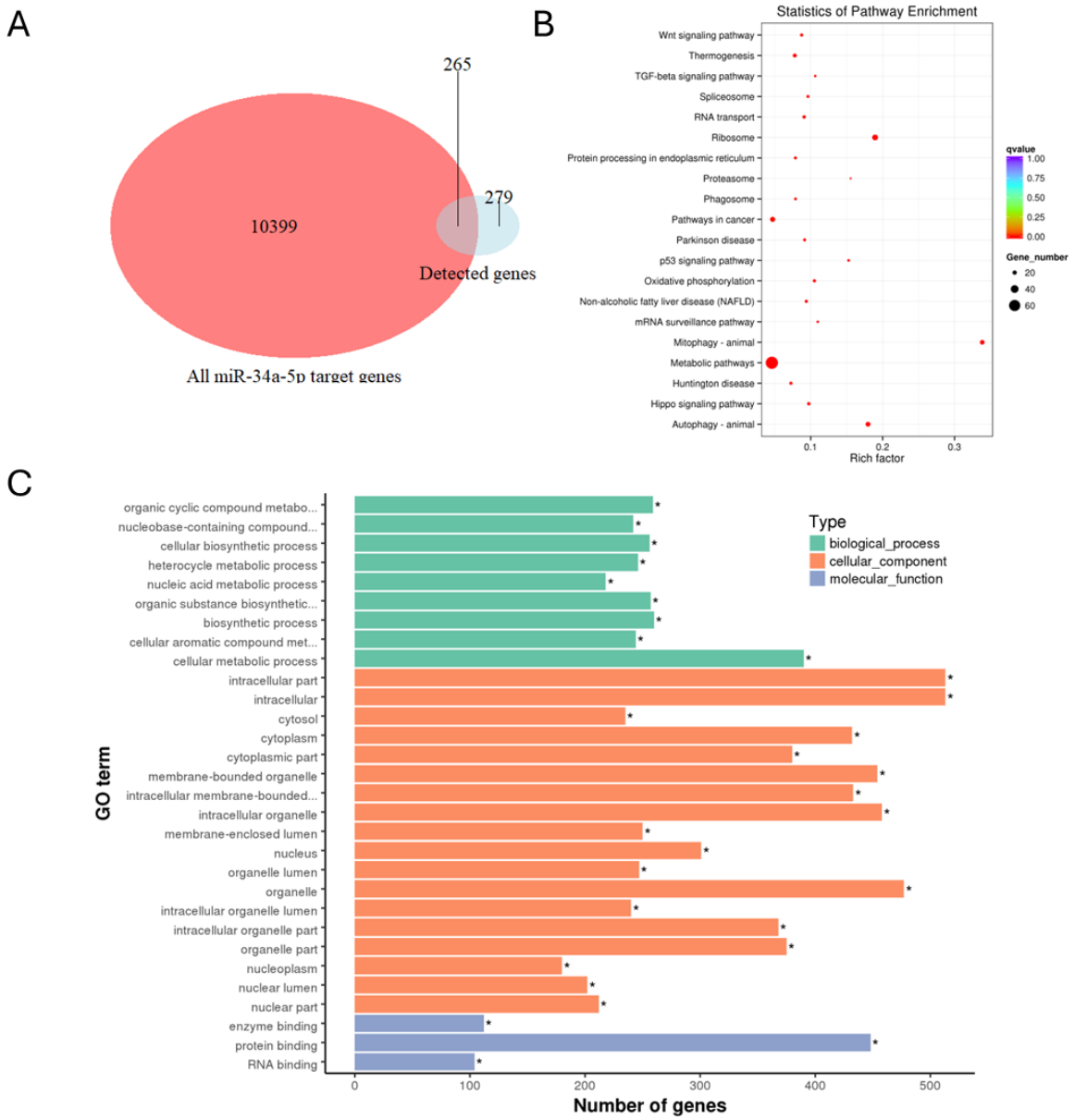

Figure 27. RIP-seq of miR-34a-5p transfected cells. A) Venn-diagram of potential miR-34a-5p target genes with in RIP-seq detected genes. B) KEGG pathway analysis of significantly up pathways. Previously published in [261] *C) GO analysis of upregulated pathways*

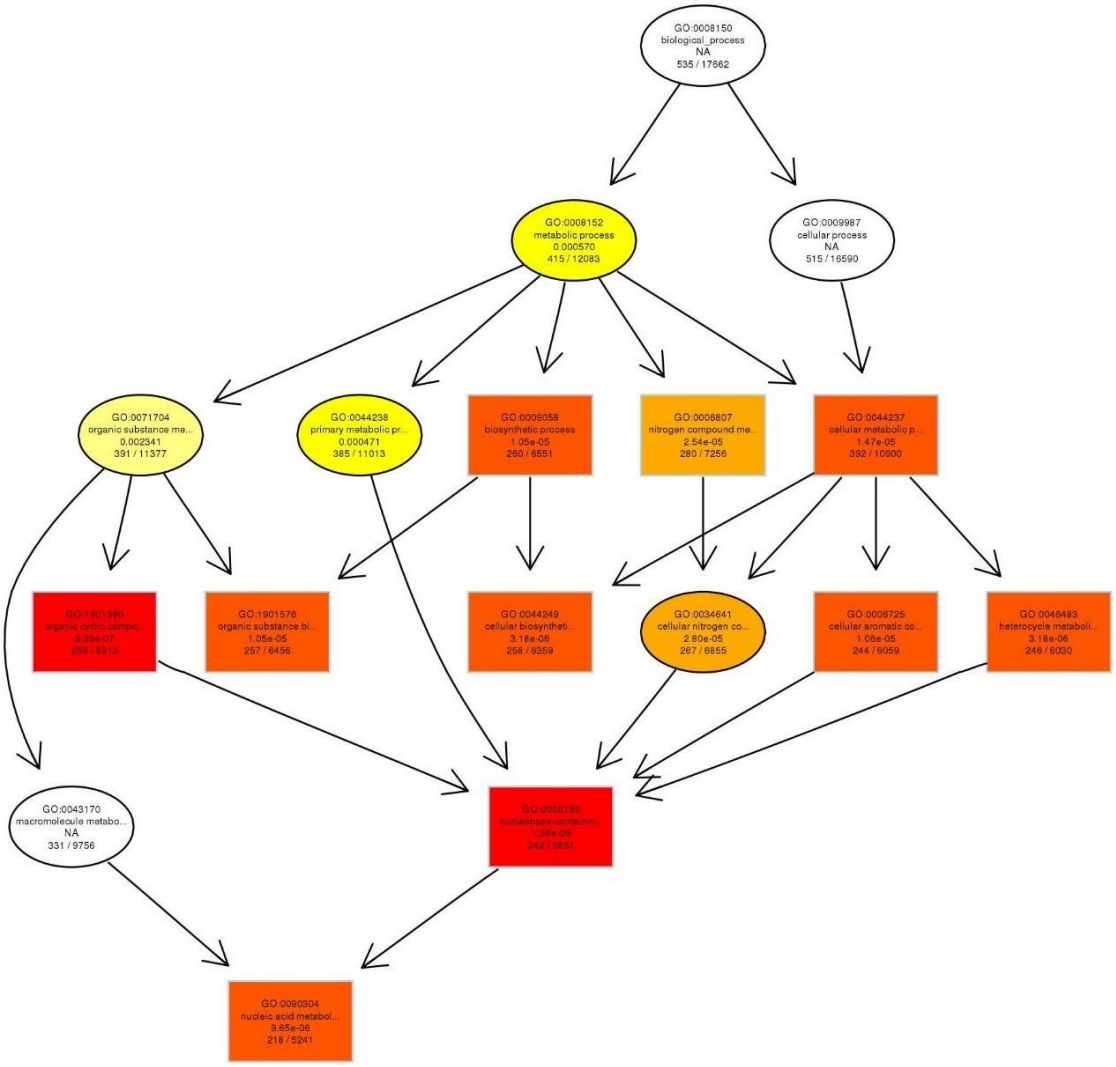

Figure 28. Metabolic processes detected by RIP-seq GO analysis

While these results are promising there was a high variation between the biological repeats as can be observed in Figure 29A and B. The amount of detected peaks varies greatly between the experiments and the overlap of detected peaks, while in experiment one a total of 8240 peaks were detected with 2769 uniquely in the AGO2-miR-34a-5p fraction, experiment three only detected a total of 177 peaks with 29 only in the AGO2-miR-34a-5p fraction. This discrepancy translates into less detected genes in the last experiment than in the first, additionally the detected genes vary between experiments, showing only 70 and 88 overlapping peaks in the AGO2-miR-34a-5p and AGO2-nc#1 samples respectively. These inconsistencies between experiments could very well reduce the validity of the results and it is possible that many miR-34a-5p targeted genes are not recorded.

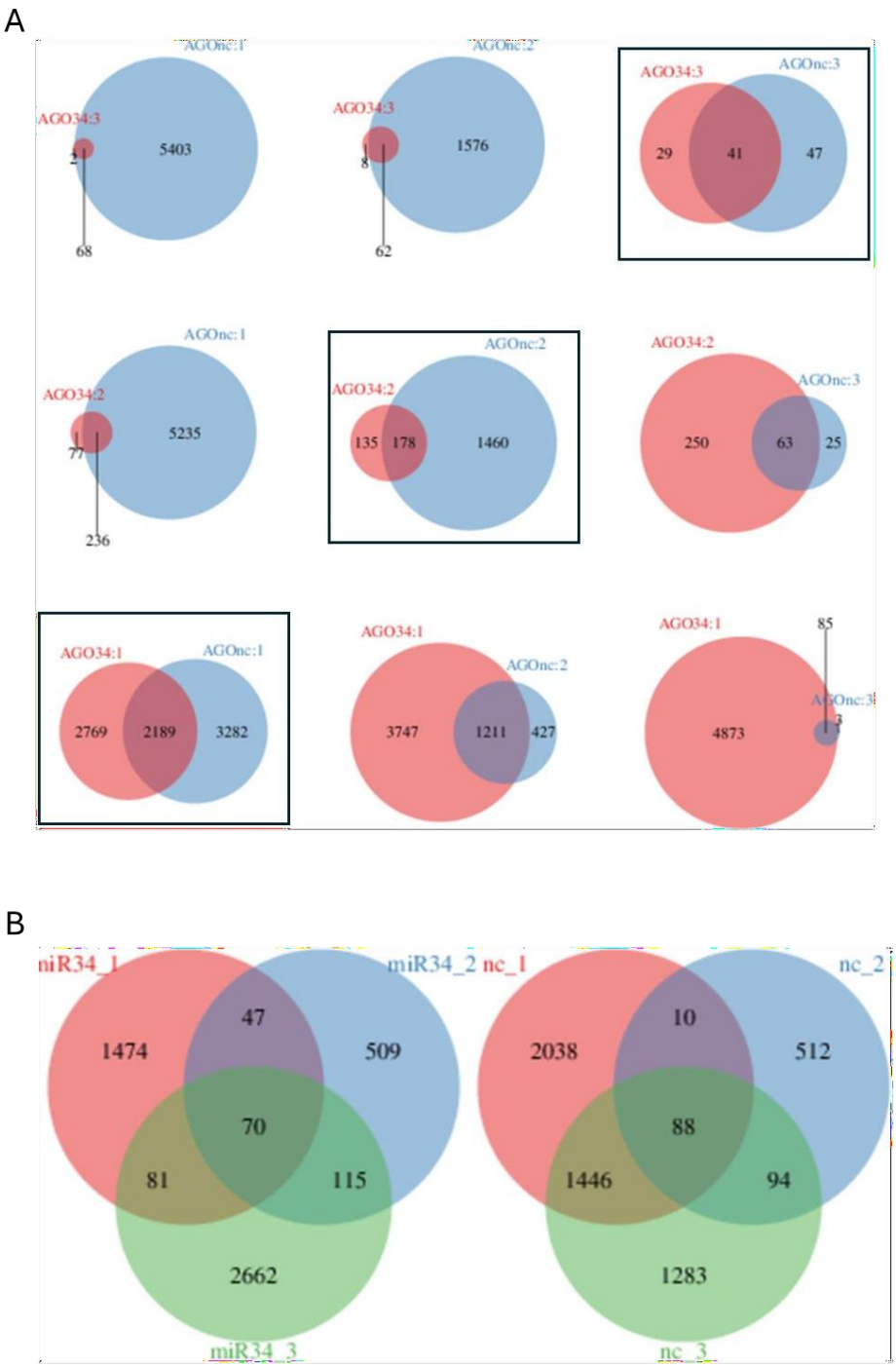

Figure 29. Overlap of RIP-seq data between experiments of the AGO-miR-34a5-5p and AGO-nc#1 samples. A)Inter group overlap of peaks. Samples with their respective controls are marked by frame. B) Intra group overlaps of peaks.

6.2. DNA methylation

Gene expression is not only regulated by one epigenetic mechanism but by multiple factors playing together. To investigate the full picture of epigenetic regulation of the TH metabolism and miR-34a-5p in the liver during MASH the next part of this thesis investigates the role of DNA methylation. The results of the *THRB* methylation analysis have already been published in the European Thyroid Journal [261].

6.2.1. THRB

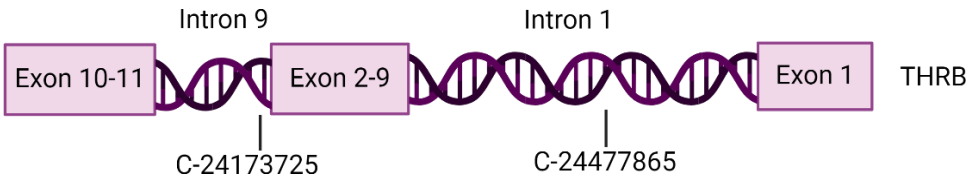

Figure 30. Schematic view of THRB gene with investigated CpG sites.

Due to the reduction of *THRB* expression during MASH and the tendency of increased DNA methylation in the promotor and intron 1 region to reduce gene expression [154] a CpG site with multiple transcription factor binding sites of potential interest was identified using JASPAR 2022 [264]. Using pyrosequencing the CpG at chromosome 3 position 24477865 (C-24477865) was identified as differentially methylated with a significant increase in methylation of 9.71% (p-value = 0.002) in the liver of MASH patients compared to non-MASH controls (Figure 31A). The increase in methylation did indeed correlate negatively with the expression of *THRB* ($r = -0.5132$, $p = <0.001$) (Figure 31B) and showed positive correlation with MAS ($r = 0.4674$, $p = 0.004$), HbA1c ($r = 0.4444$, $p = 0.02$), aspartate aminotransferase (AST) ($r = 0.5641$, $p = <0.001$), alanine aminotransferase (ALT) ($r = 0.4885$, $p = 0.003$) and liver fat ($r = 0.4857$, $p = 0.02$) (Figure 31C-G). All results were corrected for the confounding factors age and gender.

Due to the possible effect of methylation in the gene body, CpG site C-24173725 was investigated. Methylation at the CpG was reduced by 2.17% but without significance and no further methylation investigation was conducted.

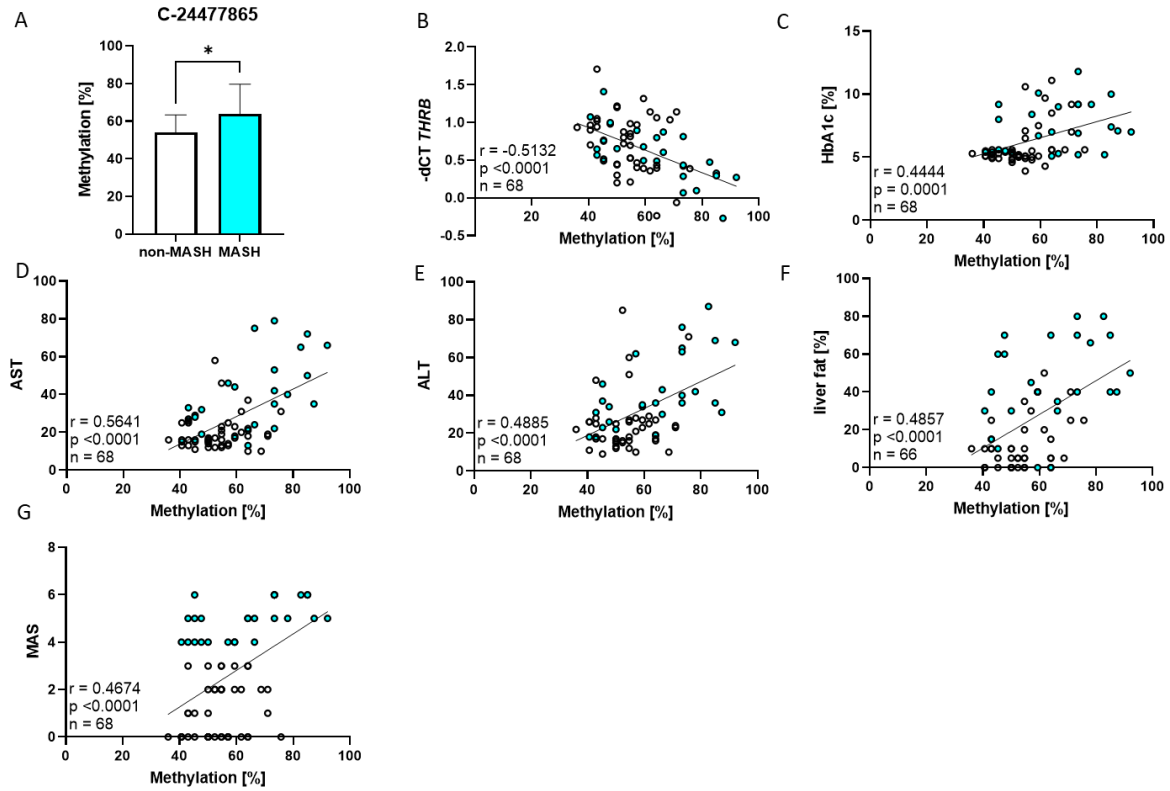

*Figure 31. Methylation of THRB in human liver tissue. A) Methylation differences in THRB for patients with and without MASH analyzed after Man-Whitney. Spearmen correlation of methylation with B) THRB, C) HbA1c, D) aspartate aminotransferase (AST), E) alanine aminotransferase (ALT), F) liver fat and G) MASLD activity score (MAS). * > 0.05.* [261]

6.2.2. *MIR34AHG*

Since the miR-34a-5p expression is significantly induced in patients with MASH and the induction od miR-34a-5p expression in cell culture with metabolic stimulation was not successful methylation was considered as alternative cause for the dysregulation of miR-34a-5p expression. MiR-34a-5p is encoded on the minus strand of chromosome 1 within the second exon of the host gene *MIR34AHG*. While the expression of miR-34a-5p is only partially dependent on the expression of *MIR34AHG* the promotor region of *MIR34AHG* was selected for methylation analysis, due to the presence of CpG islands. A CpG island containing 7 CpGs was analyzed (Figure 32) (chromosome 1 positions 9243171-9243202), neither the mean, nor analysis of each individual CpG resulted in significant methylation differences between the non-MASH and MASH group. While further CpG areas of interest were identified, the high CG content of the DNA resulted in difficulties designing functioning pyrosequencing assays and was therefore, not further conducted.

Figure 32. Schematic view of MIR34AHG and MIR34A genes on chromosome 1 with the CpG island used for methylation analysis.

6.3. *THRB* tag

To solve the problem that there are no functioning *THRB* antibodies and qPCRs only give information of the transcription of a gene and not the actual amount of translated protein *THRB* tags were designed for future CRISPR/Cas modification of iPSC derived hepatocyte-like cells. Three plasmids were designed, one containing the *THRB* gene without any modifications, one with THRB and a C-terminal 3xHis tag and one with *THRB* and a C-terminal 3xFLAG tag (see vector cards in 11.1). To determine the effect of the added tags on THRB function, Huh-7 cells were stimulated with different concentrations of T_3 for 48 h. The THRB regulated genes *DIO1*, *THRSP*, *FASN* and *CYP27A* were measured. The expression of *THRB* itself was measured and increased as expected according to the respective plasmid concentrations. Meanwhile there were no significant differences in the T_3 response between the gene expression of tagged and untagged *THRB*, notably there was also no difference between the two tags (Figure 33A-D).

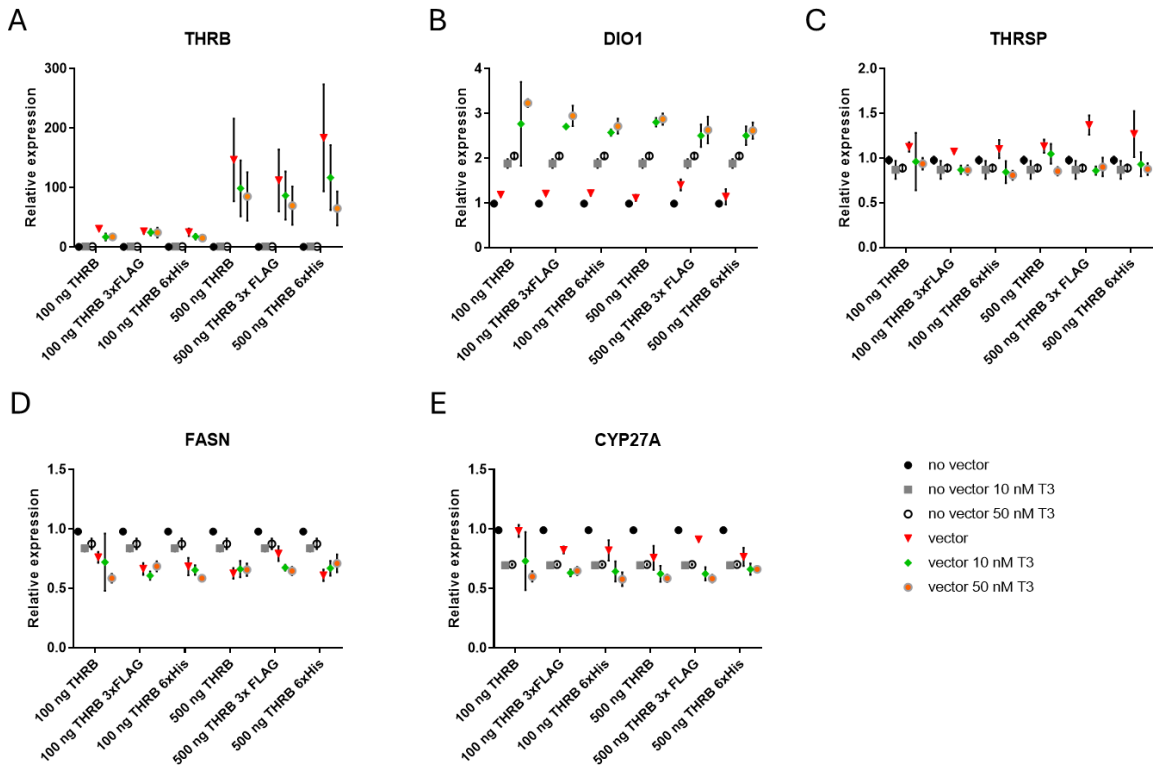

Figure 33. THRB tag test mRNA expression of THRB regulated targets. Expression of A) THRB, B) DIO1, C) THRSP, D) FASN and E) CYP27A. Data were analyzed with two-way ANOVA and are depicted as mean with SEM.

To ascertain that the selected tags not only have no negative influence the THRB function but are also accessible for Western blot detection, the plasmids were transfected into HEK293T cells and incubated for 72 h. Both antibodies, 6xHis and 3xFLAG were tested with a dilution of 1:500 and 1:1000. The molecular weight of THRB is 52.7 kDa, with the weight of the 3xFLAG tag (3 kDa) or the 6xHis tag (0.8 kDa) a detection at approximately 55 kDa can be expected. Indeed both antibodies show binding at the expected weight. The 6xHis antibody shows an additional unspecific band at approximately 70 kDa in both the sample containing the tagged THRB as well as in the negative control without tag. The 3xFLAG antibody only shows an unspecific band at around 90 kDa in the tagged sample (Figure 34A). The housekeeper HSP90 showed the expected band at 90 kDa, another band can be seen on the blots of the tagged samples which are presumably residues of the tagged antibodies which were not stripped thoroughly enough (Figure 34B). Taken together the results show no effect of the tags on the THRB function and both antibodies show clear and distinct bands on the Western blot, meaning that both tags have the potential for future experiments. Adding one of the tags to cell lines could bypass the problem of ineffective THRB antibodies and could visualize the effect of the conducted treatments on the protein level.

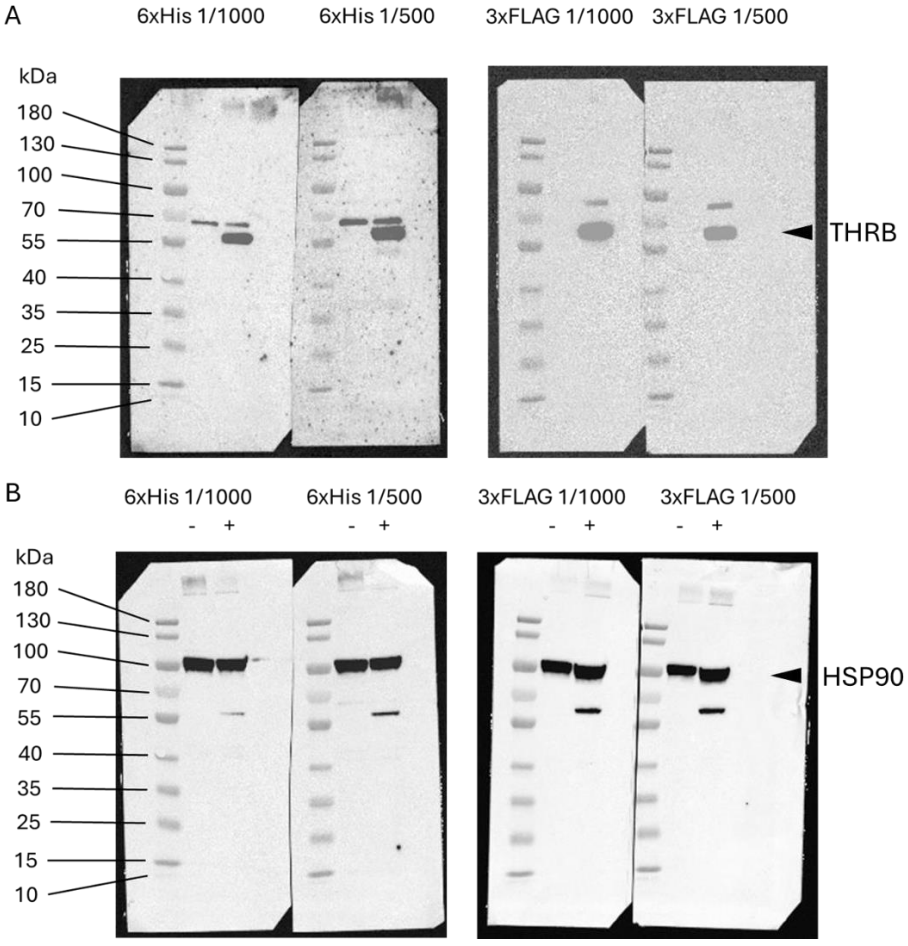

Figure 34. Western blot of THRB tag tests with His and FLAG tags. A) HIS and FLAG , B) HSP90 as housekeeper

7. Discussion

The aim of this thesis was to join the known contributors of MASLD, epigenetic changes and dysregulation of thyroid hormone signaling. To achieve this aim miRNAs were identified that were increased in MASH patients and mouse models that potentially target THRB. One identified miRNA was miR-34a-5p. The relevance and binding of miR-34a-5p was verified in cell culture studies. Additionally, changes in methylation of THRB were observed in MASH patients that correlated with THRB expression. Taken together the results show the connection of epigenetics and thyroid hormone signaling in MASLD and propose a new target for MASLD therapies.

7.1. MASLD, TH and miRNAs

While the results of this thesis could not confirm the relevance of miR-224-3p and miR-155-5p in the TH metabolism in MASLD, there is a clear connection between miR-34a-5p and TH metabolism. We were able to verify increased miR-34a-5p expression in a human MASH cohort and in multiple mouse models. The miR-34a-5p expression correlated with the MAS in humans and luciferase assays verified binding of miR-34a-5p to *THRB* and *DIO1*. RIP-seq could additionally prove the binding of the miRNA to *THRB* and overexpression of the miRNA in vitro verified the role of miR-34a-5p in TH signaling. Studies on the role of miR-34a-5p in MASLD have until now mainly concentrated on the regulation of lipid metabolism by inhibition of SIRT1 [235,236], PPARA [236] and HNF4a [209,226], which contribute to the pathogenesis of the disease, by inducing steatosis, fibrosis and mitochondria dysfunction. We previously published our results on the regulation of TH signaling by miR-34a-5p [261]. These results are presented here again with additional mouse and cell culture models. The relevance of miR-34a-5p in MASLD in mouse models was highlighted by a miR-34a knock-out model that showed reduced manifestation of MASLD after being fed a high-fat, cholesterol, fructose diet [227]. This thesis focused on the local control of TH action and takes additionally the TH receptors, hepatic TH transporters SCL10A1 and SLC16A2 and TH activating enzyme DIO1 into account.

Additionally to the human data four different mouse models, investigating different aspects of MASLD, were analyzed. Both models containing HFD (CD-HFD model and HFD-metformin model) showed an induction of miR-34a-5p expression, as expected, surprisingly the MCDD model did not. Differently to the HFD models the MCDD does not induce metabolic syndrome and should only be used as a model to study the liver independently from systemic affects, due to the loss of weight and absence of metabolic syndrome [74]. In contrast to that, another study performed by Katsura et al. observed an increase of miR-34a expression in MCDD fed mice after 15 weeks compared to the only 6 weeks of the here studied cohort [265]. This implicates that the development of metabolic syndrome might not be necessary to induce miR-34a expression. But that miR-34a expression can also be induced by later stages of liver injury like the ones caused by the lack of methionine and choline. This early increase in miR-34a expression observed in HFD mouse models might be explained by the changes in the microbiome induced by the increased fat content. Indeed, increased expression of miR-34a has been linked to changes in microbiome which is observed in obese patients and mice fed a HFD and treatment of HFD mice with G*ynostemma pentaphylla,* a substance from traditional Chinese medicine that has been used to treat hyperlipidemia, reduced miRNA expression and induced changes in the microbiome composition [234]. Mice on HFD develop dysbiosis after one week. The MCDD mice do not have this change in microbiome and therefore, not the increased induction of miR-34a-5p expression, at least in early stages of liver injury. This also highlights that the MCDD model is only partially able to mimic MASLD and might not be the best model to investigate epigenetic changes. Taking into account that in the MCDD model the liver injury is induced by dysregulation of the methionine cycle and not a consequence of disease progression. In reverse, increased intake of

methionine has also been associated with MASLD risk [266]. On the other hand, the CCl_4 model, which is mainly used as a fibrosis control and also does not manifest metabolic syndrome shows increased miR-34a-5p expression. This liver model directly induces fibrosis in the liver, without steatosis through oxidative stress which recruits proinflammatory Kupffer cells and activates hepatic stellate cells [267]. While the role of miR-34a-5p in fibrosis is well established [268], CCl_4 itself represses the expression of FXR, which negatively regulates miR-34a-5p expression, leading to an increased expression [269]. Intriguingly, the expression of miR-34a-5p was reduced in HFD mice after 6 weeks of metformin treatment. Metformin targets the glucose metabolism and induces insulin sensitivity [270] and treated mice show improved steatosis [251]. This increase and decrease on miR-34a expression after methionine treatment was also observed in a MCDD mouse model by Katsura et al. [265]. In contrast to our findings and of Katsura et al., there are multiple studies that observe an increase in miR-34a expression after metformin treatment. Metformin treatment of cancer cells induced an increase of p53 expression, a miR-34a regulator in multiple cancer cell lines, though that effect was not observed in p53 mutant cancers. This increase in miR-34a expression leads to a downregulation of SIRT1 and resulted in a susceptibility of the cancer cells to oxidative stress and apoptosis [271]. Additionally, there is data, that metformin stimulates Dicer which increases miR-34a availability and positively influences liver inflammation [272]. These studies observing an increase in miR-34a expression upon metformin treatment were conducted in cell culture and treatment duration was 24 h, meanwhile the decrease in miR-34a expression was observed in animal models after 6 and 15 weeks of treatment. Consequently, the increase of miR-34a might be a short term reaction. Additionally, the decrease might be a systemic effect of metformin on the body compared to the effect on only one cell type. Considering the mechanism of metformin is only partially understood more studies have to be conducted.

We were able to confirm binding of miR-34a-5p to *THRB* and *DIO1*. The observed increased expression of miR-34a-5p dysregulates the TH signaling in more than one way. The reduced production of TRβ reduces the ability of the receptor to regulate respective target genes resulting in an increase of de novo lipogenesis and a reduction in β-oxidation. Indeed in patients with a thyroid hormone resistance to TRβ, caused by a mutation in the THRB gene that results in a loss-of function of TRβ, a significantly higher liver fat content was observed [140]. Additionally, *THRB* knockout mice show changes in liver gene expression and the loss of TRβ results in changes of the diurnal rhythms of cholesterol and fatty acid metabolism leading to an accumulation of cholesterol, fatty acids and TGs in the liver [273]. Considering the role TH signaling plays in cholesterol, lipid and carbohydrate metabolism these changes are not surprising and are also observed in hypothyroidism, which is associated with MASLD [120]. Local hepatic hypothyroidism can also be induced through the reduction in *THRB* expression. One of the TRβ target genes affected by the reduction in TRβ signaling is *DIO1* [274]. As a miR-34a-5p and TRβ target, the expression of *DIO1* is inhibited by two different mechanisms. This inhibition of *DIO1* expression leads to a reduced amount of available T_3 in the hepatocyte, which in turn reduces activation TH induced TRβ signaling. A reduced activity of DIO1 and therefore, activation of T_4 to T_3 has also been observed in people with *DIO1* polymorphism with reduced DIO1 function [275], leading to a hypothyroid state in the liver. Similarly, reduced DIO1 action on TH signaling is likely the reason older humans, which have reduced *DIO1* expression levels are more likely to develop MASLD [32]. Reduced availability of T_3 also influences the mitochondria and less oxygen consumption has been observed in hypothyroid animals as well as changes in mitochondrial gene expression and a reduction in mitochondriogenesis [116]. Despite multiple regulatory interference in *DIO1* expression during the early stages of MASLD development, a compensatory induction of *Dio1* is observed in mouse models [276]. This early induction was also present in the analyzed HFD-metformin model as well as the CD-HFD model. The increase of *Dio1*

has a protective effect on steatosis progression [276]. Surprisingly the treatment with metformin had no effect on the increased *Dio1* expression, despite the improved steatosis and is slightly higher than the not treated HFD group. Considering the reduced expression of miR-34a-5p after metformin treatment, this would reduce the negative regulation of *Dio1* through the miRNA and could contribute to the improve in steatosis. While the lack of T_3 and lack of TRβ both negatively affect the hepatic metabolism, they result in different changes in gene expression, with TRα potentially compensating for TRβ through the ability to bind the same TREs [277]. This illustrates the non-receptor dependent activity of thyroid hormones. An increased expression of *Thra2* was only observed in the MCDD mice. The *Thra2* isoform contains a DNA binding domain, by which it can compete for binding with other TRs, but lacks a ligand binding site. Due to limited data the function of *Thra2* is not yet known and more studies have to be conducted to ascertain its role in MASLD [278]. Considering that *Thra2* potentially competes with *Thrb* DNA binding, this would further reduce signaling of TH in the liver of MCDD mice. Meanwhile, the expression of *Thra1* was induced in the CD-HFD mice after 52 weeks, but not in any other mouse model or human sample. The induction could be a compensatory effect in a late stage of MASLD, though no comparable observations have been reported in literature.

The effect of increased miR-34a-5p expression on the predicted and confirmed targets was further investigated in cell culture experiments. The resulting decrease of the TH receptors, *DIO1* and *SLC10A1* further highlighted the potential of miR-34a-5p to regulate the local thyroid hormone action. The TH transporter channels T4 and T_3 into the hepatocyte, contributing to the availability of TH to activate TH signaling. Repression of transporter expression, subsequently prevents transport of TH into the cells. The effect on the TRβ action could be verified by the reduced response of TRβ regulated genes *CYP7A1* and *DIO1* to T_3 stimulation. Surprisingly the predicted target *SLC16A2* increases expression after miR-34a-5p overexpression. This might be explained by a disruption of the diurnal rhythm of the expression due to the changes in TH levels in the cells [279]. SIRT1 also is involved in regulation of circadian clock gene expression [280]. As a target of miR-34a-5p it is downregulated upon miR-34a-5p transfection, which could lead to further disruption of the circadian rhythm in hepatocytes. Decreased SIRT1 expression and the resulting changes in the circadian rhythm , have been shown to reduce cell survival and increases the risk of cancers [281].

Metabolic stimulation results not in induction of miR-34a-5p but insulin resistance seems to influence TH signaling

Induced expression of miR-34a in cell culture has only been conducted by the activation of p53 [229] and demethylation of MIR34AHG [282], but not through metabolic stimulation. Due to the central role of fructose in the development of MASLD and its ability to affect lipid metabolism and induce hepatic insulin resistance [33–35], the stimulation of cells with high fructose levels for 24 h to induce miR-34a-5p expression was the trial of first choice. This stimulation did not result in the desired increase in expression and did not affect the expression of miR-34a-5p target genes. On the other hand, treatment of HepG2 cells using an oleate and palmitate mixture did induce miRNA expression, but without effects on the miRNA target gene expression. This effect was only observed after 48 but not 72 h of treatment. Other studies observed changes in the expression of miRNAs 6 to 36 h after cell stimulation or injury [283,284], indicating that the peak of miR-34a-5p expression might have occurred earlier and was not detected. However, the increase of miR-34a-5p expression, while significant, was only a slight increase and its lacking impact on miR-34a-5p target gene expression indicates that the increase was not high enough to reach biological significance.

Interestingly the stimulation of HepG2 cells with high fructose in addition to high insulin concentrations resulted in a downregulation of miR-34a-5p targets *THRA*, *THRB*, *DIO1* and *SLC10A1*

and upregulation of *SLC16A2*, identical to the effects observed after overexpression of miR-34a-5p after 48 h. To rule out any effects of the miRNA, the experiment was repeated with the addition of a miR-34a-5p inhibitor, which had no effect on the expression levels of the target genes. To rule out compensatory upregulation by miR-34b-5p and miR-34c-5p, their levels were measured as well and did not increase with metabolic stimulation. The downregulation of TH metabolism genes was also not observed in cells treated with high fructose and high glucose levels, implying that the effect is induced by the high insulin levels. THs and insulin indeed overlap in some of their functions, through the regulation of metabolic pathways. Moreover, some studies that show a connection between THs and insulin resistance. Both hypothyroidism as well as hyperthyroidism seem to facilitate the development of insulin resistance, though studies are not entirely conclusive [285,286]. During hyperthyroidism THs antagonize insulin action through an increased glucose production [287] and regulate insulin signaling through the modulation of FOXO1 [135]. Despite the connection between insulin signaling and THs there is little information on the effect of insulin on thyroid hormone signaling. One study reported an increase in TRα1 and TRα expression upon insulin stimulation in bovine aortic endothelial cells and observed no changes in TH transport into the cells [288]. This would contradict the results of this study, since we observed a decrease in both TRα and TRβ. However, we conducted the experiment in HepG2 in which TRβ is the predominant receptor while in aortic endothelial cells TRα is the predominant form. Meanwhile, reduced expression of *Dio1* has been observed in mice with a liver-specific insulin receptor knockout [289]. While disruption of insulin signaling through the loss of insulin receptor and induced insulin resistance through high doses of insulin are not entirely equivalent, there is evidence that high doses of insulin do reduce the expression of the insulin receptor gene [290], emphasizing the involvement of loss of insulin receptor on the reduced expression of *DIO1*. Apart from the influence of insulin on DIO1 and therefore, the TH availability in the cells, there is no evidence that insulin influences the expression of TH transporters.

To get a better understanding of the affected pathways, RNA sequencing was performed using the samples treated with fructose and insulin for 48 h and the ones treated with miR-34a-5p inhibitor and fructose and insulin for 48 h compared to a control. The KEGG pathway analysis shows differently regulated genes for both conditions in the MAPK pathway which is induced by insulin [291] but repressed by TH action [105]. This fits nicely with the observed reduction of TH metabolism related genes. Thyroid hormones also play a role in cell proliferation and differentiation, by repressing or activating gene expression, depending on tissue and developmental stage [292]. It is therefore not surprising that reduction of TH metabolism gene expression in both conditions leads to upregulation in cell cycle, DNA replication and cellular senescence pathways. A downregulation of the TH signaling pathway was, as expected observed in both conditions as were changes in cholesterol and carbohydrate metabolism. Surprisingly, there were no changes in insulin signaling detected, though the cells treated with fructose and insulin showed differently expressed genes in the AGE-RAGE signaling pathway in diabetic complications. The inhibition of miR-34a-5p in combination with the metabolic stimulation led to an enrichment in liver injury pathways observed in hepatitis c infection and hepatocellular carcinoma. Considering that miR-34a-5p expression is well known to change during liver injury, an increase in expression has been observed after hepatitis C infection [293,294]. The expression of miR-34a changes in hepatocellular carcinoma depending on the p53 status [228,229], so changes upon miRNA inhibition are not surprising. To determine the connection between insulin stimulation and the expression of TH metabolism genes, more experiments need to be conducted.

Validation of miRNA target gene binding

Target gene prediction of miR-34a-5p indicated binding sites in *THRA*, *THRB*, *DIO1*, *SLC10A1* and *SCL16A2*, though only binding to *THRB* and *DIO1* could be validated by luciferase reporter assays and the binding to *THRB* additionally with RIP-seq. The luciferase reporter assay and RIP-seq results are further confirmation of miRNA and mRNA interaction due to the downregulation of the predicted targets after miR-34a-5p transfection. Considering the induced expression of *SLC16A2* after the miR-34a-5p transfection, *SLC16A2* was not further investigated for miRNA binding. The prediction of miRNA target genes is easy if the miRNA is completely complementary to the target, though the majority of miRNA bind with only the seed sequence to the target mRNA. The seed sequence also can be between 6 and 8 nt long and target prediction tools only take sequence complementarity and rarely the accessibility of the mRNA sequence into account. Therefore, target prediction of miRNAs generates many false positive and false negative predictions [179]. Though accuracy for 8mer seed sequences is quite good, with reducing success rate for shorter seed sequences [175] and the predicted targets have to be verified by experimental methods. Because multiple binding sites were predicted for some of the potential targets, RNA secondary structure prediction was used to determine the most likely accessible miRNA binding sites. The CentroidFold tool was used, which is reliable but the accuracy reduces with increase in sequence length [257]. The secondary structure of the mRNA 3'UTR influences the accessibility of the binding of the miRNA [295,296]. Though the CentroidFold prediction was limited to a length of 400 nt, which corresponds to approximately the same length of insert that was used for the luciferase reporter assays (± 200 nt from the seed sequence binding site). Considering the 3'UTRs can reach lengths of a few thousand nucleotides [297] the predicted structures can only depict the actual secondary structures to a certain extend. Similarly, the most accurate way to test miRNA to target binding using the luciferase reporter assay would be the cloning of the complete 3'UTR of the target mRNA into the luciferase plasmid. While the cloning of large inserts in possible, the efficiency decreases with increased insert length. Therefore, smaller inserts were chosen. Since binding sites were more than 200 nt apart, only one binding site could be examined at a time. It is possible that despite less favorable prediction of the secondary structure, the actual structure would be more accessible or that the complete 3'UTR forms a different structure compared to the predicted sections. The distance between the binding sites of miRNAs can have an effect on the miRNA function. Distances between 10-50 nt tend to increase the repressing nature of miRNAs, while binding sites closer than 8 nt together compete for miRNA binding [298,299]. Considering the large distance between the binding sites such an effect was not to be expected, though binding to more than one binding site in the 3'UTR would increase the efficacy of miRNA action without the cooperative nature of close binding sites. Despite these drawbacks the luciferase reporter assay is the gold standard to verify miRNA and mRNA specific interactions [300].

For further confirmation of the interaction of miR-34a-5p and the predicted target genes RIP-seq was conducted. After transfection of miR-34a-5p into the cells to saturate the miRISC with miR-34a-5p and target mRNAs, a total of 544 different mRNAs were detected. Of these 265 were predicted miR-34a-5p targets and 279 not associated with the miRNA. Considering that miR-34a-5p is predicted to have 10399 target genes, the detected quantity is quite low especially considering the quantity of unspecific binding. This indicates that a number of housekeeper genes were detected, despite an input control to prevent this. Unfortunately the AGO genes are predicted targets of miR-34a-5p which could influence the amount of miRISC formation and distort the results. The detected genes were further processed with KEGG and GO pathway analysis. Both analyses detect metabolic pathways, the KEGG pathway analysis additionally detects changes in NAFLD pathways and p53 signaling. Considering the role of miR-34a-5p in metabolic dysregulation in MASLD and the reciprocal regulation of p53 and miR-34a-5p [301] the detection of these pathways emphasizes the validity of the experiment.

Nevertheless, there is a high variation between the three replicates of the RIP-seq experiment with a high difference between detected peaks and a low overlap of peaks between the repeats. For this thesis the protocol of Meier *et al*. [180] was adapted. Meier *et al*. generate a stable cell line with continuous miRNA of interest expression. In contrast in this study the cells were transfected once with a miR-34a-5p mimic to generate the increased availability of the miRNA. A stable cell line producing miRNAs has a more homogeneous expression pattern than what can be achieved with single transfections of miRNA, with varying transfection efficiencies. This was already observed in earlier experiments see Figure 22A, but did not impede the effect of miR-34a-5p overexpression on the target genes. A variation in the transfection could contribute to the variance in the detected target genes, especially considering that the AGO2 production might be reduced by miR-34a-5p. A variation in miR-34a-5p levels, though variations in transfection would also lead to variations in AGO2 availability. Verification of reduced AGO2 protein production upon miR-34a-5p overexpression would be helpful for the planning of further experiments. If the miRNA indeed impedes AGO2 production , creating a cell line with a AGO2 plasmid in addition to stable miR-34a-5p could be helpful to counteract the effect of the miRNA to improve miRISC assembly.

7.2. MASLD, TH and DNA methylation

As already reported in [261] we were able to show an increased methylation in *THRB* at chromosome 3 position 24477865 (C-24477865) which negatively correlated with THRB expression and positively with MAS, once more validating the importance of *THRB* in MASLD. Similar to the reduced expression of *THRB* through miR-34a-5p, increased methylation of *THRB* dysregulates the TH signaling and increases lipid accumulation. As expected *THRB* methylation explains one part of the dysregulation and is described in further detail above (7.1). The methylation site was selected for investigation due to the association of increased DNA methylation in the promotor and intron 1 to reduce gene expression [154] and a high number of transcription factor binding sites in the vicinity of the CpG site. The reduction of *THRB* gene expression could therefore be expected and contributes to the relevance of changes in DNA methylation in metabolic diseases [144].

While we were unable to show a difference in *MIR34AHG* methylation, which might be due to difficulties in assay design for pyrosequencing in the CpG island. To prevent the formation of secondary structures the PCR product used for pyrosequencing should be limited to a length less than 350 bp, though the utilized PyroMark from Qiagen recommends sequence lengths of less than 200 bp. Additionally, the designed primer should not overlap with CpG sites to prevent the preferential amplification of a subset of molecules and not contain palindromes to ensure specific binding [302]. The design of primer with binding specificity for only one binding site, that also does not overlap with a CpG site can be difficult within CpG islands, due to the repetitive CpG motif and the high AT content in bisulfite converted DNA. The complete CpG island has a length of 433 bp (chromosome 1 position 9243032-9243465). Therefore, the length limitation of the investigated sequence prevents the analysis of the complete CpG island, and it could be possible that there is a change in DNA methylation within the CpG island, but not in the investigated part. The difficulties of developing appropriate primers prevented the investigation of other parts of the CpG island via pyrosequencing. While pyrosequencing is a reliable DNA methylation detection method for short sequences, longer sequences are better investigated using whole genome bisulfite sequencing. Additionally, there is less variability in replicates of whole genome bisulfite sequencing experiments compared to pyrosequencing assays due to a lower PCR amplification bias [303]. There are no studies that show changes in *MIR34AHG* methylation in metabolic disease but, *MIR34AHG* is frequently

hypermethylated in multiple cancer types which interferes with the binding of p53 to the DNA and therefore, reduces miR-34a-5p expression [304]. To further investigate the DNA methylation of *MIR34AHG*, established primers that were successfully used to detect aberrant DNA methylation in cancer could be used to detect changes in MASLD patients. Changes in DNA methylation have also been observed in the *TP53* gene [305], a miR-34a-5p regulator. Therefore, it would be interesting to further measure DNA methylation if *TP53* of MASLD patients compared to healthy controls and whether there is an association with disease severity. Considering that the expression of miR-34a-5p can change from over expression to a reduced expression in HCC depending of the p53 status a change in *TP53* methylation might be observed as the disease progresses from MASH to HCC.

While there are CpG sites in and around the *DIO1* gene, there are no CpG islands and none of the CpG sites are associated with any disease. Whole genome bisulfite sequencing in a subset of the human cohort (unpublished data by Christin Krause) did also not identify any differentially methylated CpG sites in the *DIO1* gene or promotor region. Therefore, no pyrosequencing was performed to determine DNA methylation changes in the *DIO1* gene.

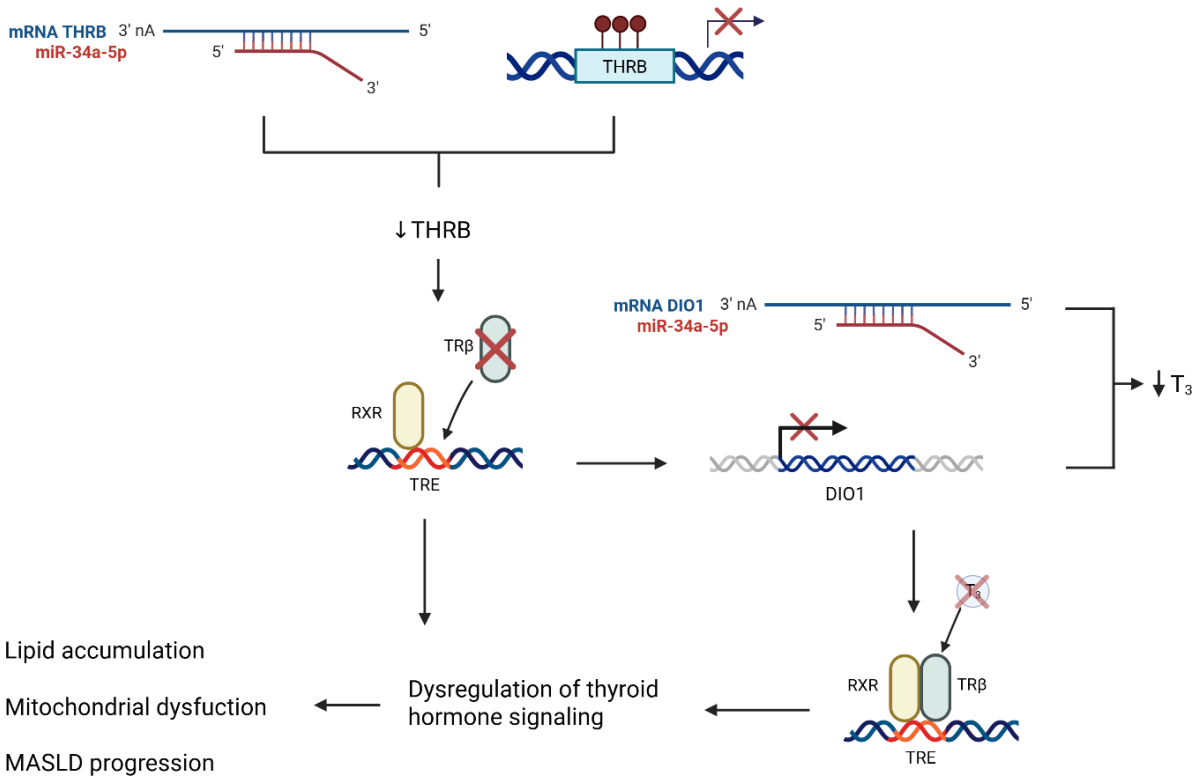

Figure 35. Epigenetic regulation of hepatic thyroid hormone signaling in metabolic dysfunction-associated steatotic liver disease (MASLD). The increased expression of miR-34a-5p during MASLD leads reduced expression of the thyroid hormone receptor beta gene (THRB) by binding of the miRNA to the THRB mRNA. Simultaneously, the increased methylation of the THRB gene reduces THRB expression, contributing to the reduced availability of thyroid hormone receptor beta (TRβ) in MASLD. The reduced TRβ level lower the binding probability of TRβ to the thyroid hormone response element (TRE) and prevents TRβ from regulating gene expression. The resulting loss of TRβ regulation of the deiodinase type 1 gene (DIO1) leads to less DIO1 expression. The binding of miR-34a-5p to the DIO1 mRNA also reduces DIO1 availability. Consequently less thyroid hormone T_4 is converted into

the active form T_3. The reduced availability of T_3, also means less binding of T_3 to TRβ and therefore, less thyroid hormone mediated regulation of gene expression. The combination of reduced TRβ and T_3 availability and activity results in a dysregulation of the hepatic thyroid hormone signaling. This induces accumulation of lipids in the liver, dysregulation of mitochondrial function and MASLD progression. RXR: retinoid X receptor

7.3. Limitations of the study

The investigated human cohort consisted of obese individuals with and without MASH, however, no healthy control individuals were included. While this cohort rules out distortion of the results caused by obesity a control sub cohort of healthy individuals without obesity and comorbidities would be beneficial to detect early onset changes in MASLD development.

The mouse models utilized in this thesis encompass different stages of MASLD and while none of them mimic the development of human MALSD completely they are useful, as long as their limitations are considered. Unfortunately the investigation of epigenetic changes is complicated by the lack of conservation od miRNAs between mouse and human which limited the investigation of miR-224-3p to cell culture. While there is generally a conservation of miRNAs between human and mice, especially in miRNAs relevant for fundamental biological functions, the conservation varies between miRNA families, tissues and developmental stage [306]. Even conserved miRNAs across species might have different functions, due to a lack of conserved binding sites, indeed about 30 % of validated miRNA targets are not conserved between species [300]. Therefore, miRNAs in mice can act differently than a miRNA with the same seed sequence in humans. The binding of miR-34a-5p to *THRB* and *DIO1* was validated using parts of the 3'UTRs of the human genes. Considering possible differences in the secondary structure of the 3'UTRs in mice, the luciferase reporter assays would have to be repeated using the mouse genome. That also means that the effects of miRNAs in model organisms are not always transferable to human conditions. Additionally, the interpretation of miRNA literature is difficult at times because the two miRNA strands of the duplex miRNA have different seed sequences and subsequently different targets and functions. While the loading to the miRISC can have a preferential miRNA due to stability, both miRNAs have the potential to be regulatory active. Since many publications do not differentiate between the 5p and 3p miRNA contradicting results are difficult to interpret, whether the discrepancy is caused by differences in models and experiments or investigated miRNA strand.

Another limitation of this study are the utilized cell lines. The effect on the TH metabolism related genes by insulin was only observed in HepG2 cells and could not be replicated in Huh-7 cells. The HepG2 cells were selected as main hepatocyte model due to the expression of TH metabolism related genes, while Huh-7 cells lack *SLC16A2* expression and would therefore, not accurately depict the effect of TH signaling. Nevertheless, both cell lines showed expected increase in TRβ regulated gene expression after T_3 stimulation (see 6.1.4.1.1. and 6.3.). Considering, that both cell lines are immortalized cancer cell lines, changes in gene expression are to be expected. Additionally, Huh-7 cells are derived from a hepatocellular carcinoma while HepG2 cells are from a hepatoblastoma. A key difference between both cell lines is the absence of miR-122 expression in HepG2 cells [307], the most abundant miRNA expressed in the liver [308]. The loss of miR-122 in HepG2 cells leads to a disruption of liver homeostasis and suppression of hepatic phenotype [309]. This could make HepG2 cells more sensitive to changes in miRNA concentration compared to Huh-7 cells, but also underlines the differences between cancer cell models and actual hepatocytes. Indeed there are differences in the lipid metabolism with both cell lines exceeding the rate of DNL compared to the rate observed in MASLD patients. The rate of DNL in HepG2 cells is significantly smaller than in Huh -7 cells and while still supraphysiological closer to MASLD conditions [310]. To ascertain that insulin and miR-

34a-5p affect the TH signaling in MASLD, experiments would have to be conducted in a MASLD model closer to healthy hepatocytes. To that effect, preliminary experiments were conducted using iPSC derived hepatocytes with fructose and insulin stimulation. Unfortunately the maintenance medium of the differentiated hepatocytes contains a not disclosed amount of insulin, which could distort the results. Additionally, transfection of the cells with miR-34a-5p showed a low transfection efficiency. Therefore, the protocols for metabolic stimulation and transfection need to be optimized for further experiments.

Lastly the effect of miRNAs on their targets does not always translate into a measurable degradation of mRNA but can also effect the protein levels without causing changes in mRNA levels [173]. Unfortunately, there are no reliable antibodies available to measure TRβ. Therefore, it is possible that changes in protein levels were overlooked, due to no changes in mRNA levels. To circumvent this problem we successfully designed tags that can be added to the C-terminal end of the THRB gene without disrupting the function of the protein (Figure 33). These tags have been added using CRISPR/Cas to iPSC cell lines which can be differentiated into hepatocyte-like cells, though at the conclusion of this thesis the cells were undergoing quality control and were not yet available for experiments.

7.4. Implementation

We were able to show that the increase of miR-34a-5p negatively affects the TH signaling and increased expression in the liver. The only recently approved MASH medication, resmetirom, is a TRβ agonist and improves steatohepatitis by induction of TH signaling [70]. Still there are unresponsive patients, which have no other option than to use life style changes to manage their disease. Overexpression of mir-34a-5p can be detected in blood serum levels and could therefore, indicate patients that could potentially profit from a reduction of miR-34a-5p levels. Indeed miR-34a has been proposed as a biomarker for MASLD severity [224], though considering that miR-34a is also increased in other liver diseases it should not be used for initial diagnosis. We were able to show that treatment of HFD fed mice with metformin reduced miR-34a-5p levels in the liver and thus propose that patients with increased miR-34a-5p levels, who are unresponsive to resmetirom could benefit from the miR-34a-5p lowering quality of metformin. Additionally to metformin, while not currently in development, an antagomir or miRNA sponge could be developed that targets miR-34a-5p levels and would present another option for the improvement of resmetirom function. Considering the tumor suppressor activity of miR-34a-5p a complete loss of miR-34a-5p function might not be beneficial for MALSD patients and the level might need tight controls. Additionally, after progression of MASLD to HCC, treatment with miR-34a-5p might depend on the p53 status and after loss of p53 function patients might benefit from an increase in miR-34a-5p. There was indeed a trial for a miR-34a mimic in cancer therapy (MRX34), which had to be terminated early due to severe side effects and death [230] and displayed a very heterogeneous distribution from organ to organ [311].

8. Outlook and conclusion

In this thesis we were able to show miR-34a-5p as a master-regulator of thyroid hormone signaling in the liver during MASH, we could prove binding of the miRNA to the targets THRB and DIO1 and show impaired TH signaling after miR-34a-5p overexpression in vitro. Human and mouse data highlight the relevance of miR-34a-5p in the disease and we were additionally able to show that methylation of the THRB gene contributes to the reduced TRβ expression in MASH patients. Furthermore, while we were only able to induce miR-34a-5p expression with fatty acid treatment in vitro, stimulation of cells with fructose and insulin dysregulated expression of TH related genes, as observed after miR-34a-5p overexpression, indicating an influence of insulin resistance on TH signaling.

Further experiments should be conducted to investigate the effect of insulin resistance on the TH genes and additional stimulation to induce miR-34a-5p could be investigated in cell lines with more hepatocyte characteristics. Since we were unable to detect the effect of the fatty acid induced expression of miR-34a-5p on the target genes, due to the discrepancy between miRNA regulation on mRNA and protein level, the experiment should be repeated in iPSC derived hepatocyte-like cells containing one of the tested tags for verification of protein levels using Western blot , after optimization of the iPCS protocol. More complex cell culture models should be investigated to better mimic MASLD in cell culture and incorporate hepatic stellate cells for investigation of fibrosis or Kupffer cells for inflammation.

In addition, we were unable to measure changes in MIR34AHG methylation analysis using other methods than pyrosequencing could be used to close the gap. WGBS, Microarray or nanopore could be used. Further, due to the regulatory effect of p53 on miR-34a-5p expression and observed changes in methylation in some cancers, potential differential methylation in MASH patients should be investigated.

Lastly the effect of miR-34a-5p reduction, through metformin or potentially miR-34a-5p antagomirs, on the efficacy of resmetirom and whether the miRNA improves response and phenotype should be investigated in cell culture and other suitable model systems.

9. Literature

1 Oosterveer MH, Schoonjans K. Hepatic glucose sensing and integrative pathways in the liver. Cell Mol Life Sci. 2014;71(8):1453–67.

2 Trefts E, Gannon M, Wasserman DH. The liver. Curr Biol. 2017 Nov;27(21):R1147–51.

3 Hijmans BS, Grefhorst A, Oosterveer MH, Groen AK. Zonation of glucose and fatty acid metabolism in the liver: Mechanism and metabolic consequences. Biochimie. 2014 Jan;96(1):121–9.

4 Guzman M, Castro J. Zonation of fatty acid metabolism in rat liver. 1989.

5 Rui L. Energy metabolism in the liver. Compr Physiol. 2014;4(1):177–97.

6 Adeva-Andany MM, Pérez-Felpete N, Fernández-Fernández C, Donapetry-García C, Pazos-García C. Liver glucose metabolism in humans. Biosci Rep. 2016 Dec;36(6). DOI: 10.1042/BSR20160385

7 Agius L. Glucokinase and molecular aspects of liver glycogen metabolism. Biochem J. 2008 Aug;414(1):1–18.

8 Han HS, Kang G, Kim JS, Choi BH, Koo SH. Regulation of glucose metabolism from a liver-centric perspective. Exp Mol Med. 2016 Mar;48(3). DOI: 10.1038/emm.2015.122

9 Titchenell PM, Lazar MA, Birnbaum MJ. Unraveling the Regulation of Hepatic Metabolism by Insulin. Trends Endocrinol Metab. 2017 Jul;28(7):497–505.

10 Nguyen P, Leray V, Diez M, Serisier S, Le Bloc'H J, Siliart B, et al. Liver lipid metabolism. J Anim Physiol Anim Nutr (Berl). 2008;92(3):272–83.

11 Saponaro C, Gaggini M, Carli F, Gastaldelli A. The Subtle Balance between Lipolysis and Lipogenesis: A Critical Point in Metabolic Homeostasis. Nutrients. 2015 Nov;7(11):9453–74.

12 Kawano Y, Cohen DE. Mechanisms of hepatic triglyceride accumulation in non-alcoholic fatty liver disease. J Gastroenterol. 2013 Apr;48(4):434–41.

13 Huh JY, Saltiel AR. Roles of IκB kinases and TANK-binding kinase 1 in hepatic lipid metabolism and nonalcoholic fatty liver disease. Exp Mol Med. 2021 Nov;53(11):1697–705.

14 Wilson CG, Tran JL, Erion DM, Vera NB, Febbraio M, Weiss EJ. Hepatocyte-specific disruption of CD36 attenuates fatty liver and improves insulin sensitivity in HFD-fed mice. Endocrinology. 2016 Feb;157(2):570–85.

15 Yamaguchi K, Yang L, McCall S, Huang J, Xing XY, Pandey SK, et al. Inhibiting triglyceride synthesis improves hepatic steatosis but exacerbates liver damage and fibrosis in obese mice with nonalcoholic steatohepatitis. Hepatology. 2007 Jun;45(6):1366–74.

16 Noncommunicable diseases [Internet]. 2024 Aug [cited 2024 Aug 23]. Available from: https://www.who.int/news-room/fact-sheets/detail/noncommunicable-diseases

17 Supreeya Swarup, Intisar Ahmed, Yulia Grigorova, Roman Zeltser. Metabolic Syndrome. Treasure Island: StatPearls Publishing; 2024.

18 Huang PL. A comprehensive definition for metabolic syndrome. DMM Dis Model Mech. 2009 May;2(5–6):231–7.

19 Younossi ZM, Golabi P, Paik JM, Henry A, Van Dongen C, Henry L. The global epidemiology of nonalcoholic fatty liver disease (NAFLD) and nonalcoholic steatohepatitis (NASH): a systematic review. Hepatology. 2023 Apr;77(4):1335–47.

20 Marjot T, Moolla A, Cobbold JF, Hodson L, Tomlinson JW. Nonalcoholic Fatty Liver Disease

in Adults: Current Concepts in Etiology, Outcomes, and Management. Endocr Rev. 2020;41(1):66–117.

21 Benedict M, Zhang X. Non-alcoholic fatty liver disease: An expanded review. World J Hepatol. 2017;9(16):715–32.

22 Rinella ME, Lazarus J V., Ratziu V, Francque SM, Sanyal AJ, Kanwal F, et al. A multi-society Delphi consensus statement on new fatty liver disease nomenclature. J Hepatol. 2023 Jun DOI: 10.1016/j.jhep.2023.06.003

23 Loomba R, Wong VW. Implications of the new nomenclature of steatotic liver disease and definition of metabolic dysfunction-associated steatotic liver disease. Aliment Pharmacol Ther. 2024 Jan;59(2):150–6.

24 Vanni E, Bugianesi E, Kotronen A, De Minicis S, Yki-Järvinen H, Svegliati-Baroni G. From the metabolic syndrome to NAFLD or vice versa? Dig Liver Dis. 2010 May;42(5):320–30.

25 Chalasani N, Younossi Z, Lavine JE, Charlton M, Cusi K, Rinella M, et al. The Diagnosis and Management of Nonalcoholic Fatty Liver Disease: Practice Guidance From the American Association for the Study of Liver Diseases. Hepatology. 2017;67(1):328–57.

26 Di Ciaula A, Baj J, Garruti G, Celano G, De Angelis M, Wang HH, et al. Liver steatosis, gut - liver axis, microbiome and environmental factors. A never-ending bidirectional cross-talk. J Clin Med. 2020 Aug;9(8):1–44.

27 Fakhoury-Sayegh N, Younes H, Heraoui GNHA, Sayegh R. Nutritional profile and dietary patterns of lebanese non-alcoholic fatty liver disease patients: A case-control study. Nutrients. 2017 Nov;9(11). DOI: 10.3390/nu9111245

28 Wehmeyer MH, Zyriax BC, Jagemann B, Roth E, Windler E, Wiesch JS Zur, et al. Nonalcoholic fatty liver disease is associated with excessive calorie intake rather than a distinctive dietary pattern. Med (United States). 2016;95(23). DOI: 10.1097/MD.0000000000003887

29 Ouyang X, Cirillo P, Sautin Y, Mccall S, Bruchette JL, Diehl AM, et al. Fructose Consumption as a Risk Factor for Non-alcoholic Fatty Liver Disease

30 Mahdessian H, Taxiarchis A, Popov S, Silveira A, Franco-Cereceda A, Hamsten A, et al. TM6SF2 is a regulator of liver fat metabolism influencing triglyceride secretion and hepatic lipid droplet content. Proc Natl Acad Sci U S A. 2014;111(24):8913–8.

31 Ittermann T, Haring R, Wallaschofski H, Baumeister SE, Nauck M, Dörr M, et al. Inverse association between serum free thyroxine levels and hepatic steatosis: Results from the study of health in pomerania. Thyroid. 2012 Jun;22(6):568–74.

32 Krause C, Grohs M, El Gammal AT, Wolter S, Lehnert H, Mann O, et al. Reduced expression of thyroid hormone receptor beta in human nonalcoholic steatohepatitis. Endocr Connect. 2018;7(12):1448–56.

33 Softic S, Cohen DE, Kahn CR. Role of Dietary Fructose and Hepatic De Novo Lipogenesis in Fatty Liver Disease. Dig Dis Sci. 2016 May;61(5):1282–93.

34 Faeh D, Minehira K, Schwarz J-M, Periasami R, Seongsu P, Tappy L. Effect of Fructose Overfeeding and Fish Oil Administration on Hepatic De Novo Lipogenesis and Insulin Sensitivity in Healthy Men. 1907.Available from: http://diabetesjournals.org/diabetes/article-pdf/54/7/1907/382267/zdb00705001907.pdf

35 Stanhope KL, Schwarz JM, Keim NL, Griffen SC, Bremer AA, Graham JL, et al. Consuming fructose-sweetened, not glucose-sweetened, beverages increases visceral adiposity and lipids and decreases insulin sensitivity in overweight/obese humans. J Clin Invest. 2009

May;119(5):1322–34.

36 Lambert JE, Ramos-Roman MA, Browning JD, Parks EJ. Increased de novo lipogenesis is a distinct characteristic of individuals with nonalcoholic fatty liver disease. Gastroenterology. 2014;146(3):726–35.

37 Cusi K. Role of obesity and lipotoxicity in the development of nonalcoholic steatohepatitis: Pathophysiology and clinical implications. Gastroenterology. 2012;142(4). DOI: 10.1053/j.gastro.2012.02.003

38 Petersen MC, Shulman GI. Roles of Diacylglycerols and Ceramides in Hepatic Insulin Resistance. Trends Pharmacol Sci. 2017 Jul;38(7):649–65.

39 Ioannou GN. The Role of Cholesterol in the Pathogenesis of NASH. Trends Endocrinol Metab. 2016 Feb;27(2):84–95.

40 Marra F, Svegliati-Baroni G. Lipotoxicity and the gut-liver axis in NASH pathogenesis. J Hepatol. 2018 Feb;68(2):280–95.

41 Szabo G, Momen-Heravi F. Extracellular vesicles in liver disease and potential as biomarkers and therapeutic targets. Nat Rev Gastroenterol Hepatol. 2017 Aug;14(8):455–66.

42 Serviddio G, Bellanti F, Vendemiale G. Free radical biology for medicine: learning from nonalcoholic fatty liver disease. Free Radic Biol Med. 2013 Dec;65:952–68.

43 Chen Z, Tian R, She Z, Cai J, Li H. Role of oxidative stress in the pathogenesis of nonalcoholic fatty liver disease. Free Radic Biol Med. 2020 May;152:116–41.

44 Jensen T, Abdelmalek MF, Sullivan S, Nadeau KJ, Green M, Roncal C, et al. Fructose and sugar: A major mediator of non-alcoholic fatty liver disease. J Hepatol. 2018 May;68(5):1063–75.

45 Cox CL, Stanhope KL, Schwarz JM, Graham JL, Hatcher B, Griffen SC, et al. Consumption of fructose-sweetened beverages for 10 weeks reduces net fat oxidation and energy expenditure in overweight/obese men and women. Eur J Clin Nutr. 2012 Feb;66(2):201–8.

46 Santoleri D, Titchenell PM. Resolving the Paradox of Hepatic Insulin Resistance. Cell Mol Gastroenterol Hepatol. 2019 Jan;7(2):447–56.

47 Branković M, Jovanović I, Dukić M, Radonjić T, Oprić S, Klašnja S, et al. Lipotoxicity as the Leading Cause of Non-Alcoholic Steatohepatitis. Int J Mol Sci. 2022 May;23(9):5146.

48 Armandi A, Rosso C, Caviglia GP, Bugianesi E. Insulin resistance across the spectrum of nonalcoholic fatty liver disease. Metabolites. 2021 Mar;11(3). DOI: 10.3390/metabo11030155

49 Armstrong MJ, Hazlehurst JM, Hull D, Guo K, Borrows S, Yu J, et al. Abdominal subcutaneous adipose tissue insulin resistance and lipolysis in patients with non -alcoholic steatohepatitis. Diabetes, Obes Metab. 2014;16(7):651–60.

50 Buechler C, Wanninger J, Neumeier M. Adiponectin, a key adipokine in obesity related liver diseases. World J Gastroenterol. 2011;17(23):2801–11.

51 Ohtani N, Kamiya T, Kawada N. Recent updates on the role of the gut-liver axis in the pathogenesis of NAFLD/NASH, HCC, and beyond. Hepatol Commun. 2023 Sep;7(9). DOI: 10.1097/HC9.0000000000000241

52 Gudan A, Jamioł-Milc D, Hawryłkowicz V, Skonieczna-Żydecka K, Stachowska E. The Prevalence of Small Intestinal Bacterial Overgrowth in Patients with Non -Alcoholic Liver Diseases: NAFLD, NASH, Fibrosis, Cirrhosis—A Systematic Review, Meta-Analysis and Meta-Regression. Nutrients. 2022 Dec;14(24). DOI: 10.3390/nu14245261

53 Carpino G, Del Ben M, Pastori D, Carnevale R, Baratta F, Overi D, et al. Increased Liver Localization of Lipopolysaccharides in Human and Experimental NAFLD. Hepatology. 2020 Aug;72(2):470–85.

54 Seki E, De Minicis S, Österreicher CH, Kluwe J, Osawa Y, Brenner DA, et al. TLR4 enhances TGF-β signaling and hepatic fibrosis. Nat Med. 2007 Nov;13(11):1324–32.

55 Cai J, Zhang X, Li H. The Role of Innate Immune Cells in Nonalcoholic Steatohepatitis. Hepatology. 2019 Sep;70(3):1026–37.

56 Zhou Z, Xu M-J, Gao B. Hepatocytes: a key cell type for innate immunity. Cell Mol Immunol. 2016 May;13(3):301–15.

57 Tacke F, Zimmermann HW. Macrophage heterogeneity in liver injury and fibrosis. J Hepatol. 2014 May;60(5):1090–6.

58 Ramachandran P, Pellicoro A, Vernon MA, Boulter L, Aucott RL, Ali A, et al. Differential Ly-6C expression identifies the recruited macrophage phenotype, which orchestrates the regression of murine liver fibrosis. Proc Natl Acad Sci U S A. 2012 Nov;109(46). DOI: 10.1073/pnas.1119964109

59 Arrese M, Cabrera D, Kalergis AM, Feldstein AE. Innate Immunity and Inflammation in NAFLD/NASH. Dig Dis Sci. 2016 May;61(5):1294–303.

60 Crespo J, Cayón A, Fernández-Gil P, Hernández-Guerra M, Mayorga M, Domínguez-Díez A, et al. Gene expression of tumor necrosis factor α and TNF-receptors, p55 and p75, in nonalcoholic steatohepatitis patients. Hepatology. 2001;34(6):1158–63.

61 Ribeiro C, Rodrigues CM. Expression of Death Receptors, and Activation of NF-κ B in the Liver of Nonalcoholic and Alcoholic Steatohepatitis Patients. Am J Gastroenterol. 2004;99(9):1708–17.

62 Leroux A, Ferrere G, Godie V, Cailleux F, Renoud M-L, Gaudin F, et al. Toxic lipids stored by Kupffer cells correlates with their pro-inflammatory phenotype at an early stage of steatohepatitis. J Hepatol. 2012 Jul;57(1):141–9.

63 Lanthier N. Targeting Kupffer cells in non-alcoholic fatty liver disease/non-alcoholic steatohepatitis: Why and how? World J Hepatol. 2015;7(19):2184.

64 Kazankov K, Jørgensen SMD, Thomsen KL, Møller HJ, Vilstrup H, George J, et al. The role of macrophages in nonalcoholic fatty liver disease and nonalcoholic steatohepatitis. Nat Rev Gastroenterol Hepatol. 2019 Mar;16(3):145–59.

65 Schwabe RF, Tabas I, Pajvani UB. Mechanisms of Fibrosis Development in Nonalcoholic Steatohepatitis. Gastroenterology. 2020 May;158(7):1913–28.

66 Hynes RO. The Extracellular Matrix: Not Just Pretty Fibrils. Science (80-). 2009 Nov;326(5957):1216–9.

67 Tsuchida T, Friedman SL. Mechanisms of hepatic stellate cell activation. Nat Rev Gastroenterol Hepatol. 2017 Jul;14(7):397–411.

68 Campos-Murguía A, Ruiz-Margáin A, González-Regueiro JA, Macías-Rodríguez RU. Clinical assessment and management of liver fibrosis in nonalcoholic fatty liver disease. World J Gastroenterol. 2020;26(39):5919–43.

69 Bruinstroop E, Dalan R, Cao Y, Bee YM, Chandran K, Cho LW, et al. Low-dose levothyroxine reduces intrahepatic lipid content in patients with type 2 diabetes mellitus and NAFLD. J Clin Endocrinol Metab. 2018;103(7):2698–706.

70 Kokkorakis M, Boutari C, Hill MA, Kotsis V, Loomba R, Sanyal AJ, et al. Resmetirom, the

first approved drug for the management of metabolic dysfunction-associated steatohepatitis: Trials, opportunities, and challenges. Metabolism. 2024 May;154:155835.

71 Fang T, Wang H, Pan X, Little PJ, Xu S, Weng J. Mouse models of nonalcoholic fatty liver disease (NAFLD): pathomechanisms and pharmacotherapies. Int J Biol Sci. 2022;18(15):5681–97.

72 Teufel A, Itzel T, Erhart W, Brosch M, Wang XY, Kim YO, et al. Comparison of Gene Expression Patterns Between Mouse Models of Nonalcoholic Fatty Liver Disease and Liver Tissues From Patients. Gastroenterology. 2016;151(3):513-525.e0.

73 Vacca M, Kamzolas I, Harder LM, Oakley F, Trautwein C, Hatting M, et al. An unbiased ranking of murine dietary models based on their proximity to human metabolic dysfunction - associated steatotic liver disease (MASLD). Nat Metab. 2024 Jun DOI: 10.1038/s42255-024-01043-6

74 Van Herck MA, Vonghia L, Francque SM. Animal models of nonalcoholic fatty liver disease—a starter's guide. Nutrients. 2017 Sep;9(10). DOI: 10.3390/nu9101072

75 Santhekadur PK, Kumar DP, Sanyal AJ. Preclinical models of non-alcoholic fatty liver disease. J Hepatol. 2018 Feb;68(2):230–7.

76 Kamli-Salino SEJ, Brown PAJ, Haschler TN, Liang L, Feliers D, Wilson HM, et al. Induction of experimental diabetes and diabetic nephropathy using anomer-equilibrated streptozotocin in male C57Bl/6J mice. Biochem Biophys Res Commun. 2023 Apr;650:109–16.

77 Szkudelski T. The mechanism of alloxan and streptozotocin action in B cells of the rat pancreas. Physiol Res. 2001;537–46.

78 Márquez-Quiroga LV, Arellanes-Robledo J, Vásquez-Garzón VR, Villa-Treviño S, Muriel P. Models of nonalcoholic steatohepatitis potentiated by chemical inducers leading to hepatocellular carcinoma. Biochem Pharmacol. 2022 Jan;195. DOI: 10.1016/j.bcp.2021.114845

79 Kubota N, Kado S, Kano M, Masuoka N, Nagata Y, Kobayashi T, et al. A high-fat diet and multiple administration of carbon tetrachloride induces liver injury and pathological features associated with non-alcoholic steatohepatitis in mice. Clin Exp Pharmacol Physiol. 2013 Jul;40(7):422–30.

80 Im YR, Hunter H, De D, Hahn G, Duret A, Cheah Q, et al. A Systematic Review of Animal Models of NAFLD Finds High-Fat, High-Fructose Diets Most Closely Resemble Human NAFLD. 1884 Hepatol. 2021;74(4):2021.

81 Im YR, Hunter H, de Gracia Hahn D, Duret A, Cheah Q, Dong J, et al. A Systematic Review of Animal Models of NAFLD Finds High-Fat, High-Fructose Diets Most Closely Resemble Human NAFLD. Hepatology. 2021;74(4):1884–901.

82 Raubenheimer PJ, Nyirenda MJ, Walker BR. A choline-deficient diet exacerbates fatty liver but attenuates insulin resistance and glucose intolerance in mice fed a high-fat diet. Diabetes. 2006;55(7):2015–20.

83 Chikamoto K, Misu H, Takayama H, Kikuchi A, Ishii KA, Lan F, et al. Rapid response of the steatosis-sensing hepatokine LECT2 during diet-induced weight cycling in mice. Biochem Biophys Res Commun. 2016;478(3):1310–6.

84 Capel F, Rolland-Valognes G, Dacquet C, Brun M, Lonchampt M, Ktorza A, et al. Analysis of sterol-regulatory element-binding protein 1c target genes in mouse liver during aging and high-fat diet. J Nutrigenet Nutrigenomics. 2013 Jun;6(2):107–22.

85 Bell CC, Dankers ACA, Lauschke VM, Sison-Young R, Jenkins R, Rowe C, et al. Comparison

of hepatic 2D sandwich cultures and 3d spheroids for long-term toxicity applications: A multicenter study. Toxicol Sci. 2018 Apr;162(2):655–66.

86 Castell J V., Jover R, Martínez-Jiménez CP, Gómez-Lechón MJ. Hepatocyte cell lines: Their use, scope and limitations in drug metabolism studies. Expert Opin Drug Metab Toxicol. 2006 Apr;2(2):183–212.

87 Müller FA, Sturla SJ. Human in vitro models of nonalcoholic fatty liver disease. Curr Opin Toxicol. 2019;16(Figure 1):9–16.

88 López-Terrada D, Cheung SW, Finegold MJ, Knowles BB. Hep G2 is a hepatoblastoma-derived cell line. Hum Pathol. 2009 Oct;40(10):1512–5.

89 Godoy P, Hewitt NJ, Albrecht U, Andersen ME, Ansari N, Bhattacharya S, et al. Recent advances in 2D and 3D in vitro systems using primary hepatocytes, alternative hepatocyte sources and non-parenchymal liver cells and their use in investigating mechanisms of hepatotoxicity, cell signaling and ADME. Arch Toxicol. 2013 Aug;87(8):1315–530.

90 Kelm JM, Timmins NE, Brown CJ, Fussenegger M, Nielsen LK. Method for generation of homogeneous multicellular tumor spheroids applicable to a wide variety of cell types. Biotechnol Bioeng. 2003 Jul;83(2):173–80.

91 Chang TT, Hughes-Fulford M. Monolayer and Spheroid Culture of Human Liver Hepatocellular Carcinoma Cell Line Cells Demonstrate Distinct Global Gene Expression Patterns and Functional Phenotypes

92 Parent R, Marion MJ, Furio L, Trépo C, Petit MA. Origin and Characterization of a Human Bipotent Liver Progenitor Cell Line. Gastroenterology. 2004;126(4):1147–56.

93 Leite SB, Roosens T, El Taghdouini A, Mannaerts I, Smout AJ, Najimi M, et al. Novel human hepatic organoid model enables testing of drug-induced liver fibrosis in vitro. Biomaterials. 2016 Feb;78:1–10.

94 Sung JH, Wang YI, Narasimhan Sriram N, Jackson M, Long C, Hickman JJ, et al. Recent Advances in Body-on-a-Chip Systems. Anal Chem. 2019 Jan;91(1):330–51.

95 Kozyra M, Johansson I, Nordling Å, Ullah S, Lauschke VM, Ingelman-Sundberg M. Human hepatic 3D spheroids as a model for steatosis and insulin resistance. Sci Rep. 2018 Dec;8(1). DOI: 10.1038/s41598-018-32722-6

96 Sinha RA, Yen PM. Metabolic Messengers: Thyroid Hormones. Nat Metab. 2024 Apr;6(4):639–50.

97 Mayerl S, Müller J, Bauer R, Richert S, Kassmann CM, Darras VM, et al. Transporters MCT8 and OATP1C1 maintain murine brain thyroid hormone homeostasis. J Clin Invest. 2014;124(5):1987–99.

98 Friesema ECH, Jansen J, Jachtenberg JW, Visser WE, Kester MHA, Visser TJ. Effective cellular uptake and efflux of thyroid hormone by human monocarboxylate transporter 10. Mol Endocrinol. 2008 Jun;22(6):1357–69.

99 Visser WE, Wong WS, van Mullem AAA, Friesema ECH, Geyer J, Visser TJ. Study of the transport of thyroid hormone by transporters of the SLC10 family. Mol Cell Endocrinol. 2010 Feb;315(1–2):138–45.

100 Russo SC, Salas-Lucia F, Bianco AC. Deiodinases and the Metabolic Code for Thyroid Hormone Action. Endocrinol (United States). 2021 Aug;162(8). DOI: 10.1210/endocr/bqab059

101 Flamant F, Cheng SY, Hollenberg AN, Moeller LC, Samarut J, Wondisford FE, et al. Thyroid hormone signaling pathways: Time for a more precise nomenclature. Endocrinology. 2017 Jul;158(7):2052–7.

102 Lazar MA. Thyroid Hormone Receptors: Multiple Forms, Multiple Possibilities*. Endocr Rev. 1993;14(2).

103 Shabtai Y, Nagaraj NK, Batmanov K, Cho YW, Guan Y, Jiang C, et al. A coregulator shift, rather than the canonical switch, underlies thyroid hormone action in the liver. Genes Dev. 2021;35(5–6):367–78.

104 Saatciqglu F, Bartunek P, Deng T, Zenke M, Karin M. A Conserved C-Terminal Sequence That Is Deleted in v-ErbA Is Essential for the Biological Activities of c-ErbA (the Thyroid Hormone Receptor). 1993.

105 Martínez-Iglesias O, Garcia-Silva S, Tenbaum SP, Regadera J, Larcher F, Paramio JM, et al. Thyroid hormone receptor β1 acts as a potent suppressor of tumor invasiveness and metastasis. Cancer Res. 2009 Jan;69(2):501–9.

106 Davis PJ, Leonard JL, Lin HY, Leinung M, Mousa SA. Molecular Basis of Nongenomic Actions of Thyroid Hormone. Vitamins and Hormones. Academic Press Inc.; 2018; pp 67–96.

107 Sinha RA, Singh BK, Yen PM. Direkt effects of thyroid hormones on hepatic lipid metabolism. Nat Rev Endocrinol. 2018;14(5):259–69.

108 Sinha RA, Singh BK, Yen PM. Direct effects of thyroid hormones on hepatic lipid metabolism. Nat Rev Endocrinol. 2018;14(5):259–69.

109 Schultze SM, Hemmings BA, Niessen M, Tschopp O. PI3K/AKT, MAPK and AMPK signalling: Protein kinases in glucose homeostasis. Expert Rev Mol Med. 2012 Jan;14. DOI: 10.1017/S1462399411002109

110 Sinha RA, You SH, Zhou J, Siddique MM, Bay BH, Zhu X, et al. Thyroid hormone stimulates hepatic lipid catabolism via activation of autophagy. J Clin Invest. 2012;122(7):2428–38.

111 Sinha RA, You SH, Zhou J, Siddique MM, Bay BH, Zhu X, et al. Thyroid hormone stimulates hepatic lipid catabolism via activation of autophagy. J Clin Invest. 2012 Jul;122(7):2428–38.

112 Weitzel JM, Alexander Iwen K. Coordination of mitochondrial biogenesis by thyroid hormone. Mol Cell Endocrinol. 2011 Aug;342(1–2):1–7.

113 Jackson-Hayes L, Song S, Lavrentyev EN, Jansen MS, Hillgartner FB, Tian L, et al. A thyroid hormone response unit formed between the promoter and first intron of the carnitine palmitoyltransferase-Iα gene mediates the liver-specific induction by thyroid hormone. J Biol Chem. 2003 Mar;278(10):7964–72.

114 Singh BK, Sinha RA, Tripathi M, Mendoza A, Ohba K, Sy JAC, et al. Thyroid hormone receptor and ERRa coordinately regulate mitochondrial fission, mitophagy, biogenesis, and function. 2018.Available from: https://www.science.org

115 Cingolani F, Czaja MJ. Regulation and Functions of Autophagic Lipolysis. Trends Endocrinol Metab. 2016 Oct;27(10):696–705.

116 Wrutniak-Cabello C, Casas F, Cabello G. Thyroid hormone action in mitochondria. J Mol Endocrinol. 2001 Feb;26(1):67–77.

117 Djouadi F, Riveau atrice, Merlet-benichou C, Bastin J. Tissue-specific regulation of medium-chain acyl-CoA dehydrogenase gene by thyroid hormones in the developing rat. 1997.

118 Holness MJ, Bulmer K, Smith ND, Sugden MC. Investigation of potential mechanisms regulating protein expression of hepatic pyruvate dehydrogenase kinase isoforms 2 and 4 by fatty acids and thyroid hormone. 2003.

119 Jekabsons MB, Gregoire FM, Schonfeld-Warden NA, Warden CH, Horwitz BA. T 3 stimulates resting metabolism and UCP-2 and UCP-3 mRNA but not nonphosphorylating mitochondrial

respiration in mice. 1999.

120 Ritter MJ, Amano I, Hollenberg AN. Thyroid Hormone Signaling and the Liver. Hepatology. 2020 Aug;72(2):742–52.

121 Hua X, Yokoyama C, Wu J, Briggs MR, Brown MS, Goldstein JL, et al. SREBP-2, a second basic-helix-loop-helix-leucine zipper protein that stimulates transcription by binding to a sterol regulatory element (cDNA cloning/cholesterol/low density lipoprotein receptor/3-hydroxy-3-methylglutaryl-coenzyme A synthase). 1993.

122 O'BRIEN T, DINNEEN SF, O'BRIEN PC, PALUMBO PJ. Hyperlipidemia in Patients With Primary and Secondary Hypothyroidism. Mayo Clin Proc. 1993;68(9):860–6.

123 Bonde Y, Breuer O, Lütjohann D, Sjöberg S, Angelin B, Rudling M. Thyroid hormone reduces PCSK9 and stimulates bile acid synthesis in humans. J Lipid Res. 2014 Nov;55(11):2408–15.

124 Rader DJ, Alexander ET, Weibel GL, Billheimer J, Rothblat GH. The role of reverse cholesterol transport in animals and humans and relationship to atherosclerosis. J Lipid Res. 2009 Apr;50(SUPPL.). DOI: 10.1194/jlr.R800088-JLR200

125 Ness GC, Pendleton LC, Li YC, Chiang JYL. EFFECT OF THYROID HORMONE ON HEPATIC CHOLESTEROL 7a HYDROXYLASE, LDL RECEPTOR, HMG-CoA REDUCTASE, FARNESYL PYROPHOSPHATE SYNTHETASE AND APOLIPOPROTEIN A-I mRNA LEVELS IN HYPOPHYSECTOMIZED RATS. 1990;172(3).

126 Tan KCB, Shiu SWM, Kung AWC. Effect of Thyroid Dysfunction on High-Density Lipoprotein Subfraction Metabolism: Roles of Hepatic Lipase and Cholesteryl Ester Transfer Protein*. 1998.Available from: https://academic.oup.com/jcem/article/83/8/2921/2660623

127 Lammel Lindemann JA, Angajala A, Engler DA, Webb P, Ayers SD. Thyroid hormone induction of human cholesterol 7 alpha-hydroxylase (Cyp7a1) in vitro. Mol Cell Endocrinol. 2014 May;388(1–2):32–40.

128 Yu L, Li-Hawkins J, Hammer RE, Berge KE, Horton JD, Cohen JC, et al. Overexpression of ABCG5 and ABCG8 promotes biliary cholesterol secretion and reduces fractional absorption of dietary cholesterol. J Clin Invest. 2002 Sep;110(5):671–80.

129 Repa JJ, Berge KE, Pomajzl C, Richardson JA, Hobbs H, Mangelsdorf DJ. Regulation of ATP-binding cassette sterol transporters ABCG5 and ABCG8 by the liver X receptors α and β. J Biol Chem. 2002 May;277(21):18793–800.

130 Park EA, Song S, Vinson C, Roesler WJ. Role of CCAAT Enhancer-binding Protein in the Thyroid Hormone and cAMP Induction of Phosphoenolpyruvate Carboxykinase Gene Transcription*Available from: http://www.jbc.org

131 Suh JH, Sieglaff DH, Zhang A, Xia X, Cvoro A, Winnier GE, et al. SIRT1 is a Direct Coactivator of Thyroid Hormone Receptor β1 with Gene-Specific Actions. PLoS One. 2013 Jul;8(7). DOI: 10.1371/journal.pone.0070097

132 Attia RR, Connnaughton S, Boone LR, Wang F, Elam MB, Ness GC, et al. Regulation of pyruvate dehydrogenase kinase 4 (PDK4) by thyroid hormone role of the peroxisome proliferator-activated receptor γ coactivator (PGC-1α). J Biol Chem. 2010 Jan;285(4):2375–85.

133 Singh BK, Sinha RA, Yen PM. Novel transcriptional mechanisms for regulating metabolism by thyroid hormone. Int J Mol Sci. 2018 Oct;19(10). DOI: 10.3390/ijms19103284

134 Chalkiadaki A, Guarente L. Sirtuins mediate mammalian metabolic responses to nutrient availability. Nat Rev Endocrinol. 2012;8(5):287–96.

135 Singh BK, Sinha RA, Zhou J, Tripathi M, Ohba K, Wang ME, et al. Hepatic FOXO1 target genes are co-regulated by thyroid hormone via RICTOR protein deacetylation and MTORC2-

AKT protein inhibition. J Biol Chem. 2016 Jan;291(1):198–214.

136 Sinha RA, Singh BK, Yen PM. Thyroid hormone regulation of hepatic lipid and carbohydrate metabolism. Trends Endocrinol Metab. 2014 Oct;25(10):538–45.

137 Seifert J, Chen Y, Schöning W, Mai K, Tacke F, Spranger J, et al. Hepatic Energy Metabolism under the Local Control of the Thyroid Hormone System. Int J Mol Sci. 2023 Mar;24(5):4861.

138 He W, Huang C, Wang L, Su W, Wang S, Huang P, et al. The correlation between triiodothyronine and the severity of liver fibrosis. BMC Endocr Disord. 2022 Dec;22(1):313.

139 Oppenheimer JH, Schwartz HL, Lane JT, Thompson MP. Functional relationship of thyroid hormone-induced lipogenesis, lipolysis, and thermogenesis in the rat. J Clin Invest. 1991;87(1):125–32.

140 Chaves C, Bruinstroop E, Refetoff S, Yen PM, Anselmo J. Increased Hepatic Fat Content in Patients with Resistance to Thyroid Hormone Beta. Thyroid. 2021 Jul;31(7):1127–34.

141 Zhao M, Xie H, Shan H, Zheng Z, Li G, Li M, et al. Development of Thyroid Hormones and Synthetic Thyromimetics in Non-Alcoholic Fatty Liver Disease. Int J Mol Sci. 2022;23(3). DOI: 10.3390/ijms23031102

142 Waddington CH. The epigenotype. 1942. Int J Epidemiol. 2012 Feb;41(1):10–3.

143 Wu C-T, Morris JR. Genes, Genetics, and Epigenetics: A Correspondence. Science (80-). 2001 Aug;293(10):1103–5.

144 Wu YL, Lin ZJ, Li CC, Lin X, Shan SK, Guo B, et al. Epigenetic regulation in metabolic diseases: mechanisms and advances in clinical study. Signal Transduct Target Ther. 2023 Dec;8(1). DOI: 10.1038/s41392-023-01333-7

145 Peterson CL, Laniel M-A. Histones and histone modifications. Curr Biol. 2004 Jul;14(14):R546–51.

146 Reyes AA, Marcum RD, He Y. Structure and Function of Chromatin Remodelers. J Mol Biol. 2021 Jul;433(14). DOI: 10.1016/j.jmb.2021.166929

147 Ma X, Kang S. Functional implications of DNA methylation in adipose biology. Diabetes. 2019;68(5):871–8.

148 Maiti A, Drohat AC. Thymine DNA glycosylase can rapidly excise 5-formylcytosine and 5-carboxylcytosine: Potential implications for active demethylation of CpG sites. J Biol Chem. 2011 Oct;286(41):35334–8.

149 Tahiliani M, Koh KP, Shen Y, Pastor WA, Bandukwala H, Brudno Y, et al. Conversion of 5-methylcytosine to 5-hydroxymethylcytosine in mammalian DNA by MLL partner TET1. Science (80-). 2009 May;324(5929):930–5.

150 Chen Z, Zhang Y. Role of Mammalian DNA Methyltransferases in Development. 2020;10. DOI: 10.1146/annurev-biochem-103019

151 Yin Y, Morgunova E, Jolma A, Kaasinen E, Sahu B, Khund-Sayeed S, et al. Impact of cytosine methylation on DNA binding specificities of human transcription factors. Science (80-). 2017 May;356(6337). DOI: 10.1126/science.aaj2239

152 Zhu H, Wang G, Qian J. Transcription factors as readers and effectors of DNA methylation. Nat Rev Genet. 2016 Sep;17(9):551–65.

153 Illingworth RS, Bird AP. CpG islands - “A rough guide.” FEBS Lett. 2009 Jun;583(11):1713–20.

154 Anastasiadi D, Esteve-Codina A, Piferrer F. Consistent inverse correlation between DNA

methylation of the first intron and gene expression across tissues and species. Epigenetics and Chromatin. 2018 Jun;11(1). DOI: 10.1186/s13072-018-0205-1

155 Ball MP, Li JB, Gao Y, Lee JH, Leproust EM, Park IH, et al. Targeted and genome-scale strategies reveal gene-body methylation signatures in human cells. Nat Biotechnol. 2009 Apr;27(4):361–8.

156 Hibler E, Huang L, Andrade J, Spring B. Impact of a diet and activity health promotion intervention on regional patterns of DNA methylation. Clin Epigenetics. 2019 Sep;11(1). DOI: 10.1186/s13148-019-0707-0

157 Kurdyukov S, Bullock M. DNA methylation analysis: Choosing the right method. Biology (Basel). 2016 Jan;5(1). DOI: 10.3390/biology5010003

158 Gouil Q, Keniry A. Latest techniques to study DNA methylation. Essays Biochem. 2019;63(6):639–48.

159 Ahsan MU, Gouru A, Chan J, Zhou W, Wang K. A signal processing and deep learning framework for methylation detection using Oxford Nanopore sequencing. Nat Commun. 2024 Dec;15(1). DOI: 10.1038/s41467-024-45778-y

160 Sharp PA. The Centrality of RNA. Cell. 2009 Feb;136(4):577–80.

161 St.Laurent G, Wahlestedt C, Kapranov P. The Landscape of long noncoding RNA classification. Trends Genet. 2015 May;31(5):239–51.

162 Ling H, Fabbri M, Calin GA. MicroRNAs and other non-coding RNAs as targets for anticancer drug development. Nat Rev Drug Discov. 2013 Nov;12(11):847–65.

163 Kim VN. MicroRNA biogenesis: Coordinated cropping and dicing. Nat Rev Mol Cell Biol. 2005;6(5):376–85.

164 Bartel DP. Review MicroRNAs: Genomics, Biogenesis, Mechanism, and Function. 2004.

165 Ruby JG, Jan CH, Bartel DP. Intronic microRNA precursors that bypass Drosha processing. 2007.Available from: http://www.targetscan.org

166 Okamura K, Hagen JW, Duan H, Tyler DM, Lai EC. The Mirtron Pathway Generates microRNA-Class Regulatory RNAs in Drosophila. Cell. 2007 Jul;130(1):89–100.

167 Ha M, Kim VN. Regulation of microRNA biogenesis. Nat Rev Mol Cell Biol. 2014;15(8):509–24.

168 Knight SW, Bass BL. A Role for the RNase III Enzyme DCR-1 in RNA Interference and Germ Line Development in Caenorhabditis elegans. Science (80-). 2001 Sep;5538(293):2269–71.

169 Chendrimada TP, Finn KJ, Ji X, Baillat D, Gregory RI, Liebhaber SA, et al. MicroRNA silencing through RISC recruitment of eIF6. Nature. 2007 Jun;447(7146):823–8.

170 Frank F, Sonenberg N, Nagar B. Structural basis for 5′-nucleotide base-specific recognition of guide RNA by human AGO2. Nature. 2010 Jun;465(7299):818–22.

171 Schwarz DS, Rgy Hutvá Gner G, Du T, Xu Z, Aronin N, Zamore PD. Asymmetry in the Assembly of the RNAi Enzyme Complex (Lagos-Quintana et al. Cell. 2003 Oct;115:199–208.

172 Khvorova A, Reynolds A, Jayasena SD. Functional siRNAs and miRNAs Exhibit Strand Bias. 2003.Available from: http://www.sanger.ac.uk/Software/Rfam/mirna/

173 Carthew RW, Sontheimer EJ. Origins and Mechanisms of miRNAs and siRNAs. Cell. 2009;136(4):642–55.

174 Bartel DP. MicroRNAs: Target Recognition and Regulatory Functions. Cell. 2009;136(2):215–

33.

175 Friedman RC, Farh KK-H, Burge CB, Bartel DP. Most mammalian mRNAs are conserved targets of microRNAs. Genome Res. 2009 Jan;19(1):92–105.

176 Kiriakidou M, Tan GS, Lamprinaki S, De Planell-Saguer M, Nelson PT, Mourelatos Z. An mRNA m7G Cap Binding-like Motif within Human Ago2 Represses Translation. Cell. 2007 Jun;129(6):1141–51.

177 Lytle JR, Yario TA, Steitz JA. Target mRNAs are repressed as efficiently by microRNA-binding sites in the 5 UTR as in the 3 UTR. 2007.Available from: www.pnas.orgcgidoi10.1073pnas.0703820104

178 Filipowicz W, Bhattacharyya SN, Sonenberg N. Mechanisms of post -transcriptional regulation by microRNAs: Are the answers in sight? Nat Rev Genet. 2008 Feb;9(2):102–14.

179 Nicolas FE. Experimental Validation of MicroRNA Targets Using a Luciferase Reporter System. Methods in Molecular Biology. Humana Press Inc.; 2011; pp 139–52.

180 Meier J, Hovestadt V, Zapatka M, Pscherer A, Lichter P, Seiffert M. Genome-wide identification of translationally inhibited and degraded miR-155 targets using RNA-interacting protein-IP. RNA Biol. 2013;10(6):1017–29.

181 Tan LP, Seinen E, Duns G, De jong D, Sibon OCM, Poppema S, et al. A high throughput experimental approach to identify miRNA targets in human cells. Nucleic Acids Res. 2009 Sep;37(20). DOI: 10.1093/nar/gkp715

182 Easow G, Teleman AA, Cohen SM. Isolation of microRNA targets by miRNP immunopurification. RNA. 2007 Aug;13(8):1198–204.

183 Wang WX, Wilfred BR, Hu Y, Stromberg AJ, Nelson PT. Anti-Argonaute RIP-Chip shows that miRNA transfections alter global patterns of mRNA recruitment to microribonucleoprotein complexes. RNA. 2010 Feb;16(2):394–404.

184 Goff LA, Davila J, Swerdel MR, Moore JC, Cohen RI, Wu H, et al. Ago2 immunoprecipitation identifies predicted MicroRNAs in human embryonic stem cells and neural precursors. PLoS One. 2009 Sep;4(9). DOI: 10.1371/journal.pone.0007192

185 Hoffman AE, Liu R, Fu A, Zheng T, Slack F, Zhu Y. Targetome profiling, pathway analysis and genetic association study implicate miR-202 in lymphomagenesis DOI: 10.1158/1055-9965.EPI-12-1131

186 Fang Z, Dou G, Wang L. MicroRNAs in the Pathogenesis of Nonalcoholic Fatty Liver Disease. Int J Biol Sci. 2021;17(7):1851–63.

187 Chang J, Guo J-T, Jiang D, Guo H, Taylor JM, Block TM. Liver-Specific MicroRNA miR-122 Enhances the Replication of Hepatitis C Virus in Nonhepatic Cells. J Virol. 2008 Aug;82(16):8215–23.

188 López-Sánchez GN, Dóminguez-Pérez M, Uribe M, Chávez-Tapia NC, Nuño-Lámbarri N. Non-alcoholic fatty liver disease and microRNAs expression, how it affects the development and progression of the disease. Ann Hepatol. 2021;21. DOI: 10.1016/j.aohep.2020.04.012

189 Thomas M, Deiters A. MicroRNA miR-122 as a Therapeutic Target for Oligonucleotides and Small Molecules. Curr Med Chem. 2013 Aug;20(29):3629–40.

190 Long JK, Dai W, Zheng YW, Zhao SP. MiR-122 promotes hepatic lipogenesis via inhibiting the LKB1/AMPK pathway by targeting Sirt1 in non-alcoholic fatty liver disease. Mol Med. 2019 Jun;25(1). DOI: 10.1186/s10020-019-0085-2

191 Pirola CJ, Gianotti TF, Castaño GO, Mallardi P, Martino JS, Ledesma MMGL, et al.

Circulating microRNA signature in non-alcoholic fatty liver disease: From serum non-coding RNAs to liver histology and disease pathogenesis. Gut. 2015;64(5):800–12.

192 Cheung O, Puri P, Eicken C, Contos MJ, Mirshahi F, Maher JW, et al. Nonalcoholic steatohepatitis is associated with altered hepatic MicroRNA expression. Hepatology. 2008;48(6):1810–20.

193 Miyaaki H, Ichikawa T, Kamo Y, Taura N, Honda T, Shibata H, et al. Significance of serum and hepatic microRNA-122 levels in patients with non-alcoholic fatty liver disease. Liver Int. 2014;34(7). DOI: 10.1111/liv.12429

194 Lee YH, Jang HJ, Kim S, Choi SS, Khim KW, Eom HJ, et al. Hepatic MIR20B promotes nonalcoholic fatty liver disease by suppressing PPARA. Elife. 2021 Dec;10. DOI: 10.7554/eLife.70472

195 Vega-Badillo J, Gutiérrez-Vidal R, Hernández-Pérez HA, Villamil-Ramírez H, León-Mimila P, Sánchez-Muñoz F, et al. Hepatic miR-33a/miR-144 and their target gene ABCA1 are associated with steatohepatitis in morbidly obese subjects. Liver Int. 2016 Sep;36(9):1383–91.

196 Rayner KJ, Esau CC, Hussain FN, McDaniel AL, Marshall SM, Van Gils JM, et al. Inhibition of miR-33a/b in non-human primates raises plasma HDL and lowers VLDL triglycerides. Nature. 2011 Oct;478(7369):404–7.

197 Dávalos A, Goedeke L, Smibert P, Ramírez CM, Warrier NP, Andreo U, et al. miR-33a/b contribute to the regulation of fatty acid metabolism and insulin signaling. Proc Natl Acad Sci U S A. 2011 May;108(22):9232–7.

198 Sun C, Huang F, Liu X, Xiao X, Yang M, Hu G, et al. miR-21 regulates triglyceride and cholesterol metabolism in non-alcoholic fatty liver disease by targeting HMGCR. Int J Mol Med. 2015 Mar;35(3):847–53.

199 Ahn J, Lee H, Jung CH, Ha T. Lycopene inhibits hepatic steatosis via microRNA-21-induced downregulation of fatty acid-binding protein 7 in mice fed a high-fat diet. Mol Nutr Food Res. 2012 Nov;56(11):1665–74.

200 Calo N, Ramadori P, Sobolewski C, Romero Y, Maeder C, Fournier M, et al. Stress-activated miR-21/miR-21∗ in hepatocytes promotes lipid and glucose metabolic disorders associated with high-fat diet consumption. Gut. 2016 Nov;65(11):1871–81.

201 Zeng N, Huang R, Li N, Jiang H, Li R, Wang F, et al. MiR-451a attenuates free fatty acids–mediated hepatocyte steatosis by targeting the thyroid hormone responsive spot 14 gene. Mol Cell Endocrinol. 2018 Oct;474:260–71.

202 Csak T, Bala S, Lippai D, Kodys K, Catalano D, Iracheta-Vellve A, et al. MicroRNA-155 deficiency attenuates liver steatosis and fibrosis without reducing inflammation in a mouse model of steatohepatitis. PLoS One. 2015 Jun;10(6). DOI: 10.1371/journal.pone.0129251

203 Wang L, Zhang N, Wang Z, Ai DM, Cao ZY, Pan HP. Decreased MiR-155 Level in the Peripheral Blood of Non-Alcoholic Fatty Liver Disease Patients may Serve as a Biomarker and may Influence LXR Activity. Cell Physiol Biochem. 2016 Nov;39(6):2239–48.

204 Miller AM, Gilchrist DS, Nijjar J, Araldi E, Ramirez CM, Lavery CA, et al. MiR-155 Has a Protective Role in the Development of Non-Alcoholic Hepatosteatosis in Mice. PLoS One. 2013 Aug;8(8). DOI: 10.1371/journal.pone.0072324

205 Mansour RM, Abdel Mageed SS, Abulsoud AI, Sayed GA, Lutfy RH, Awad FA, et al. From fatty liver to fibrosis: the impact of miRNAs on NAFLD and NASH. Funct Integr Genomics. 2025 Dec;25(1). DOI: 10.1007/s10142-025-01544-x

206 Loyer X, Paradis V, Hénique C, Vion AC, Colnot N, Guerin CL, et al. Liver microRNA-21 is

overexpressed in non-alcoholic steatohepatitis and contributes to the disease in experimental models by inhibiting PPARα expression. Gut. 2016 Nov;65(11):1882–94.

207 Erhartova D, Cahova M, Dankova H, Heczkova M, Mikova I, Sticova E, et al. Serum miR-33a is associated with steatosis and inflammation in patients with nonalcoholic fatty liver disease after liver transplantation. PLoS One. 2019 Nov;14(11). DOI: 10.1371/journal.pone.0224820

208 Zhang T, Hu J, Wang X, Zhao X, Li Z, Niu J, et al. MicroRNA-378 promotes hepatic inflammation and fibrosis via modulation of the NF-κB-TNFα pathway. J Hepatol. 2019;70(1):87–96.

209 López-Sánchez GN, Dóminguez-Pérez M, Uribe M, Chávez-Tapia NC, Nuño-Lámbarri N. Non-alcoholic fatty liver disease and microRNAs expression, how it affects the development and progression of the disease. Ann Hepatol. 2021 Mar;21. DOI: 10.1016/j.aohep.2020.04.012

210 Hou X, Yin S, Ren R, Liu S, Yong L, Liu Y, et al. Myeloid-Cell–Specific IL-6 Signaling Promotes MicroRNA-223-Enriched Exosome Production to Attenuate NAFLD-Associated Fibrosis. Hepatology. 2021 Jul;74(1):116–32.

211 Jampoka K, Muangpaisarn P, Khongnomnan K, Treeprasertsuk S, Tangkijvanich P, Payungporn S. Serum miR-29a and miR-122 as Potential Biomarkers for Non-Alcoholic Fatty Liver Disease (NAFLD). MicroRNA. 2018 May;7(3):215–22.

212 Ramírez CM, Goedeke L, Rotllan N, Yoon J-H, Cirera-Salinas D, Mattison JA, et al. MicroRNA 33 Regulates Glucose Metabolism. Mol Cell Biol. 2013 Aug;33(15):2891–902.

213 Wang X, Wang M, Li H, Lan X, Liu L, Li J, et al. Upregulation of miR-497 induces hepatic insulin resistance in E3 rats with HFD-MetS by targeting insulin receptor. Mol Cell Endocrinol. 2015 Nov;416:57–69.

214 Yang W, Jeong H, Park S, Lee W. Obesity-induced miR-15b is linked causally to the development of insulin resistance through the repression of the insulin receptor in hepatocytes. Mol Nutr Food Res. 2015 Nov;59(11):2303–14.

215 Wang S, Wang L, Dou L, Guo J, Fang W, Li M, et al. MicroRNA 152 regulates hepatic glycogenesis by targeting PTEN. FEBS J. 2016 May;283(10):1935–46.

216 Ashraf NU, Sheikh TA. Endoplasmic reticulum stress and Oxidative stress in the pathogenesis of Non-alcoholic fatty liver disease. Free Radic Res. 2015 Aug;49(12):1405–18.

217 Xu H, Tian Y, Tang D, Zou S, Liu G, Song J, et al. An Endoplasmic Reticulum Stress–MicroRNA-26a Feedback Circuit in NAFLD. Hepatology. 2021 Apr;73(4):1327–45.

218 Cheng Y, Mai J, Hou T, Ping J. MicroRNA-421 induces hepatic mitochondrial dysfunction in non-alcoholic fatty liver disease mice by inhibiting sirtuin 3. Biochem Biophys Res Commun. 2016 May;474(1):57–63.

219 Bader AG. miR-34 – a microRNA replacement therapy is headed to the clinic. Front Genet. 2012;3(JUL). DOI: 10.3389/fgene.2012.00120

220 Hsu S Da, Chu CH, Tsou AP, Chen SJ, Chen HC, Hsu PWC, et al. miRNAMap 2.0: Genomic maps of microRNAs in metazoan genomes. Nucleic Acids Res. 2008 Jan;36(SUPPL. 1). DOI: 10.1093/nar/gkm1012

221 Guo Y, Xiong Y, Sheng Q, Zhao S, Wattacheril J, Flynn CR. A micro-RNA expression signature for human NAFLD progression. J Gastroenterol. 2016 Oct;51(10):1022–30.

222 Liu CH, Ampuero J, Gil-Gómez A, Montero-Vallejo R, Rojas Á, Muñoz-Hernández R, et al. miRNAs in patients with non-alcoholic fatty liver disease: A systematic review and meta-analysis. J Hepatol. 2018 Dec;69(6):1335–48.

223 Castro RE, Ferreira DMS, Afonso MB, Borralho PM, MacHado M V., Cortez-Pinto H, et al. MiR-34a/SIRT1/p53 is suppressed by ursodeoxycholic acid in the rat liver and activated by disease severity in human non-alcoholic fatty liver disease. J Hepatol. 2013 Jan;58(1):119–25.

224 Liu XL, Pan Q, Zhang RN, Shen F, Yan SY, Sun C, et al. Disease-specific miR-34a as diagnostic marker of nonalcoholic steatohepatitis in a Chinese population. World J Gastroenterol. 2016;22(44):9844–52.

225 Shao M, Ye Z, Qin Y, Wu T. Abnormal metabolic processes involved in the pathogenesis of non-alcoholic fatty liver disease (Review). Exp Ther Med. 2020;20(5):1–1.

226 Xu Y, Zalzala M, Xu J, Li Y, Yin L, Zhang Y. A metabolic stress-inducible miR-34a-HNF4α pathway regulates lipid and lipoprotein metabolism. Nat Commun. 2015 Jun;6. DOI: 10.1038/ncomms8466

227 Xu Y, Zhu Y, Hu S, Pan X, Bawa FC, Wang HH, et al. Hepatocyte miR-34a is a key regulator in the development and progression of non-alcoholic fatty liver disease. Mol Metab. 2021 Sep;51(April):101244.

228 Lee J, Padhye A, Sharma A, Song G, Miao J, Mo YY, et al. A pathway involving farnesoid X receptor and small heterodimer partner positively regulates hepatic sirtuin 1 levels via MicroRNA-34a inhibition. J Biol Chem. 2010 Apr;285(17):12604–11.

229 Chang T-C, Wentzel EA, Kent OA, Ramachandran K, Mullendore M, Lee KH, et al. Transactivation of miR-34a by p53 Broadly Influences Gene Expression and Promotes Apoptosis. Mol Cell. 2007 Jun;26(5):745–52.

230 Hong DS, Kang YK, Borad M, Sachdev J, Ejadi S, Lim HY, et al. Phase 1 study of MRX34, a liposomal miR-34a mimic, in patients with advanced solid tumours. Br J Cancer. 2020 May;122(11):1630–7.

231 Jiao Y, Lu Y, Li XY. Farnesoid X receptor: A master regulator of hepatic triglyceride and glucose homeostasis. Acta Pharmacol Sin. 2015;36(1):44–50.

232 Kumar J, Hasan M, Mohsin S, Alzaher MH, Nagar T, Jamil A, et al. Assessing the efficacy of farnesoid X receptor agonists in the management of metabolic dysfunction-associated steatotic liver disease: A systematic review and meta-analysis. Clin Res Hepatol Gastroenterol. 2025 Feb;49(2):102530.

233 Wang JM, Qiu Y, Yang Z, Kim H, Qian Q, Sun Q, et al. IRE1 prevents hepatic steatosis by processing and promoting the degradation of select microRNAs. Sci Signal. 2018 May;11(530). DOI: 10.1126/scisignal.aao4617

234 Jia N, Lin X, Ma S, Ge S, Mu S, Yang C, et al. Amelioration of hepatic steatosis is associated with modulation of gut microbiota and suppression of hepatic miR-34a in Gynostemma pentaphylla (Thunb.) Makino treated mice. Nutr Metab. 2018 Dec;15(1). DOI: 10.1186/s12986-018-0323-6

235 Wen Y, Huang H, Huang B, Liao X. HSA-miR-34a-5p regulates the SIRT1/TP53 axis in prostate cancer. Am J Transl Res. 2022;14(7):4493–504.

236 Ding J, Li M, Wan X, Jin X, Chen S, Yu C, et al. Effect of MIR-34a in regulating steatosis by targeting PPARα expression in nonalcoholic fatty liver disease. Sci Rep. 2015 Sep;5. DOI: 10.1038/srep13729

237 Anggreini P, Kuncoro H, Sumiwi SA, Levita J. Role of the AMPK/SIRT1 pathway in non-alcoholic fatty liver disease (Review). Mol Med Rep. 2023 Feb;27(2). DOI: 10.3892/mmr.2022.12922

238 Hochreuter MY, Dall M, Treebak JT, Barrès R. MicroRNAs in non-alcoholic fatty liver

disease: Progress and perspectives. Mol Metab. 2022 Aug;101581.

239 Li M, Hong W, Hao C, Li L, Wu D, Shen A, et al. SIRT1 antagonizes liver fibrosis by blocking hepatic stellate cell activation in mice. FASEB J. 2018 Jan;32(1):500–11.

240 Li X, Chen Y, Wu S, He J, Lou L, Ye W, et al. MicroRNA-34a and microRNA-34c promote the activation of human hepatic stellate cells by targeting peroxisome proliferator-activated receptor γ. Mol Med Rep. 2015 Feb;11(2):1017–24.

241 Ding J, Li M, Wan X, Jin X, Chen S, Yu C, et al. Effect of miR-34a in regulating steatosis by targeting PPARα expression in nonalcoholic fatty liver disease. Sci Rep. 2015 Sep;5(1):13729.

242 Zhang J, Wang H, Yao L, Zhao P, Wu X. MiR-34a promotes fibrosis of hepatic stellate cells via the TGF-β pathway. Ann Transl Med. 2021 Oct;9(20):1520–1520.

243 Lai Z, Chen J, Ding C, Wong K, Chen X, Pu L, et al. Association of Hepatic Global DNA Methylation and Serum One-Carbon Metabolites with Histological Severity in Patients with NAFLD. Obesity. 2020 Jan;28(1):197–205.

244 Pogribny IP, Tryndyak VP, Bagnyukova T V., Melnyk S, Montgomery B, Ross SA, et al. Hepatic epigenetic phenotype predetermines individual susceptibility to hepatic steatosis in mice fed a lipogenic methyl-deficient diet. J Hepatol. 2009 Jul;51(1):176–86.

245 Baumeier C, Saussenthaler S, Kammel A, Jähnert M, Schlüter L, Hesse D, et al. Hepatic DPP4 DNA methylation associates with fatty liver. Diabetes. 2017 Jan;66(1):25–35.

246 Baumeier C, Schlüter L, Saussenthaler S, Laeger T, Rödiger M, Alaze SA, et al. Elevated hepatic DPP4 activity promotes insulin resistance and non-alcoholic fatty liver disease. Mol Metab. 2017 Oct;6(10):1254–63.

247 Hosseini H, Teimouri M, Shabani M, Koushki M, Babaei Khorzoughi R, Namvarjah F, et al. Resveratrol alleviates non-alcoholic fatty liver disease through epigenetic modification of the Nrf2 signaling pathway. Int J Biochem Cell Biol. 2020 Feb;119. DOI: 10.1016/j.biocel.2019.105667

248 Sookoian S, Rosselli MS, Gemma C, Burgueño AL, Fernández Gianotti T, Castaño GO, et al. Epigenetic regulation of insulin resistance in nonalcoholic fatty liver disease: Impact of liver methylation of the peroxisome proliferator-activated receptor γ coactivator 1α promoter. Hepatology. 2010 Dec;52(6):1992–2000.

249 Ahrens M, Ammerpohl O, Von Schönfels W, Kolarova J, Bens S, Itzel T, et al. DNA methylation analysis in nonalcoholic fatty liver disease suggests distinct disease-specific and remodeling signatures after bariatric surgery. Cell Metab. 2013 Aug;18(2):296–302.

250 Nishida N, Yada N, Hagiwara S, Sakurai T, Kitano M, Kudo M. Unique features associated with hepatic oxidative DNA damage and DNA methylation in non-alcoholic fatty liver disease. J Gastroenterol Hepatol. 2016 Sep;31(9):1646–53.

251 Geißler C, Krause C, Neumann AM, Britsemmer JH, Taege N, Grohs M, et al. Dietary induction of obesity and insulin resistance is associated with changes in Fgf21 DNA methylation in liver of mice. J Nutr Biochem. 2022 Feb;100. DOI: 10.1016/j.jnutbio.2021.108907

252 da Silva Lima N, Fondevila MF, Nóvoa E, Buqué X, Mercado-Gómez M, Gallet S, et al. Inhibition of ATG3 ameliorates liver steatosis by increasing mitochondrial function. J Hepatol. 2022 Jan;76(1):11–24.

253 Fondevila MF, Fernandez U, Heras V, Parracho T, Gonzalez-Rellan MJ, Novoa E, et al. Inhibition of carnitine palmitoyltransferase 1A in hepatic stellate cells protects against fibrosis. J Hepatol. 2022 Jul;77(1):15–28.

254 Fondevila MF, Novoa E, Gonzalez-Rellan MJ, Fernandez U, Heras V, Porteiro B, et al. p63 controls metabolic activation of hepatic stellate cells and fibrosis via an HER2-ACC1 pathway. Cell Reports Med. 2024 Feb;5(2). DOI: 10.1016/j.xcrm.2024.101401

255 Fondevila MF, Fernandez U, Gonzalez-Rellan MJ, Da N, Lima S, Buque X, et al. The L-α-Lysophosphatidylinositol/G Protein-Coupled Receptor 55 System Induces the Development of Nonalcoholic Steatosis and Steatohepatitis. Hepatology. 2021;73(2):606–24.

256 Krause C, Britsemmer JH, Bernecker M, Molenaar A, Taege N, Geißler C, et al. Liver microRNA transcriptome reveals miR-182 as link between type 2 diabetes and fatty liver disease in obesity. Elife. 2023;12(RP92075). DOI: 10.7554/eLife.92075.1

257 Hamada M, Kiryu H, Sato K, Mituyama T, Asai K. Prediction of RNA secondary structure using generalized centroid estimators. Bioinformatics. 2009 Feb;25(4):465–73.

258 Sato K, Hamada M, Asai K, Mituyama T. CENTROIDFOLD: a web server for RNA secondary structure prediction. Nucleic Acids Res. 2009 Jul;37(Web Server):W277–80.

259 Pfaffl MW, Hageleit M. Validities of mRNA quantification using recombinant RNA and recombinant DNA external calibration curves in real-time RT-PCR. Biotechnol Lett. 2001;23(4):275–82.

260 Ulgen E, Ozisik O, Sezerman OU. PathfindR: An R package for comprehensive identification of enriched pathways in omics data through active subnetworks. Front Genet. 2019 Sep;10(SEP). DOI: 10.3389/fgene.2019.00858

261 Naujack A-M, Krause C, Britsemmer JH, Taege N, Mittag J, Kirchner H. Epigenetic regulation of thyroid hormone action in human metabolic dysfunction associated steatohepatitis. Eur Thyroid J. 2024 DOI: https://doi.org/10.1530/ETJ-24-0080

262 Uhlen M, Zhang C, Lee S, Sjöstedt E, Fagerberg L, Bidkhori G, et al. A pathology atlas of the human cancer transcriptome. Science (80-). 2017 Aug;357(6352). DOI: 10.1126/science.aan2507

263 Version 24.0. The Human Protein Atlas [Internet]. [cited 2025 Mar 5]. Available from: https://www.proteinatlas.org/ENSG00000147100-SLC16A2/cell+line#liver_cancer

264 Castro-Mondragon JA, Riudavets-Puig R, Rauluseviciute I, Berhanu Lemma R, Turchi L, Blanc-Mathieu R, et al. JASPAR 2022: The 9th release of the open-access database of transcription factor binding profiles. Nucleic Acids Res. 2022 Jan;50(D1):D165–73.

265 Katsura A, Morishita A, Iwama H, Tani J, Sakamoto T, Tatsuta M, et al. MicroRNA profiles following metformin treatment in a mouse model of non-alcoholic steatohepatitis. Int J Mol Med. 2015;35(4):877–84.

266 Yang Y, Lu M, Xu Y, Qian J, Le G, Xie Y. High dietary methionine intake may contribute to the risk of nonalcoholic fatty liver disease by inhibiting hepatic H2S production. Food Res Int. 2022 Aug;158. DOI: 10.1016/j.foodres.2022.111507

267 Kanno K, Tazuma S, Chayama K. AT1A-deficient mice show less severe progression of liver fibrosis induced by CCl4. Biochem Biophys Res Commun. 2003 Aug;308(1):177–83.

268 Jiang X-P, Ai W-B, Wan L-Y, Zhang Y-Q, Wu J-F. The roles of microRNA families in hepatic fibrosis. Cell Biosci. 2017 Dec;7(1):34.

269 Meng Z, Wang Y, Wang L, Jin W, Liu N, Pan H, et al. FXR regulates liver repair after CCl4-induced toxic injury. Mol Endocrinol. 2010 May;24(5):886–97.

270 Rena G, Hardie DG, Pearson ER. The mechanisms of action of metformin. Diabetologia. 2017 Sep;60(9):1577–85.

271 Truong Do M, Gyun Kim H, Ho Choi J, Gwang Jeong H. Metformin induces microRNA-34a to downregulate the Sirt1/Pgc-1α/Nrf2 pathway, leading to increased susceptibility of wild-type p53 cancer cells to oxidative stress and therapeutic agents. Free Radic Biol Med. 2014 Sep;74:21–34.

272 Luo X, Hu R, Zheng Y, Liu S, Zhou Z. Metformin shows anti-inflammatory effects in murine macrophages through Dicer/microribonucleic acid-34a-5p and microribonucleic acid-125b-5p. J Diabetes Investig. 2020 Jan;11(1):101–9.

273 de Assis LVM, Harder L, Inderhees J, Jöhren O, Mittag J, Oster H. Thyroid hormone receptor beta (THRB) dependent regulation of diurnal hepatic lipid metabolism in adult male mice. npj Metab Heal Dis. 2024 Aug;2(1). DOI: 10.1038/s44324-024-00023-4

274 Bruinstroop E, van der Spek AH, Boelen A. Role of hepatic deiodinases in thyroid hormone homeostasis and liver metabolism, inflammation, and fibrosis. Eur Thyroid J. 2023 Jun;12(3). DOI: 10.1530/ETJ-22-0211

275 De Jong FJ, Peeters RP, Heijer T Den, Van Der Deure WM, Hofman A, Uitterlinden AG, et al. The association of polymorphisms in the type 1 and 2 deiodinase genes with circulating thyroid hormone parameters and atrophy of the medial temporal lobe. J Clin Endocrinol Metab. 2007;92(2):636–40.

276 Bruinstroop E, Zhou J, Tripathi M, Yau WW, Boelen A, Singh BK, et al. Early induction of hepatic deiodinase type 1 inhibits hepatosteatosis during NAFLD progression. Mol Metab. 2021;53(June):101266.

277 Yen PM, Feng X, Flamant F, Chen Y, Walker RL, Weiss RE, et al. Effects of ligand and thyroid hormone receptor isoforms on hepatic gene expression profiles of thyroid hormone receptor knockout mice. EMBO Rep. 2003 Jun;4(6):581–7.

278 Paisdzior S, Schuelke M, Krude H. What is the Role of Thyroid Hormone Receptor Alpha 2 (TRα2) in Human Physiology? Exp Clin Endocrinol Diabetes. 2022 May;130(05):296–302.

279 de Assis LVM, Harder L, Lacerda JT, Parsons R, Kaehler M, Cascorbi I, et al. Rewiring of liver diurnal transcriptome rhythms by triiodothyronine (T3) supplementation. Elife. 2022 Jul;11:1–35.

280 Asher G, Gatfield D, Stratmann M, Reinke H, Dibner C, Kreppel F, et al. SIRT1 Regulates Circadian Clock Gene Expression through PER2 Deacetylation. Cell. 2008 Jul;134(2):317–28.

281 Jung-Hynes B, Ahmad N. SIRT1 controls circadian clock circuitry and promotes cell survival: a connection with age-related neoplasms. FASEB J. 2009 Sep;23(9):2803–9.

282 Liao H, Xiao Y, Hu Y, Xiao Y, Yin Z, Liu L, et al. Methylation-induced silencing of miR-34a enhances chemoresistance by directly upregulating ATG4B-induced autophagy through AMPK/mTOR pathway in prostate cancer. Oncol Rep. 2016 Jan;35(1):64–72.

283 Zheng K, Chen D-S, Wu Y-Q, Xu X-J, Zhang H, Chen C-F, et al. MicroRNA Expression Profile in RAW264.7 cells in Response to Brucella melitensis Infection. Int J Biol Sci. 2012 Aug;8(7):1013–22.

284 Ziu M, Fletcher L, Rana S, Jimenez DF, Digicaylioglu M. Temporal Differences in MicroRNA Expression Patterns in Astrocytes and Neurons after Ischemic Injury. PLoS One. 2011 Feb;6(2):e14724.

285 Spira D, Buchmann N, Dörr M, Markus MRP, Nauck M, Schipf S, et al. Association of thyroid function with insulin resistance: data from two population-based studies. Eur Thyroid J. 2022 Apr;11(2). DOI: 10.1530/ETJ-21-0063

286 Choi YM, Kim MK, Kwak MK, Kim D, Hong E-G. Association between thyroid hormones

and insulin resistance indices based on the Korean National Health and Nutrition Examination Survey. Sci Rep. 2021 Nov;11(1):21738.

287 Brenta G. Why Can Insulin Resistance Be a Natural Consequence of Thyroid Dysfunction? J Thyroid Res. 2011;2011:1–9.

288 Ren-Ming H, Li-Min W, Frank HJL, Pedram A, Levin ER. Insulin stimulates thyroid hormone receptor α gene expression in cultured bovine aortic endothelial cells. Mol Cell Endocrinol. 1994 Jul;103(1–2):65–71.

289 Liu J, Hernandez-Ono A, Graham MJ, Galton VA, Ginsberg HN. Type 1 Deiodinase Regulates ApoA-I Gene Expression and ApoA-I Synthesis Independent of Thyroid Hormone Signaling. Arterioscler Thromb Vasc Biol. 2016 Jul;36(7):1356–66.

290 Zhang Z, Li X, Liu G, Gao L, Guo C, Kong T, et al. High Insulin Concentrations Repress Insulin Receptor Gene Expression in Calf Hepatocytes Cultured in Vitro. Cell Physiol Biochem. 2011;27(6):637–40.

291 Boucher J, Kleinridders A, Ronald Kahn C. Insulin receptor signaling in normal and insulin - resistant states. Cold Spring Harb Perspect Biol. 2014 Jan;6(1). DOI: 10.1101/cshperspect.a009191

292 Pascual A, Aranda A. Thyroid hormone receptors, cell growth and differentiation. Biochim Biophys Acta - Gen Subj. 2013 Jul;1830(7):3908–16.

293 Badami E, Carcione C, Chinnici CM, Tinnirello R, Conaldi PG, Iannolo G. HCV Interplay With Mir34a: Implications in Hepatocellular Carcinoma. Front Oncol. 2022 Jan;11. DOI: 10.3389/fonc.2021.803278

294 Cermelli S, Ruggieri A, Marrero JA, Ioannou GN, Beretta L. Circulating MicroRNAs in Patients with Chronic Hepatitis C and Non-Alcoholic Fatty Liver Disease. PLoS One. 2011 Aug;6(8):e23937.

295 Haas U, Sczakiel G, Laufer S. MicroRNA-mediated regulation of gene expression is affected by disease-associated SNPs within the 3′-UTR via altered RNA structure. RNA Biol. 2012 Jun;9(6):924–37.

296 Zheng Z, Reichel M, Deveson I, Wong G, Li J, Millar AA. Target RNA Secondary Structure Is a Major Determinant of miR159 Efficacy. Plant Physiol. 2017 Jul;174(3):1764–78.

297 Hesketh J. 3′ UTRs and Regulation. Encyclopedia of Life Sciences. Wiley; 2005. DOI: 10.1038/npg.els.0005011

298 Grimson A, Farh KK-H, Johnston WK, Garrett-Engele P, Lim LP, Bartel DP. MicroRNA Targeting Specificity in Mammals: Determinants beyond Seed Pairing. Mol Cell. 2007 Jul;27(1):91–105.

299 Nielsen CB, Shomron N, Sandberg R, Hornstein E, Kitzman J, Burge CB. Determinants of targeting by endogenous and exogenous microRNAs and siRNAs. RNA. 2007 Nov;13(11):1894–910.

300 Riolo G, Cantara S, Marzocchi C, Ricci C. miRNA Targets: From Prediction Tools to Experimental Validation. Methods Protoc. 2020 Dec;4(1):1.

301 Navarro F, Lieberman J. miR-34 and p53: New Insights into a Complex Functional Relationship. PLoS One. 2015 Jul;10(7):e0132767.

302 Tost J, Gut IG. DNA methylation analysis by pyrosequencing. Nat Protoc. 2007 Sep;2(9):2265–75.

303 Crary-Dooley FK, Tam ME, Dunaway KW, Hertz-Picciotto I, Schmidt RJ, LaSalle JM. A

comparison of existing global DNA methylation assays to low-coverage whole-genome bisulfite sequencing for epidemiological studies. Epigenetics. 2017 Mar;12(3):206–14.

304 Lodygin D, Tarasov V, Epanchintsev A, Berking C, Knyazeva T, Körner H, et al. Inactivation of miR-34a by aberrant CpG methylation in multiple types of cancer. Cell Cycle. 2008 Aug;7(16):2591–600.

305 Saeed WH, Eissa AA, Al-Doski AA. Impact Of TP53 Gene Promoter Methylation On Chronic Lymphocytic Leukemia Pathogenesis And Progression. J Blood Med. 2019 Nov;Volume 10:399–404.

306 Roux J, Gonzàlez-Porta M, Robinson-Rechavi M. Comparative analysis of human and mouse expression data illuminates tissue-specific evolutionary patterns of miRNAs. Nucleic Acids Res. 2012 Jul;40(13):5890–900.

307 Jopling CL, Yi M, Lancaster AM, Lemon SM, Sarnow P. Modulation of Hepatitis C Virus RNA Abundance by a Liver-Specific MicroRNA. Science (80-). 2005 Sep;309(5740):1577–81.

308 Girard M, Jacquemin E, Munnich A, Lyonnet S, Henrion-Caude A. miR-122, a paradigm for the role of microRNAs in the liver. J Hepatol. 2008 Apr;48(4):648–56.

309 Coulouarn C, Factor VM, Andersen JB, Durkin ME, Thorgeirsson SS. Loss of miR-122 expression in liver cancer correlates with suppression of the hepatic phenotype and gain of metastatic properties. Oncogene. 2009 Oct;28(40):3526–36.

310 Gunn PJ, Green CJ, Pramfalk C, Hodson L. In vitro cellular models of human hepatic fatty acid metabolism: Differences between Huh7 and HepG2 cell lines in human and fetal bovine culturing serum. Physiol Rep. 2017 Dec;5(24). DOI: 10.14814/phy2.13532

311 Mockly S, Seitz H. Synthetic miR-34a against solid tumours: a predictable failure. Br J Cancer. 2023 Feb;128(3):478–80.

312 Wu WY, Ding XQ, Gu TT, Guo WJ, Jiao RQ, Song L, et al. Pterostilbene Improves Hepatic Lipid Accumulation via the MiR-34a/Sirt1/SREBP-1 Pathway in Fructose-Fed Rats. J Agric Food Chem. 2020;68(5):1436–46.

10. Supplemental Tables

Table 52. RNA sequencing HepG2 cells stimulated with fructose and insulin

Gene,symbol	baseMean	logFC	lfcSE	pvalue	adj,P,Val
SERPINE1	451,1679	1,724188	0,15826	6,94E-29	7,21E-25
APOC3	581,9538	-1,35682	0,143503	1,60E-22	8,33E-19
AKR1B10	502,0139	1,464611	0,159995	2,84E-21	9,85E-18
MT2A	20014,96	0,991353	0,112553	7,47E-20	1,94E-16
AKR1C1	7143,15	0,960988	0,123121	4,77E-16	9,91E-13
GDF15	3895,506	1,279526	0,165849	7,50E-16	1,30E-12
TGFBR3	1133,819	0,921558	0,123984	6,06E-15	8,99E-12
RP11-1143G9,4	3090,813	0,938955	0,127047	8,36E-15	1,09E-11
LYZ	3114,807	0,939335	0,128335	1,49E-14	1,72E-11
SLC7A11	460,5385	1,117714	0,161417	2,40E-13	2,50E-10
SOX4	1021,997	1,013158	0,146827	2,90E-13	2,74E-10
GLRX	434,254	1,158734	0,170144	5,02E-13	4,01E-10
AC132217,4	4024,786	-0,72507	0,10597	4,74E-13	4,01E-10
PDLIM1	1595,653	-0,77807	0,114271	5,95E-13	4,42E-10
JAG1	590,7857	0,880774	0,132969	2,07E-12	1,43E-09
FILIP1L	254,1311	1,283298	0,198323	5,25E-12	3,41E-09
AKAP12	643,9899	0,969985	0,150829	7,12E-12	4,35E-09
SLC6A14	317,1989	1,05782	0,167319	1,38E-11	7,96E-09
DUSP6	490,0487	1,0243	0,162837	1,71E-11	9,33E-09
ITGA2	373,8441	1,065234	0,171629	2,95E-11	1,48E-08
FSCN1	1482,584	-0,73554	0,118276	2,98E-11	1,48E-08
GCLM	415,4166	0,99221	0,162067	5,01E-11	2,37E-08
S100A6	1128,822	1,028815	0,168634	5,58E-11	2,52E-08
HOXD1	129,9273	1,748532	0,288806	6,09E-11	2,64E-08
SAT1	2070,397	0,702963	0,115693	7,91E-11	3,29E-08
ASPH	1147,874	0,757092	0,129928	3,45E-10	1,38E-07
HSPB1	1212,948	-0,80244	0,138406	3,83E-10	1,47E-07
ATP1B1	2114,163	0,671782	0,117583	7,34E-10	2,72E-07
TUBA1A	252,5834	0,979535	0,176607	1,54E-09	5,52E-07

Gene,symbol	baseMean	logFC	lfcSE	pvalue	adj,P,Val
CACNA2D4	282,2265	0,938297	0,169352	1,67E-09	5,59E-07
SERPINF2	1080,581	-0,73408	0,132021	1,63E-09	5,59E-07
MT1E	4166,104	0,626702	0,112464	1,72E-09	5,59E-07
ADH6	234,571	-0,99396	0,182227	2,51E-09	7,90E-07
PHLDA1	1559,184	0,63852	0,11661	2,67E-09	8,17E-07
TESC	759,5192	0,722196	0,134324	3,59E-09	1,07E-06
DCBLD2	1090,484	0,683983	0,128081	5,89E-09	1,70E-06
DHRS2	21623,13	-0,67428	0,128547	9,76E-09	2,74E-06
TRIB1	416,8816	0,746463	0,144627	1,46E-08	3,99E-06
SLC2A1	3043,795	0,74287	0,146338	2,34E-08	6,23E-06
IGF2	11610,51	-0,71371	0,141185	2,56E-08	6,65E-06
TXNRD1	755,3217	0,79879	0,158953	2,82E-08	7,15E-06
TM4SF1	2954,416	0,548551	0,108256	3,01E-08	7,45E-06
IL11	76,4994	1,433249	0,289917	3,67E-08	8,87E-06
LGALS3	136,3036	1,07601	0,219922	4,97E-08	1,17E-05
MALAT1	13274,9	0,784082	0,158969	5,63E-08	1,30E-05
PAQR8	406,6785	-0,79052	0,161975	5,87E-08	1,33E-05
CTGF	890,806	0,634752	0,12961	6,37E-08	1,41E-05
RAB11FIP4	601,2729	-0,72289	0,148537	6,69E-08	1,45E-05
C19orf77	442,83	-0,7445	0,154027	7,70E-08	1,63E-05
IER3	1560,01	0,814269	0,168889	7,97E-08	1,66E-05

Table 53. RNA sequencing HepG2 cells miR-34a-5p inhibitor with fructose insulin

Gene,symbol	baseMean	logFC	lfcSE	pvalue	adj,P,Val
SERPINE1	462,0959	1,867378	0,16282	1,03E-31	1,23E-27
GLRX	451,0935	1,3547	0,165939	1,70E-17	1,01E-13
MT2A	19374,48	1,027043	0,143096	4,77E-14	1,90E-10
SOX4	1010,092	1,099323	0,156922	1,32E-13	3,93E-10
S100A6	1206,481	1,272871	0,190932	1,30E-12	3,10E-09
AKR1B10	442,9763	1,303772	0,198591	2,69E-12	5,35E-09
TGFBR3	1101,644	0,962803	0,149057	5,66E-12	9,65E-09

Gene,symbol	baseMean	logFC	lfcSE	pvalue	adj,P,Val
MIR34A	31,61658	9,271686	2,778145	8,60E-12	1,28E-08
RP11-1143G9,4	2944,835	0,939602	0,148377	1,31E-11	1,74E-08
LYZ	2971,926	0,94405	0,14942	1,56E-11	1,86E-08
SLC7A11	433,4491	1,091893	0,181087	8,62E-11	9,36E-08
AKR1C1	6808,888	0,95166	0,158901	1,21E-10	1,20E-07
AKAP12	609,8944	0,962389	0,162476	1,72E-10	1,58E-07
GDF15	3253,424	1,001171	0,16993	1,87E-10	1,59E-07
FILIP1L	230,0743	1,187145	0,202852	2,60E-10	2,07E-07
JAG1	571,6102	0,915219	0,15646	2,77E-10	2,07E-07
ASPH	1100,22	0,77927	0,139463	1,37E-09	9,62E-07
SLC2A1	3042,088	0,862562	0,155085	1,48E-09	9,79E-07
GCLM	399,7077	1,014028	0,186148	2,70E-09	1,69E-06
APOC3	595,6601	-0,9654	0,17808	2,89E-09	1,72E-06
IGF2	10826,84	-0,77759	0,147496	7,71E-09	4,38E-06
CACNA2D4	270,9998	0,955217	0,183638	1,03E-08	5,59E-06
DCBLD2	1114,327	0,838748	0,161871	1,19E-08	5,94E-06
INS-IGF2	3942,957	-0,93022	0,179714	1,15E-08	5,94E-06
HPX	216,911	-1,17452	0,229682	1,39E-08	6,64E-06
TM4SF1	2922,357	0,644515	0,125507	1,84E-08	8,44E-06
ITGA2	367,6661	1,120576	0,2215	2,15E-08	9,50E-06
KANK4	155,8903	-1,21969	0,243034	2,73E-08	1,16E-05
PLAU	32,25087	2,45125	0,491189	2,84E-08	1,17E-05
ADAM9	314,7958	0,943823	0,191546	4,20E-08	1,67E-05
CCDC170	69,99307	-1,58613	0,325784	5,74E-08	2,21E-05
SAT1	1978,62	0,703482	0,14493	7,15E-08	2,67E-05
DUSP6	461,2306	0,976948	0,204332	8,60E-08	3,11E-05
TESC	721,3603	0,722744	0,151702	1,13E-07	3,86E-05
C19orf77	411,6549	-0,82052	0,173294	1,13E-07	3,86E-05
SLC6A14	283,9016	0,915925	0,195435	1,46E-07	4,83E-05
TIMP1	390,5323	0,966235	0,209185	1,85E-07	5,98E-05
RAB11FIP4	558,7911	-0,79357	0,172274	2,15E-07	6,74E-05
HOXD1	107,0181	1,442123	0,318208	2,45E-07	7,49E-05

Gene,symbol	baseMean	logFC	lfcSE	pvalue	adj,P,Val
PAQR8	376,7468	-0,87641	0,193283	2,84E-07	8,06E-05
HSPB1	1165,099	-0,73458	0,161114	2,80E-07	8,06E-05
SNORD13	79,40781	-1,35345	0,297696	2,73E-07	8,06E-05
GPR126	732,2156	0,701095	0,155302	3,73E-07	0,000104
IL11	73,22204	1,415999	0,321317	4,53E-07	0,000123
FGB	550,828	-0,72115	0,163103	5,38E-07	0,000143
HSPA13	150,2743	0,970885	0,221614	5,96E-07	0,000155
PDLIM1	1533,4	-0,69407	0,158462	6,39E-07	0,000162
APOC1	3061,85	-0,71105	0,165591	9,73E-07	0,000242
GSTA1	75,40671	-1,53645	0,360193	1,02E-06	0,000243
PEG10	11930,28	-0,57632	0,134212	1,03E-06	0,000243

Table 54. RIP-seq detected miR-34a-5p detected target genes

PLIN2+A2:E42	CYREN	PDCD5	BTG2	LRRC40	CD74
DMD	EAF1	BICRAL	RPL27	FAM171A1	CCN1
NSD1	ABI2	OTULIN	BBS5	TDRP	NUDCD2
CTTNBP2NL	ASAH2B	ZBTB10	PGK1	AGAP1	CALCOCO2
MTHFSD	CDC37L1	ARIH2	AP3B2	ZC3H14	RP2
C3	INTS8	CASP6	RFC5	FNIP2	CAP1
SNX27	CCNE2	GTF3C2	ABRAXAS1	C4orf45	TIMM23B
ZNF148	ZHX2	CITED2	TMEM199	DGAT2	PPM1A
CRTC1	GRTP1	RPL38	RBM38	PHF3	THRB
CERK	KIAA0319L	SLC35B3	RIOX2	MTM1	UBE2W
ABCD1	AKR1D1	SEPTIN1	PUS7	MRAS	IL6R
COL26A1	INO80	CAGE1	FKBP1B	CDC42EP1	RHPN2
RALGDS	SIRT1	BRK1	PLPBP	NDUFA4	EZR

CRAT	SYNCRIP	COX7B	DTD1	DYM	IGFBP1
IL11	EIF2S2	RPL18A	DPY19L4	RNF19B	DTNA
CHMP7	CCNG2	POLDIP3	TK2	CINP	DNMT3A
MTX3	GNPAT	FBXO46	TNRC6B	ZNF428	FUT8
QDPR	SMPD4	DCP1A	ZFP2	LRFN3	LYRM4
DBT	PSMD11	LSM8	RAB40B	HSPD1	PLEKHA1
MPV17L2	RNF14	NFYC	THBS1	MRPL19	MAGT1
SLC38A1	EP400	ARPC4-TTLL3	PBX4	GOLGA3	FAM193A
TESK1	CLCN3	POLR2F	STXBP5	MAPK8IP3	SMURF2
MAD2L1	E2F5	TXNIP	TSPAN6	TMEM267	RRAGC
PRMT1	NINJ1	MT1E	CDC42BPB	PSMD4	SPARC
NMT1	NCSTN	PHF6	TPD52	ITPRID2	CSTB
TTC39B	TAF10	IDS	SLC2A4RG	CSNK2A1	RAB3GAP1
TRMT61A	ACADVL	VIL1	OTX1	MSANTD3-TMEFF1	RCOR1
IMPACT	DNAJB12	PDCD4	AP2S1	TUT4	SNX17
ABHD4	SNAP29	BBIP1	UBE4A	PPARG	NEPRO
STX17	METTL16	UBAC2	LMBR1L	N4BP2L2	ACBD3
ZNF276	TUFT1	ENSA	GNPDA1	SMIM14	
PHF19	CHD4	PTPN14	NFAT5	TM9SF3	
PHYKPL	CD68	SFT2D1	SLC25A23	PRKAB2	
RPL24	RDH10	MKLN1	ZNF367	CBX3	
EIF3A	EMP2	PABPC4	ENAH	ING1	
LMAN2L	USP21	MIEF1	GORASP2	TAF5	

RPS14	LSM14B	SLC17A5	LATS1	ROCK1
NKX3-1	NFYA	RPIA	UBE2D1	GALNT1
VPS4A	DEF8	TMEM250	PECAM1	LYPLAL1
LIMD2	RABEPK	POM121C	BUD31	PSMB2
GALNT10	SLC30A1	UBE2D4	STK16	APLP2
SIDT2	ZMAT3	AAGAB	PSMF1	EIF4G3
RLIM	WWC3	RNF208	ANKH	B4GALT4
PCYT1B	TVP23A	IL6ST	NXF1	RNF170
SLX1A	POLR2L	ABCE1	KIF1C	KRT8
FAM76A	FLOT2	XBP1	GGA3	SOAT1
RAPGEF6	TRAPPC8	CYB5A	METTL14	S100PBP

11. Appendix

11.1. Vector maps

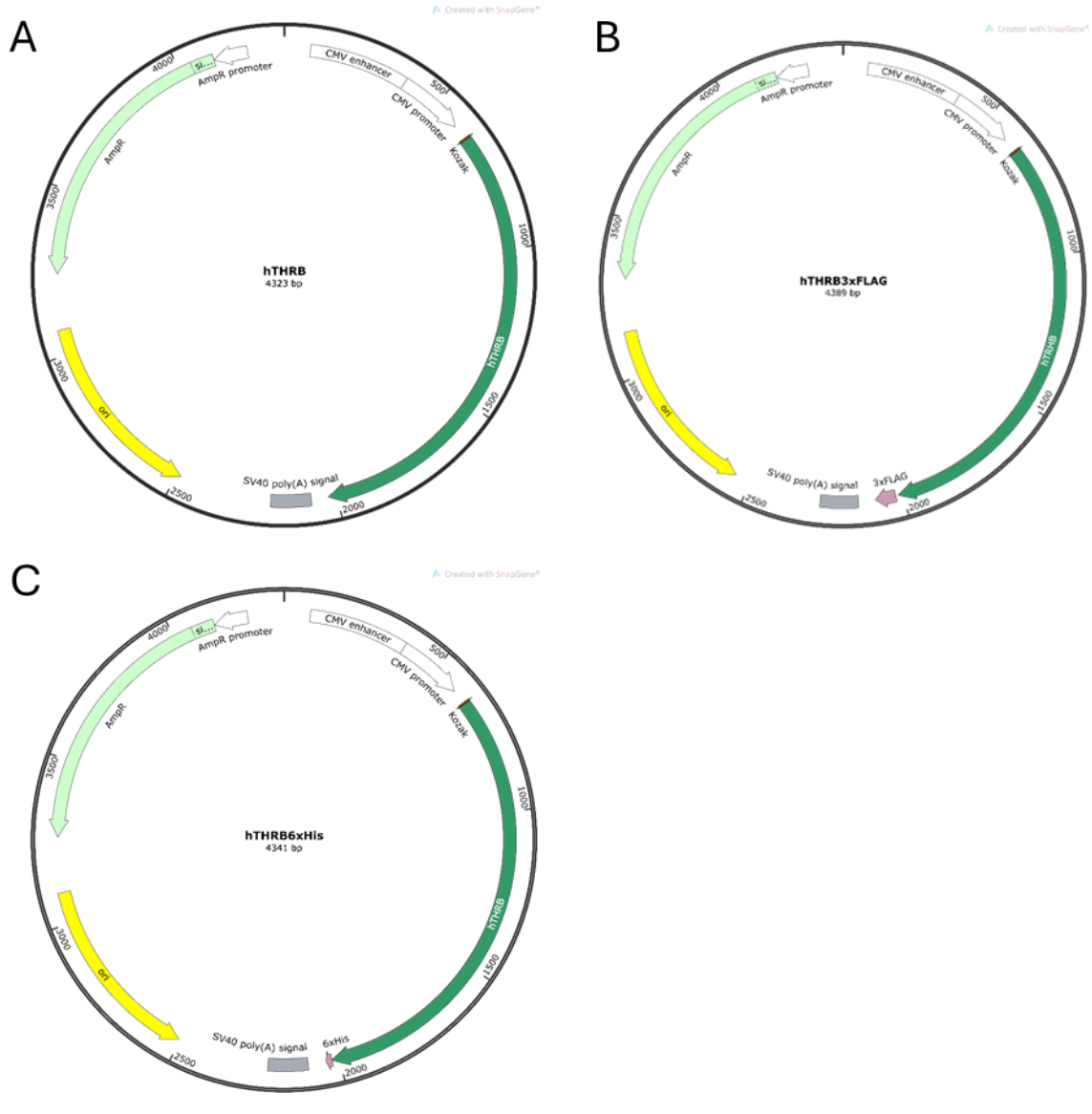

Figure 36. Vectors designed for THRB tag tests. A) Control vector containing the THRB gene, B) THRB3xFLAG vector containing a 3xFLAG tag at the C-terminal end of the THRB gene. C) THRB6xHis vector containing a THRB C-terminal 6xHis tag. All plasmids were generated using Vector Builder.

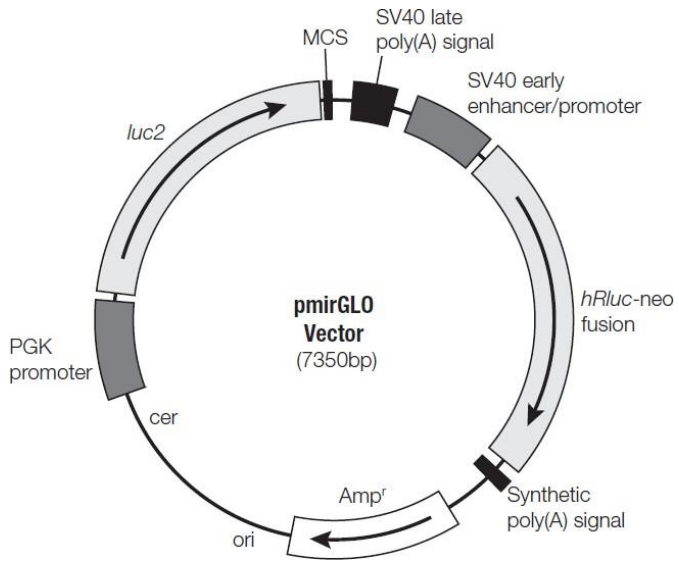

Figure 37. Plasmid used for luciferase reporter assays

11.2. Characterization of miRNA expression in iPSC derived hepatocyte-like cells

To verify the differentiation of the iPSC derived hepatocytes into hepatocyte like cell, the expression of miR-122-5p was measured, the main miRNA in the liver. As Table 55 shows, miR-122-5p is not expressed in undifferentiated iPSCs, but highly expressed after differentiation. The difference to the liver biopsy ample could be explained with either not fully matured hepatocyte like cells or that the liver biopsy contains more cell types than hepatocytes, which would distort the measurement. The other measured miRNAs miR-34a-5p and miR-155-5p, were measured due to their potential relevance to the regulation of TH signaling in MASLD and miR-24-5p was used throughout this work as a reliable housekeeper miRNA. The expression of miR-34a-5p increases during differentiation and reaches higher expressin than the biopsy sample, meanwhile the expression of miR-155-5p reduces and though still detectable is lower than the expression in the biopsy sample. MiR-24-3p increases during differentiation but does not reach the expression levels of the biopsy.

Table 55. Comparison of Ct values between iPSC, iPSC derived hepatocytes and liver biopsy isolated miRNA expression

miRNA	iPCS	iPSC derived Hep 1	iPSC derived Hep 2	Liver biopsy
miR-122-5	ND	19,91048	19,98202	16,98445
miR-34a-5p	30,59286	25,04647	26,10557	28,20375
miR-155-5p	31,57852	32,09882	34,45556	28,91682
miR-24-3p	27,62709	22,44872	22,8826	19,97168

ND Not detectable

12. Abbreviations

ΔCt	ΔCt value, calculated by $\Delta Ct = Ct_{Target} - Ct_{Housekeeper}$
5mC	5-methylcytosine
ABCA1	ATP binding cassette transporter member 1
ACACA	Acetyl-CoA carboxylase
Actb	Actin beta
ADIPOR1	adiponectin receptor 1
AGO2	Argonaut protein 2
ALT	Alanine aminotransferase
AMLD	American lifestyle diet
APOA1	Apolipoprotein A1
APOB100	Apolipoprotein B100
AST	Aspartate aminotransferase
ATP	Adenosine triphosphate
B2m	Beta-2-microglobulin
BisDNA	Bisulfite converted DNA
Bp	Base pair
CASC3	CASC3 exon junction complex subunit
CCl_4	Carbon tetrachloride
CDD	Choline deficient diet
CD-HFD	Choline deficient high-fat diet
CDHFHCD	Choline deficient high fat high cholesterol diet
cDNA	Complementary DNA
CETP	Cholesterol ester transfer protein
ChREBP	Carbohydrate-responsive element-binding protein
CpG	Cytosine-guanine dinucleotides
CPT1-Lα	β-oxidation carnitine palmitoyltransferase 1
Cyclo	Ppia gene encoding peptidylprolyl isomerase A (cyclophilin A)
CYP7A1	Cholesterol 7 alpha-hydroxylase
DAMP	Damage-associated molecular pattern
DE	Definite endoderm

DIO1	Deiodinase type 1
DIO2	Deiodinase type 2
DIO3	Deiodinase type 3
DNA	Desoxyribonucleic acid
DNL	*De novo* lipogenesis
DNMT	DNA methyltransferases
DPP4	Dipeptidyl peptidase 4
eIF4E	Eukaryotic translation initiation factor 4E
ER	Endoplasmic reticulum
ESRRA	Estrogen-related receptor α
FABP7	fatty acid-binding protein 7
FASN	Fatty acid synthase
FATP	Fatty acid transport protein
FDPS	farnesyl diphosphate synthase
FFA	Free fatty acids
FXR	Farnesoid X receptor
G6PC	Glucose-6-phosphatase
GO	Gene Ontology
GLUT2	Glucose transporter 2
HCC	Hepatocellular carcinoma
HCD	High cholesterol diet
HFD	High-fat diet
HFrD	High fructose diet
HFrHFD	High fructose high fat diet
HFrHFHCD	High fructose high fat high cholesterol diet
HMG-CoA	3-hydroxy-3-methylglutaryl coenzyme A
HMGCR	3-hydroxy-3-methylglutaryl-coenzyme A reductase
HMGCS1	hydroxy-3-methylglutaryl-coenzyme A synthase 1
HNF4α	hepatocyte nuclear factor 4α
HPT	hypothalamus-pituitary-thyroid
hRluc	Renilla luciferase

InsR Insulin receptor

iPSC Induced pluripotent stem cell

IRE1α inositol-requiring enzyme 1α

KEGG Kyoto Encyclopedia of Genes and Genomes

Kik1b4 Kallikrein 1 related peptidase b4

LDLR Low density lipoprotein receptor

LPS Lipopolysaccharide

LXR Liver X receptor

MAMP Microbial-associated molecular pattern

MAS Metabolic disfunction-associated steatotic liver disease activity score

MASH Metabolic dysfunction-associated steatohepatitis

MASL metabolic dysfunction-associated steatotic liver

MASLD Metabolic dysfunction-associated steatotic liver disease

MCAD Medium-chain acyl-CoA dehydrogenase

MCDD Methionine-choline deficient diet

MCT8 Monocarboxylate transporter 8

ME Malic enzyme

MHPS MASLD human proximity score

miRISC miRNA-induced silencing complex

miRNA Micro RNA

mRNA Messenger RNA

NASH Non-alcoholic steatohepatitis

NAFLD Non-alcoholic fatty liver disease

NCD Noncommunicable diseases

ncRNA Noncoding RNA

NFκB Nuclear factor kappa B subunit 1

Nfr2 NF-E2-reated factor 2

nt Nucleotide

NTCP Na^+/taurocholate cotransporting polypeptide

NTP Nucleoside triphosphate

PAMP Pathogen-associated molecular pattern

PCR	Polymerase chain reaction
PCSK9	Proprotein convertase subtilisin/kexin type 9
PDH	pyruvate dehydrogenase
PDK4	Pyruvate dehydrogenase kinase isoform 4
PEPCK	Phosphoenolpyruvate carboxy kinase
Pfu	Phusion Hotstart II
PGC-1α	Peroxisome proliferator-activated receptor gamma coactivator 1-alpha
PI3K	Phosphoinositide 3-kinase
PNPLA3	Patatin-like phospholipase domain containing protein 3
PTEN	Phosphatase and tensin homolog
qRT-PCR	Quantitative real time polymerase chain reaction
RNA	Ribonucleic acid
ROCKi	ROCK inhibitor
RT	Reverse transcriptase
RIP-seq	RNA-interacting protein immunoprecipitation-sequencing
ROS	Reactive oxygen species
RXR	Retinoid X receptor
SAM	S-adenosylmethionine
SCD1	Stearoyl-CoA desaturase
SD	Standard deviation
SEM	Standard error of mean
SIRT1	Sirtuin 1
SLC10A1	Solute carrier family 10 member 1
SLC16A2	Solute carrier family 16 member 2
SRB1	Scavenger receptor class B member 1 (
SREBP1c	Sterol regulatory element-binding protein 1c
SREBP2	Sterol regulatory element-binding protein 2
STD	Standard diet
STZ	Streptozotocin
T2D	Type 2 diabetes
T_3	Triiodothyronine

T_4	Thyroxine
TG	Triglyceride
TF	Transcription factor
TH	Thyroid hormones
THRA	Thyroid hormone receptor alpha (gene)
THRB	Thyroid hormone receptor beta (gene)
THRSP	Thyroid hormone responsive protein
TLR	Toll-like receptor
TM6SF2	Transmembrane 6 superfamily member 2
TNFα	Tumor necrosis factor α
TR	Thyroid hormone receptor (protein)
TRE	Thyroid hormone response element
TRH	Thyrotropin releasing hormone
TSH	Thyroid stimulating hormone
UCP2	Mitochondrial uncoupling protein 2
UTR	Untranslated region
VEH	Vehicle
VLDL	Very low density lipoprotein
WD	Western diet
WGBS	Whole genome bisulfite sequencing

13. Acknowledgements

Finally, this thesis has come to an end and it is time to thank everybody who helped, supported and encouraged me throughout the completion.

First of all, I would like to thank my supervisor Prof. Dr. Henriette Kirchner who gave me the opportunity to work in her group. Her support and excellent mentorship contributed greatly to the success of this work.

Secondly, many thanks to my second supervisor Prof. Dr. Jens Mittag who was always available with his vast knowledge and expertise.

Then there are all these people that provided me with models, be it mouse models from Dr. Natalie Taege or Prof. Rubén Nogueiras from the University Santiago de Compostela or a brand new cell model from Dr. Katarzyna Ludwik from the Charite, this work would not have been completed without their contributions. This also applies to every person that donated a liver biopsy for the human cohort and Dr. Christin Krause that isolated DNA and RNA from these samples. I would also like to thank Christin for being an awesome office buddy and mentor.

Of course I want to thank everyone in the lab, this thesis would not have been anyway near as fun without you.

And lastly I would like to thank my family, partner and friends for listening to all my complaints, cheering me on and their valuable feedback.

ACADEMIC EDUCATION

04/2021 – 09/2024 **Doctoral thesis**

- University to Lübeck
- Institute for human genetics, supervised by Prof. Henriette Kirchner
- Topic: Control of cellular TH metabolism in NASH

10/2017 – 10/2020 **Master of Science (2,1)**

- University to Lübeck
- Molecular Life Science (Master)
- Titel of the master thesis: Stem-like glioma cells with edits in the genes coding for the peroxisome proliferator-activated receptors PPARα, β/δ and γ
- Institute for neuro surgery, experimental neurooncology supervised by PD. Dr. Christina Zechel

10/2014 – 12/2017 **Bachelor of Science (2,7)**

- University to Lübeck
- Molecular Life Science (Bachelor)
- Titel of the bachelor thesis: Biochemical investigation of MERS-Coronavirus accessory protein 4a
- Institute for biochemistry, supervised by Prof. Rolf Hilgenfeld

INTERNSHIPS

10/2016 – 02/2017 **AUSTRALIAN NATIONAL UNIVERSITY**

- Gardiner Group – Mechanisms od Thrombosis and Cancer
- Topic: Platelet-Tumour cell interactions under fluid shear stress

11/2015 – 06/2016 **UNIVERSITY TO LÜBECK**

- Institute for pathology
- Topic: Determination of the HPV status of oropharynx carcinoma

PUBLICATIONS

Naujack A-M, Krause C, Britsemmer JH, Taege N, Mittag J, Kirchner H. Epigenetic regulation of thyroid hormone action in human metabolic dysfunction associated steatohepatitis. Eur Thyroid J. 2024 DOI: https://doi.org/10.1530/ETJ-24-0080

Britsemmer, J. H., Krause, C., Taege, N., Geißler, C., Lopez-Alcantara, N., Schmidtke, L., Naujack, A. M., Wagner, J., Wolter, S., Mann, O., & Kirchner, H. (2023). Fatty Acid Induced Hypermethylation in the Slc2a4 Gene in Visceral Adipose Tissue Is Associated to Insulin-Resistance and Obesity. *International Journal of Molecular Sciences*, *24*(7). https://doi.org/10.3390/ijms24076417